Stony Brook University

Base Excision DNA Repair in the Mitochondria of Differentiated Neuronal Cells

A Dissertation Presented

by

Rachel Audrey Caston

to

The Graduate School

in Partial Fulfillment of the

Requirements

for the Degree of

Doctor of Philosophy

in

Genetics

Stony Brook University

December 2017

Stony Brook University

The Graduate School

Rachel Audrey Caston

We, the dissertation committee for the above candidate for the

Doctor of Philosophy degree, hereby recommend

acceptance of this dissertation.

Bruce Demple – Dissertation Advisor
Professor, Department of Pharmacology, Stony Brook University

Styliani-Anna Tsirka - Chairperson of Defense
Professor, Department of Pharmacology, Stony Brook University

Daniel Bogenhagen
Professor, Department of Pharmacology, Stony Brook University

Holly Colognato
Associate Professor, Department of Pharmacology, Stony Brook University

Elizabeth Boon
Associate Professor, Department of Chemistry. Stony Brook University

This dissertation is accepted by the Graduate School

Charles Taber

Dean of the Graduate School

Abstract of the Dissertation

Base Excision DNA Repair in the Mitochondria of Differentiated Neuronal Cells

by

Rachel Audrey Caston

Doctor of Philosophy

in

Genetics

Stony Brook University

2017

Healthy mitochondria are vital for maintaining neuronal activity over the lifespan of an organism. Since mitochondria contain their own DNA, functional DNA repair pathways in the organelle are necessary for mitochondrial integrity. However, mitochondria do not have the complete complement of DNA repair pathways found in the nucleus. Thus far, base excision DNA repair (BER), mismatch repair, and double-strand break repair have been detected in mitochondria, although these pathways involve fewer proteins than is the case in the nucleus. Of the DNA repair pathways operating in mitochondria, BER acts on small, non-distorting base lesions, the main type of damage expected to arise from oxidative reactions.

This dissertation focuses on BER after cellular differentiation. There is mounting evidence that BER occurs more slowly in differentiated cells compared to proliferating cells. In terminally differentiated cells, the nuclear genome is no longer being replicated, and the proteins involved in DNA replication are correspondingly down-regulated in the nucleus.

However, mitochondria continue to replicate their DNA and divide even in a non-dividing cell, which necessitates efficient DNA repair. It may be that mitochondrial DNA repair proteins shared with the nucleus continue to be imported into mitochondria after differentiation. It is also possible that other, mitochondria-specific proteins compensate for the loss of shared DNA repair proteins. Of particular interest are four nuclease enzymes implicated in “long-patch” base excision DNA repair in mitochondria: Fen1, DNA2, MGME1 and ExoG.

During DNA repair synthesis in base excision repair, the DNA polymerase can add a single nucleotide, at which point the enzyme removes the resulting 5'-terminal 2-deoxyribose-5-phosphate (5’-dRP) residue, and DNA ligase III can seal the nick. However, if the DNA polymerase adds more than one nucleotide, the resulting displaced oligonucleotide flap needs to be removed before the DNA strand can be resealed by DNA ligase. That process is so-called “long-patch” BER. The nuclease(s) responsible for flap excision in the mitochondria are not yet certain. Fen1 and DNA2 are enzymes that function in the maturation of Okazaki fragments during DNA replication in the nucleus, as well as in nuclear and mitochondrial DNA repair. ExoG and MGME1 are structure-specific nucleases specific to mitochondria, and they have activities that could function in long-patch BER. Investigating the regulation and roles of these proteins should give insight into the modulation of BER during cellular differentiation.

The use of CAD cells, a mouse neuroblastoma cell line that can be differentiated into neurons in vitro, allows the comparison of proliferating progenitors and genetically identical terminally differentiated cells. Immunoblotting and immunofluorescence microscopy were used to probe the expression of these proteins in the nucleus and in mitochondria. Upon CAD cell

differentiation, Fen1 and DNA2 were indeed down-regulated at the whole cell level. ExoG was also lowered to 50% of the cycling cell level, while MGME1 was not diminished and may be modestly increased. Enzyme activity assays showed that whole-cell extracts of differentiated cells performed flap excision less effectively than did the proliferating cell extracts. Likewise, mitochondrial extracts from differentiated CAD cells had slower flap excision than observed for mitochondrial extracts from proliferating cells. Paradoxically, a PCR-based DNA repair assay for mitochondrial DNA damage revealed that differentiated cell mitochondria accumulated *less* damage than did proliferating cell mitochondria. Taken together, these data imply that long-patch BER flap excision occurs more slowly in differentiated cells, both in the nucleus and mitochondria, but that, despite the difference in the flap endonuclease activity detected, the in vivo mitochondrial DNA repair capacity of differentiated cells is comparable to that of proliferating cell mitochondria.

Dedication Page

For Carolyn, Lucille, and Charlotte Walls, without whom this dissertation would not exist.

To Madeline and Robert, who picked up the slack along the way.

Table of Contents

List of Figures

List of Tables

Chapter 1

Introduction and significance

Mitochondria are organelles which engage in a range of cellular functions, including generating ATP, calcium ion storage, and signaling for apoptosis [1]. Mitochondria contain their own genome, separate from the nuclear genome, which is maintained by mitochondrial DNA replication and repair proteins. Genes encoding proteins that are required for oxidative phosphorylation are found in the mitochondrial genome. Therefore, mitochondrial DNA (mtDNA) integrity is critical for mitochondrial function. The research reported in this dissertation explores the regulation of mtDNA repair upon cellular differentiation.

1.1 Oxidative Phosphorylation

In eukaryotic cells, mitochondria are the sites of oxidative phosphorylation, a process for generating most of the ATP in cells. Conversion of ATP to ADP releases energy, which can be used for signaling [2], motility [3,4], cell division [5,6], and numerous of other cellular functions. Unlike fermentation, which produces only 2 molecules of ATP per molecule glucose, oxidative phosphorylation produces 30-32 ATP molecules per glucose molecule [7]. Oxidative phosphorylation in the mitochondria is achieved using the electron transport chain, which is a series of four protein complexes located in the inner membrane of the mitochondrial matrix [5]. These proteins create both pH and electrical gradients across the membrane by pumping protons through the inner membrane into the inter-membrane space of the mitochondria [8]. Electrons are passed along the in a series of linked redox reactions, with oxygen being the final electron acceptor in a reaction that produces H_2O. To generate ATP, the protons that were excluded from the inner membrane flow back through ATP synthase, a spinning motor that converts ADP to ATP.

While more efficient than fermentation, oxidative phosphorylation does create a risk of generating reactive oxygen species (ROS) as a by-product (Figure 1.1). ROS are free radicals and other reactive molecules derived from oxygen. The prominent species include hydrogen peroxide, superoxide anion, and hydroxyl radical [9]. When ROS are formed as a result of oxidative phosphorylation, they pose a threat to mitochondrial function. Since mtDNA is attached to the inner mitochondrial membrane, in close proximity to the electron transport chain, it is a nearby target for oxidation [10]. However, evidence that mitochondrial DNA is more sensitive to oxidation is controversial and mitochondrial DNA does not incur more oxidative damage than nuclear DNA [11,12].

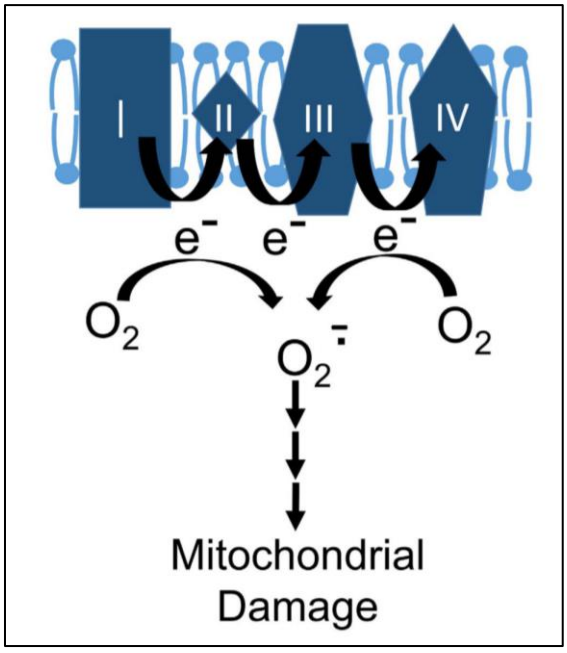

Figure 1.1. Formation of ROS from "leaks" in the electron transport chain. Transfer of electrons during oxidative phosphorylation creates the risk of ROS formation by reaction with oxygen, which initially generates superoxide as shown. This occurs mostly for Complex I and Complex III. The arrows indicate reactions producing first hydrogen peroxide, then the far more reactive hydroxyl radical. The close proximity of the mtDNA may enhance damage due to ROS generated locally.

From: Caston and Demple. Free Radical Biology and Medicine. (2017) 146–150 [13]

1.2 Mitochondrial DNA

In mammals, mitochondria have a circular genome of about 16,000 base pairs containing 37 genes: 13 electron transport chain proteins, 22 transfer RNAs, and 2 ribosomal RNAs [14]. The mitochondria-specific transfer RNAs help maintain the codon usage bias of mtDNA-encoded messenger RNA compared to nuclear DNA [15]. Most of the genes needed for mitochondrial functions are encoded in the nucleus. Why some genes are kept in the mitochondria instead of the nucleus is unclear. One theory is that hydrophobic proteins are difficult to import and sort across membranes or may be targeted to different organelles, so retention of hydrophobic proteins is favored [16]. Alternatively, a theory known as "colocalization for redox regulation" suggests that proteins necessary for ATP production are maintained in the mtDNA to allow local control of energy production [16].

The mtDNA is organized into a complex known as the nucleoid, which is associated with the inner mitochondrial membrane and composed of a single circular genome and mtDNA binding proteins such as transcription factor A (TFAM), DNA polymerase γ, and Twinkle helicase [10,17]. The mtDNA is transcribed as a polycistronic RNA, with transfer RNAs in between most messenger RNAs [18,19]. Transcription begins from a primary promoter in each direction around the circular genome [20]. As a result, DNA lesions that block transcription can prevent the expression of multiple genes.

1.3 Mitochondrial DNA Damage and Disease

Diseases caused by mutations to the mitochondrial genome account for only 15% of mitochondrial disorders [21]. The other 85% are caused by mutations to genes in the nuclear DNA that are required for mitochondrial function. There are two main categories of diseases associated with mtDNA mutations: those inherited at birth (germline), and those acquired with time through somatic accumulation of mutations. The list of inheritable mitochondrial disease is extensive, but general indications of mitochondrial disorders include poor growth, muscle weakness, visual problems, hearing problems, respiratory disorders, and neurological problems [22].

The mtDNA mutations acquired throughout life are thought to contribute to aging [23,24]. For example, the “common deletion” in mitochondria, which removes region of 4977 base pairs affecting 5 tRNAs and 7 protein-coding genes, is found more frequently with age in high-energy tissues such as neurons and muscles [25]. The common deletion is the result of recombination between two 13 base pairs GC-rich regions of the mtDNA and is considered a typical feature of the aging process. Another study has shown that general mtDNA mutations accumulate with age, though no single mutation was more likely than the others [26].

Mutations in the mtDNA are associated with neurodegenerative syndromes including Parkinson’s, Alzheimer’s, and Huntington’s diseases [27]. In the human post-mortem brain tissue of patients with Parkinson’s disease, mtDNA anomalies occur in dopamine neurons of the substantia nigra, including deletions and mutations in the mtDNA [26-30]. In a study of Parkinson’s and Alzheimer’s diseases, changes in cytosine methylation of mtDNA were found in both disease states [31]. Furthermore, control region mutations are increased in Alzheimer’s

disease and mtDNA copy number is decreased, implying that transcription of mtDNA is altered in the disease [32,33]. Some variations in mtDNA are associated with increased risk of acquiring Alzheimer's and Huntington's diseases [34]. Finally, in a mouse model of Huntington's disease, the temporal and frontal lobes of the brain exhibited 8-fold greater amounts of mtDNA lesions than did nuclear DNA [35,36]. In these diseased cells, DNA damage accumulates beyond the ability of the mitochondria to repair it. However, in healthy tissues, mitochondrial DNA repair pathways prevent the accrual of DNA lesions.

1.4 Mitochondrial Base Excision DNA Repair

Mitochondria do not have the complete complement of DNA repair pathways found in the nucleus. Thus far, mitochondria have been shown to have base excision DNA repair (BER), mismatch repair, and double-strand break repair, although with fewer proteins for each pathway than are involved in the nucleus [37]. Of these, BER is focused on repairing small, non-distorting base lesions, the type mainly expected to arise from oxidative damage [38]. When the DNA is damaged, a DNA glycosylase removes the damaged base by cleaving the N-glycosylic bond between the base and the sugar (Figure 1.1). The mitochondria do not have all 11 of the glycosylases found in the nucleus; only 7 glycosylases have been confirmed in the organelle [39]. DNA glycosylases can be mono- or bi-functional [39]. Monofunctional glycosylases remove the damaged base by hydrolysis, which yields an unmodified 2-deoxyribose apurinic/apyrimidinic (AP) site as the other product. In contrast, bifunctional DNA glycosylases act via a covalent intermediate, sometimes cleaving the DNA backbone in a ß-elimination reaction to produce a 3'-end bearing a 2,3-unsaturated derivative of 2-deoxyribose. This lyase-

generated 3’ blocking group must be removed to allow DNA repair synthesis, and a number of enzymes are proposed for this role, notably Ape1, which has a significant 3’ processing activity. It is also possible for certain AP lyases, such as Neil1 and Neil2, to cleave the DNA backbone using β, δ-elimination; the consecutive reactions eliminate the 2-deoxyribose, leaving a 3’-phosphate remains which must be removed by an enzyme such as polynucleotide kinase-phosphatase before DNA repair synthesis can occur.

After the glycosylase has removed the damaged base, Ape1 nicks the DNA on the immediate 5’ side of the AP site, allowing the DNA polymerase to access the DNA. For many years, DNA polymerase γ was thought to be the only DNA polymerase present in mitochondria. Recently, PrimPol and DNA polymerase β have both been detected in mitochondria[40-42]. Either one of these polymerases could function in DNA repair in the mitochondria, particularly polymerase β since it functions in BER in the nucleus. DNA polymerase β was found to interact with the mitochondrial DNA helicase Twinkle, and suppression of DNA polymerase β resulted in elevated endogenous mtDNA lesions[42].

During DNA repair synthesis, the DNA polymerase can add a single nucleotide, at which point the polymerase will remove the 5’ dRP if it has lyase activity. Then DNA ligase III can seal the nick. However, if the DNA polymerase adds more than one nucleotide, the resulting displaced oligonucleotide flap retaining the 5’abasic residue needs to be removed before the DNA can be closed by ligase. The endonuclease responsible for this reaction in the mitochondria is not yet clear. Fen1, DNA2, ExoG, and MGME1 are potential candidates, which is discussed and analyzed further in Chapter 2. Fen1 and DNA2 perform this role in the nucleus, with some evidence of a similar function in mitochondrial BER[43,44]. ExoG and MGME1 are

more recently discovered and mitochondria-specific enzymes, but their ability to remove such a flap in a DNA repair intermediate has not been tested [45,46]. After flap excision, the nick is sealed by ligase III, the only DNA ligase known so far in mitochondria.

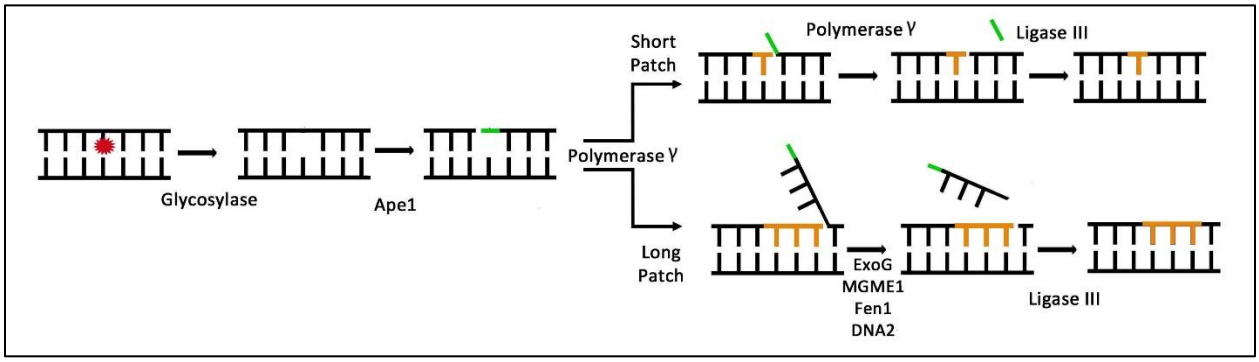

Figure 1.2. Schematic of mitochondrial base excision repair. A damaged base (red) is removed by a DNA glycosylase. The Ape1 endonuclease incises the resulting AP site at the 5' phosphodiester, leaving behind a 5'-dRP (green). In short-patch BER, one new nucleotide is added (orange) by Polγ, and the DNA is ligated by Lig III. For long-patch BER, multiple nucleotides are added, and the resulting displaced flap is excised by Fen1, DNA2, MGME1 and/or ExoG, followed by ligation by Lig III.
From: Caston and Demple. Free Radical Biology and Medicine (2017) [13]

1.5 DNA Damage Tolerance and Alternate Pathways

For DNA damage that is not yet repaired, cells may have damage tolerance pathways. For example, certain DNA polymerases can synthesize past certain lesions in a template DNA strand in a process known as translesion synthesis. The DNA lesion is not removed, but translesion synthesis may prevent cytotoxicity by allowing DNA synthesis to be completed. Currently, PrimPol is the best candidate for a mitochondrial translesion synthesis enzyme. In vitro assays have demonstrated that PrimPol can synthesize both DNA and RNA using a DNA template, with a preference for DNA, and the enzyme can perform de novo synthesis due to its activity as a primase [41]. As is common with translesion DNA polymerases, PrimPol is

potentially mutagenic, with an error rate 50 times greater than that of DNA polymerase γ [40,47]. PrimPol was proposed as a trans-lesion synthesis polymerase because it is capable in vitro of bypassing 8-oxoguanine, abasic sites, and UV adducts in the template, as well as extending from mismatched termini [40,41,47-49]. However, when combined with the mitochondrial enzymes necessary for mtDNA replication including DNA polymerase γ, PrimPol did not enhance bypass of oxidative lesions [50].

When mitochondria are excessively damaged, the entire organelle can be degraded in a process known as mitophagy [51]. The best understood pathway for mitophagy is dependent on the proteins PINK1 and Parkin. In healthy mitochondria, PINK1 is imported into the inner mitochondrial membrane and degraded. This process is reliant on the membrane potential of the outer mitochondrial membrane. If a mitochondrion is defective and the outer mitochondrial membrane becomes depolarized, PINK1 accumulates on the outer mitochondrial membrane. PINK1 is then available to activate Parkin, an E3 ubiquitin ligase. Parkin marks outer mitochondrial membrane proteins for degradation, setting up a signal for mitophagy.

In neurons, mitophagy occurs in both the cell body and the axon. Mitochondria are unequally distributed in neurons, being generated in the soma then distributed out to the axons [52]. In these cells, mitophagy occurs via the Parkin-PINK1 pathway in the cell body as well as in the neuronal process [53,54]. It is also possible for neurons to pass their dysfunctional mitochondria to nearby astrocytes for degradation in a process known as transmitophagy [55]. Failure to clear damaged mitochondria in the dendrites of neurons may lead to neuronal cell death, which would result in the loss of a synaptic connection [56]. Accumulation of dysfunctional mitochondria in the axons could signal the beginning of neurodegeneration.

1.6 Cellular Differentiation

When cells differentiate, nuclear DNA replication ceases. Correspondingly, some DNA replication proteins are down-regulated. Since proteins can perform functions in both DNA replication and repair, down-regulating these proteins may lead to slower nuclear DNA repair in differentiated cells compared to proliferating cells. For example, differentiated neuronal SH-SY5Y cells were more sensitive to hydrogen peroxide (H_2O_2) than were proliferating SH-SY5Y cells [57]. Furthermore, the differentiated SH-SY5Y cells down-regulated both short-patch and long-patch BER proteins, including Ape1, ligase I, ligase III, DNA polymerase ε, XRCC1, PCNA, and Fen1. Interestingly, when challenged with methyl methanesulfonate (MMS), the cycling and non-cycling cells responded similarly to one another, implying that the differentiated cells were more sensitive than proliferating cells to oxidative damage, but not to alkylation damage. Another study demonstrated that in C2C12 mouse myoblasts, DNA polymerase and DNA ligase activities are lower in the nucleus of differentiated cells compared to proliferating cells[58]. Moreover, in primary mouse muscle cells, DNA damage requiring either short- or long-patch BER pathways was resolved more slowly in differentiated cells compared to proliferating cells [59]. In these cells, DNA ligase I and XRCC1 proteins were down-regulated upon differentiation [59].

Despite the attenuation of nuclear DNA repair upon differentiation, the mitochondria of differentiated cells must continue to survive and reproduce for the life of the cell. Mitochondria replicate and divide even in non-dividing cells, albeit more slowly [60]. The mitochondrial genome needs to be repaired for the mitochondria to continue functioning. There is some

evidence for DNA repair in differentiated cell mtDNA. For example, the same study that revealed attenuated DNA ligase and DNA polymerase activities in the nucleus upon differentiation also showed that differentiated myotubes repair their mtDNA at a faster rate than do proliferating myoblasts after being incubated with glucose oxidase to generate a flux of H_2O_2 [58]. Additionally, differentiated muscle cells have higher survival than their proliferating counterparts after treatment with chemical agents and irradiation[61].

1.7 Conclusion

In the research for this dissertation, I addressed the effects of cellular differentiation on mitochondrial BER. I utilized a neuronal mouse cell line to explore mtDNA repair after cellular differentiation. In Chapter 2, I present evidence showing that Fen1 and DNA2 endonucleases are down-regulated after cellular differentiation, but Fen1 continues to be localized to the mitochondria of differentiated cells. The mitochondrial enzymes MGME1 and ExoG are expressed before and after differentiation. Despite the presence of these enzymes, flap excision in differentiated cell mitochondrial extracts was slower compared to proliferating cells mitochondria. Chapter 3 focuses on the overall DNA repair capacity of the mitochondria. Differentiated cells showed a greater rate of survival than proliferating cells when challenged with chemical damaging agents. Additionally, the mtDNA of differentiated cells accumulated fewer lesions than did proliferating cell mtDNA.

Chapter 4 focuses on the effects of soil toxicity on differentiated cells as well as lung epithelial cells. When astronauts visited the Moon during the Apollo missions, the lunar soil clung to spacesuits due to its electrostatic charge, and the lunar dust was tracked into the living environment by astronauts who had been exploring the lunar surface [62]. Astronaut Harrison

Schmitt described his reaction to lunar dust as “lunar hay fever”, including sneezing, watering eyes, and sore throat [63]. I demonstrate that when CAD cells are exposed to lunar soil simulants, the CAD cells reacted similarly to their response with chemical agents; differentiated cells mtDNA accumulated less DNA damage than did the proliferating cells.

Chapter 2

Expression and activity of mitochondrial endonucleases after cellular differentiation

2.1 Abstract

Mitochondrial base excision repair (BER) utilizes proteins involved in nuclear and mitochondrial DNA replication and repair. After cellular differentiation, nuclear DNA is not replicated, and many proteins are down-regulated accordingly. However, a structure-specific endonuclease remains necessary for long-patch base excision DNA repair (BER) in both the nucleus and mitochondria of differentiated cells. Four such endonucleases have been implicated in long-patch in mitochondria: Fen1, DNA2, MGME1 and EXOG. Fen1 and DNA2 are localized to both the nucleus and mitochondria, and they are down-regulated in the nucleus upon differentiation. ExoG and MGME1 are proteins localized to the mitochondria, and either of them might support long-patch BER in the mitochondria.

In this chapter, I demonstrate that Fen1 and DNA2 change their distribution after differentiation, and that Fen1 is localized to the mitochondria after differentiation. The expression levels of MGME1 and ExoG show only small changes after differentiation. Despite expression of these nucleases after differentiation, flap excision occurred more slowly in the mitochondrial extracts of differentiated cells than in those of proliferating cells.

2.2 Introduction

One common change during terminal differentiated cell types is the down-regulation of DNA replication proteins [58,59]. Some structure-specific endonucleases are a necessary component of long-patch base excision DNA repair (BER) and there is evidence that their expression may change with differentiation. The long-patch BER pathway is necessary because some lesions can be repaired only by this pathway. For example, 2-deoxyribonolactone (2-dL), a C1' oxidized AP site, forms a covalent crosslink with repair proteins during attempted short-patch BER [64-66]. DNA-protein crosslinks are avoided in long-patch BER because DNA polymerase γ moves past the oxidized site when it adds the 2^{nd} nucleotide.

Four endonucleases are discussed in this chapter: Fen1, DNA2, MGME1, and ExoG proteins. Fen1 and DNA2 are found in both the nucleus and the mitochondria [43,67,68]. These two enzymes function in nuclear DNA replication for the maturation of Okazaki fragments [69]. DNA2 cleaves long DNA "flaps" (displaced strands) to a size (30 nucleotides) that renders those substrates for Fen1. Fen1 cleaves precisely at the flap junction, yielding a ligatable product [70]. DNA2 has been shown to cleave RNA primers from mitochondrial DNA as well as long-patch BER flaps in mitochondria [43]. There is conflicting evidence on the function of Fen1 in mitochondria. In HeLa cells, an enzyme activity consistent with Fen1 was measured in mitochondrial extracts [44]. When Fen1 was depleted from mitochondrial extracts, flap – cleavage intermediate products accumulated [44]. However, in HOS and HEK cells, a Fen1 variant was found exclusively in mitochondria that was more active on RNA than on DNA, which is consistent with a role in replication and removal of RNA primers from mtDNA during replication [71].

ExoG and MGME1 are proteins localized to the mitochondria, both of which have activity consistent with long-patch flap excision [45,72]. ExoG is a paralog of EndoG, an endonuclease found in the mitochondria and involved in apoptosis [46]. ExoG functions by removing 2 nucleotides at a time from the 5' end of a DNA flap and was found to be necessary for the completion of long patch BER in Hela mitochondrial extracts [72,73]. Furthermore, over-expression of ExoG in progenitor cells increased the cells' resistance to oxidative DNA damage.

MGME1 is an endonuclease proposed to work in conjunction with DNA polymerase γ in the mitochondria [45]. MGME1 does not consistently make ligatable cuts at the flap junction, but the enzyme can work in concert with DNA polymerase γ to generate a ligatable nick [45]. The possible role of MGME1 in BER has not been assessed, but the enzyme's activities are consistent with long-patch BER flap excision in mitochondria (Figure 1.2).

In this chapter I demonstrate that Fen1 and DNA2 change their localization after differentiation, and Fen1 is localized to the mitochondria after differentiation. Additionally, MGME1 and ExoG are expressed in the mitochondria of differentiated cells. Despite availability of endonucleases, flap excision occurs more slowly in differentiated cell mitochondria extracts than in proliferating cell mitochondria extracts.

2.3 Results

2.3.1 Protein Localization

The Cath.-a-differentiated (CAD) cell line was chosen for these experiments. The CAD cell line was isolated from a mouse neuroblastoma [74]. The cells can be grown proliferatively (PCAD) or terminally differentiated (TDCAD) in culture by serum starvation [74]. CAD cells allow

for direct comparison of genetically identical proliferating progenitors and terminally differentiated neurons.

As mentioned in section 2.2, several BER proteins are down-regulated at the whole-cell during cellular differentiation. These include Ape1, DNA ligase I, DNA ligase III, DNA polymerase ε, X-ray repair cross-complementing protein 1 (XRCC1), proliferating cell nuclear antigen (PCNA), and Fen1 [57,59]. It is important to note that these proteins were down-regulated by varying degrees, with XRCC1 and Fen1 reduced to <25% of the level in proliferating cells and the other proteins expressed above 50% of proliferating cell expression. To investigate whether such changes are recapitulated during the differentiation of CAD cells, whole-cell extracts were probed for expression of several BER-related proteins (Figure 2.1A). After CAD cell differentiation, DNA2 and Fen1 were reduced to ~25% of their expression in proliferating cells and ExoG was reduced to ~50% of the proliferating cell level (Figure 2.1). The MGME1 level was not diminished, and even increased after differentiation (Figure 2.1). Ape1 was included since it is a BER protein that has not been shown to be significantly down-regulated upon differentiation [57]. The limited change in expression of Ape1 observed here was consistent with published findings [57], retaining 75% of its proliferating cell level after differentiation (Figure 2.1B).

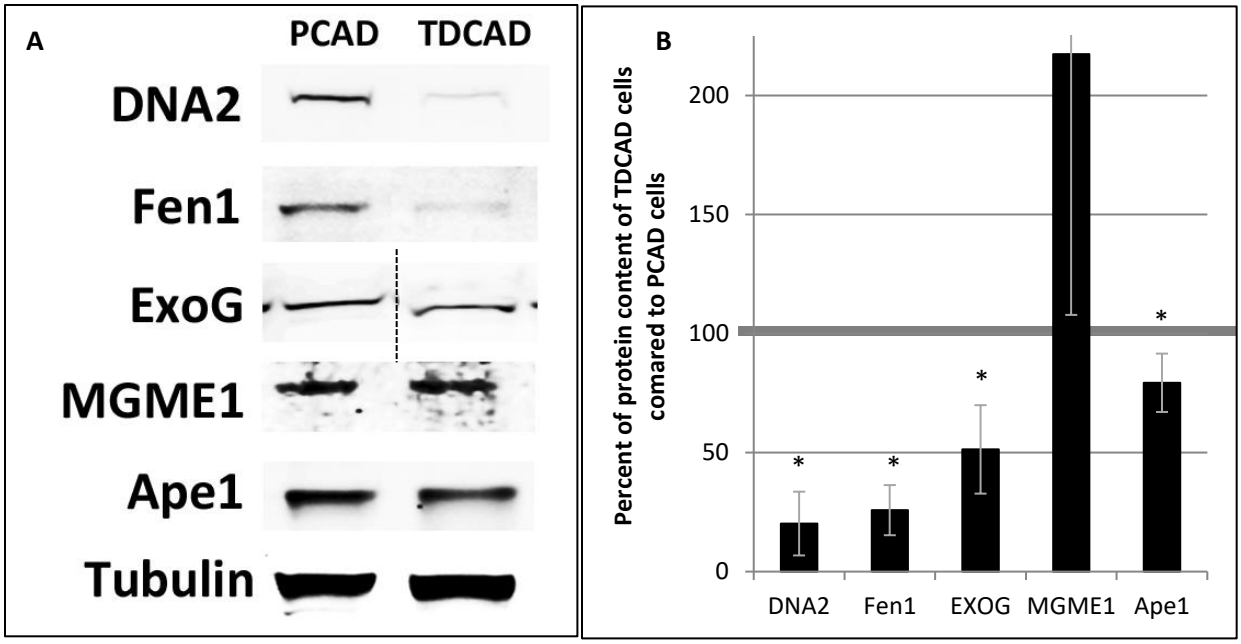

Figure 2.1. Expression of endonucleases upon differentiation. A. Western blot of PCAD and TDCAD whole-cell extracts with 25 µg of protein loaded in each lane. Protein names on left indicate the antibody specificity. The proteins were not probed for on the same blot, but representative examples for each blot are shown. The line between the ExoG bands indicates removal of an irrelevant lane. B. Quantification of 3 independent experiments by Image Studio program. Each protein was normalized to tubulin as a loading control. PCAD cells protein level for each protein was set to 100%. The TDCAD cell protein level is presented as a percent of the PCAD cell level. Error bars indicate standard deviation. * denotes where the $p<0.05$ between PCAD and TDCAD cells measured by the student's t test.

Since MGME1 and ExoG are mitochondria-specific, their continued expression in whole cell extracts is expected to reflect their expression in mitochondria. However, the immunoblotting gave no information on the localization of Fen1 and DNA2 after differentiation. These proteins may be down-regulated across the whole cell, but still localized to the mitochondria. In order to answer this question, mitochondria were isolated from the cell and probed for protein levels. Thus far, the measurement has been accomplished for Fen1 (Figure 2.2). MGME1 and ExoG are similar in size to Fen1 and could not be probed simultaneously.

While purifying the mitochondria, aliquots were taken for the nuclear and cytosolic portions of the cell. It is important to note that these are not purified fractions, as evidenced by the significant portion of complex I still present in them (Figure 2.2A). Fen1 present in the nuclear and cytosolic lanes of the western blot likely results from to mitochondria or unbroken cell in these aliquots. Failure to separate mitochondria from the nuclear and cytosolic fractions means that only ~50% of the total mitochondria are in the mitochondrial fraction.

Consistent with the data in Figure 2.1, Fen1 was more abundant in the PCAD than in the TDCAD nuclear aliquot. Tubulin, lamin, and complex I were probed as controls for the cytosolic, nuclear, and mitochondrial fractions, respectively. Quantification of band density for Fen1 is presented as a fraction of total cellular Fen1 (Figure 2.2B). In this analysis, Fen1 in the mitochondria of proliferating cells was 4% of the total, while in mitochondria of differentiated cells it was 7% of the total. However, since the total amount of Fen1 in TDCAD is one fourth of that in PCAD cells (Figure 2.1), this indicates that mitochondrial Fen1 in TDCAD cells was about 50% of that in PCAD cell mitochondria.

This quantification did not include normalization to complex I due to changes in complex I expression between experiments. In two experiments of the three immunoblots, complex I was down-regulated after differentiation (Figure 2.2D). Down-regulation of complex I contrasts with results from PC12 neuronal cells, in which components of the electron transport chain were upregulated after differentiation [75]. Further replicates of this experiment should clarify the result.

Of note, lamin was probed for in this blot as the nuclear control, but, in other blots, DNA polymerase β was probed as a nuclear control. Due to new evidence that DNA polymerase β is localized to the mitochondria [42], it is no longer an appropriate negative control for mitochondria. However, I did not detect significant expression of DNA polymerase β in the mitochondria of the CAD cells (Figure 2.3).

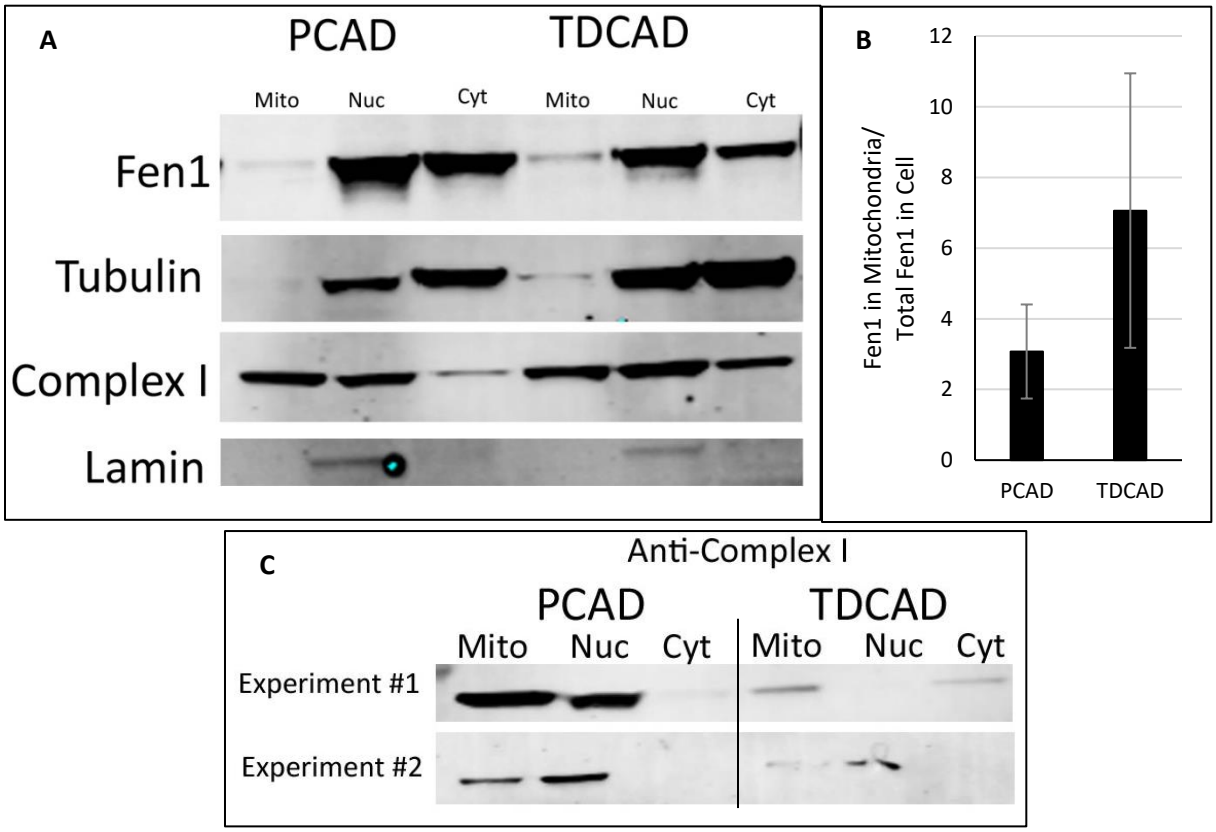

Figure 2.2. Mitochondrial expression of Fen1 after differentiation. A. Western blot of mitochondrial (Mito), nuclear (Nuc), and cytosolic (Cyt) fractions of PCAD and TDCAD cells. Proteins names on left indicate antibody specificity. Into each well was loaded 25 µg of protein. B. Amount of Fen1 in mitochondrial fractions from A, relative to total amount of Fen1 for each cell type. Quantification is of 3 biological replicates in Image Studio program. Error bars indicate standard deviations. There is no significant difference between PCAD and TDCAD Fen1 expression in mitochondria according to student's t test. C. Two western blots of mitochondrial extracts probed for complex 1 in which complex I is not detected as abundantly in TDCAD cells compared to PCAD cells.

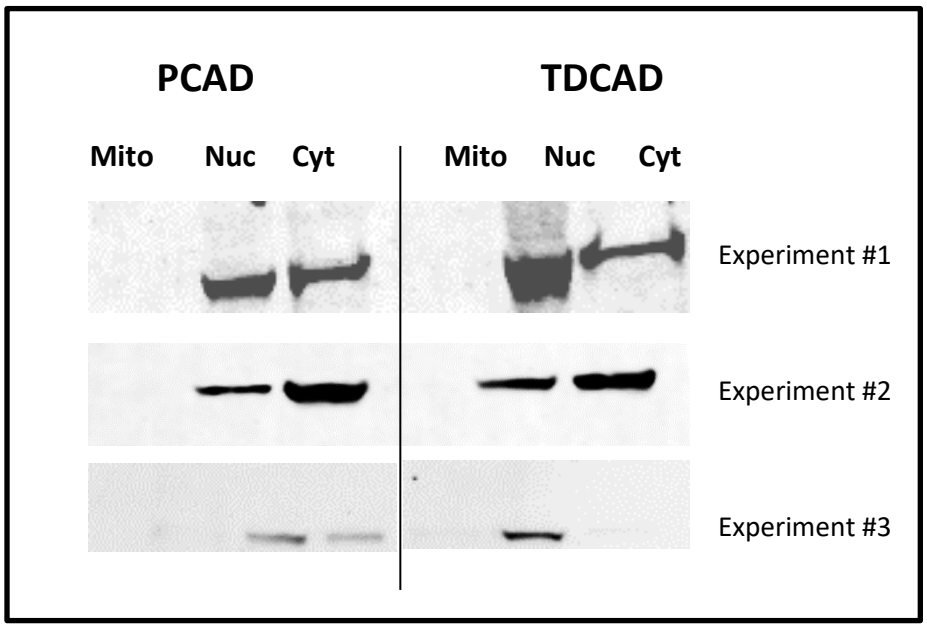

Figure 2.3. Blotting for DNA polymerase β in mitochondrial extracts. Western blots of mitochondrial (Mito), nuclear (Nuc), and cytosolic (Cyt) fractions of PCAD and TDCAD cells probed for DNA polymerase β. Into each well was loaded 25 μg of protein. Compared with nuclear and cytosolic fractions, the mitochondria have negligible expression of DNA polymerase β. Three biological replicates are shown.

The localization of Fen1 was further investigated by immunofluorescence. PCAD and TDCAD cells were labeled with Mitotracker Red to identify the mitochondria and Fen1 was labeled with a primary antibody for Fen1 and a secondary antibody against FITC. In PCAD cells, Fen1 was expressed in both the nucleus and in the mitochondria, and the protein was also detected in the cytosol (Figure 2.4A). After differentiation, Fen1 was no longer localized to the nucleus, but the observed mitochondrial and cytosolic expression remained (Figure 2.4B). Figure 2.4 also displays the morphological changes in the CAD cells resulting from differentiation. PCAD cells have a single, short dendritic process, whereas differentiated CAD cells display many long dendritic processes characteristic of neurons [74]. Data analysis

indicated that PCAD cells and TDCAD cells have nearly equal distributions of Fen1 in their mitochondria (Figure 2.4C).

Cell-by-cell quantification was performed on the immunofluorescence images by first applying a threshold to the image to remove background fluorescence (Figure 2.5). Then a region including the mitochondria of one cell was selected and the average Fen1 fluorescence intensity within the mitochondria was measured. The average intensity of Fen1 in the mitochondria was then divided by the cell area. This resulted in numbers ranging from 0.0001 to 0.009. The average intensities per cell were then binned into intervals of 0.00039 (Figure 2.4C).

A

PCAD

Fen1 **Mitochondria** **Merge**

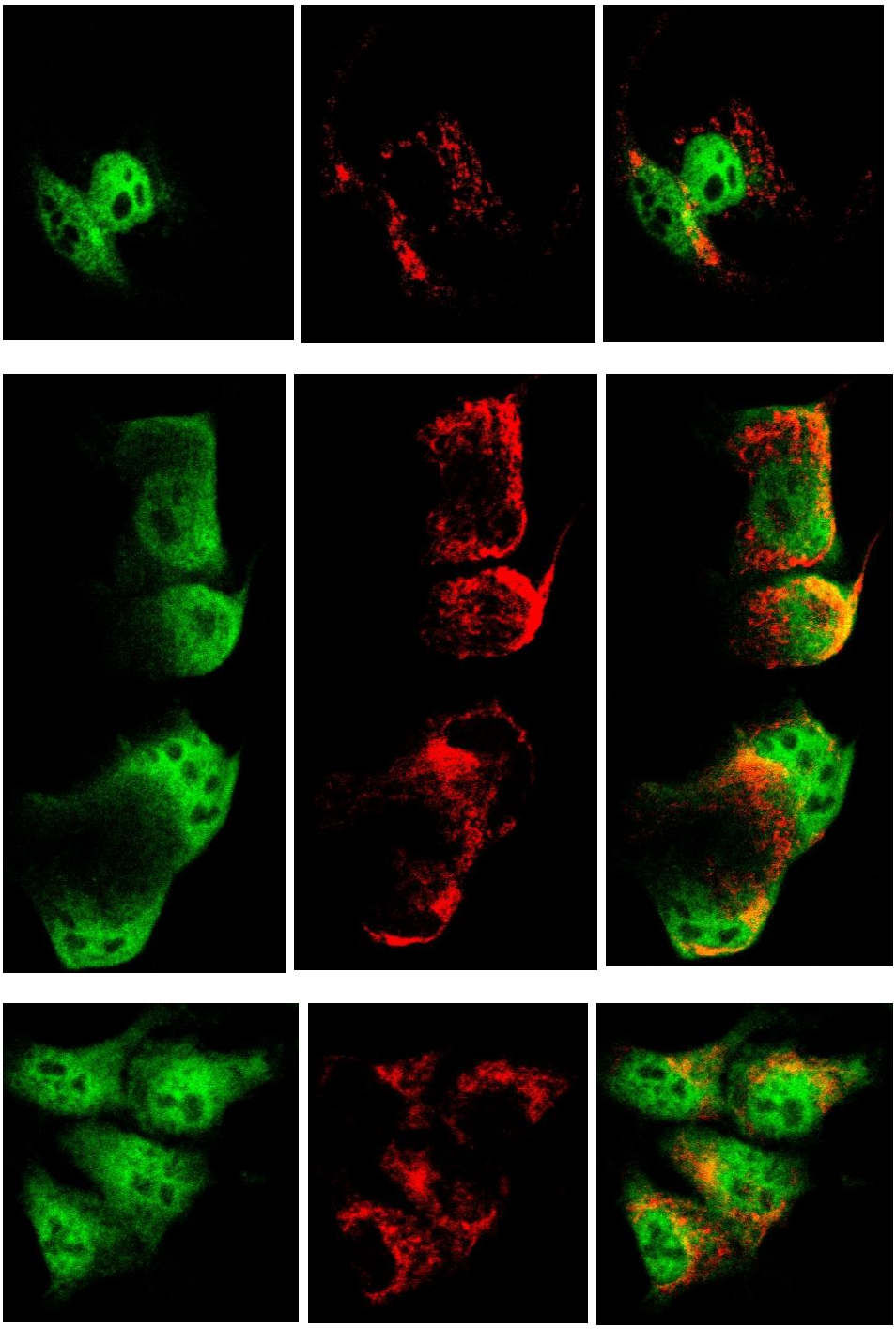

B

TDCAD

Fen1 **Mitochondria** **Merge**

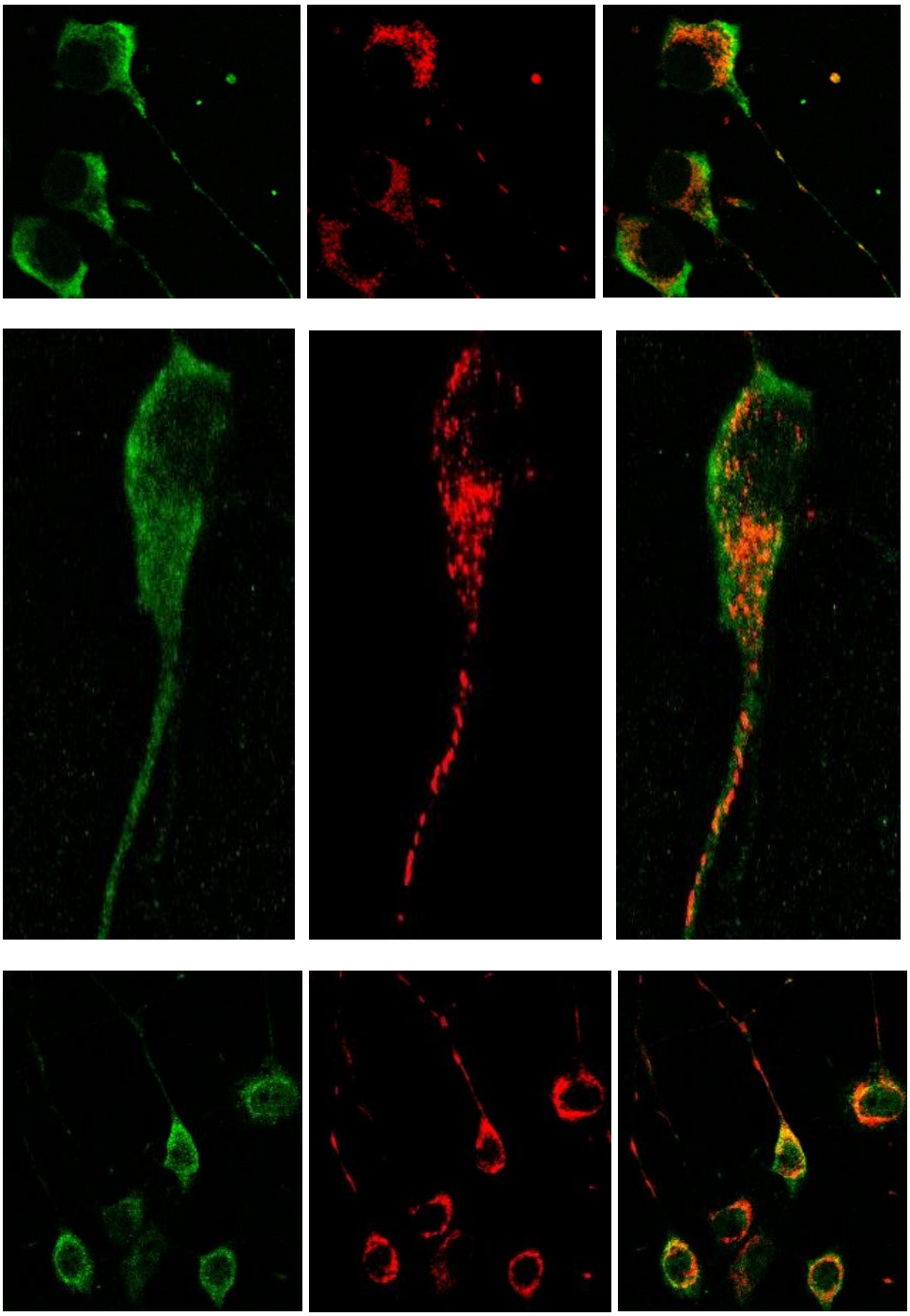

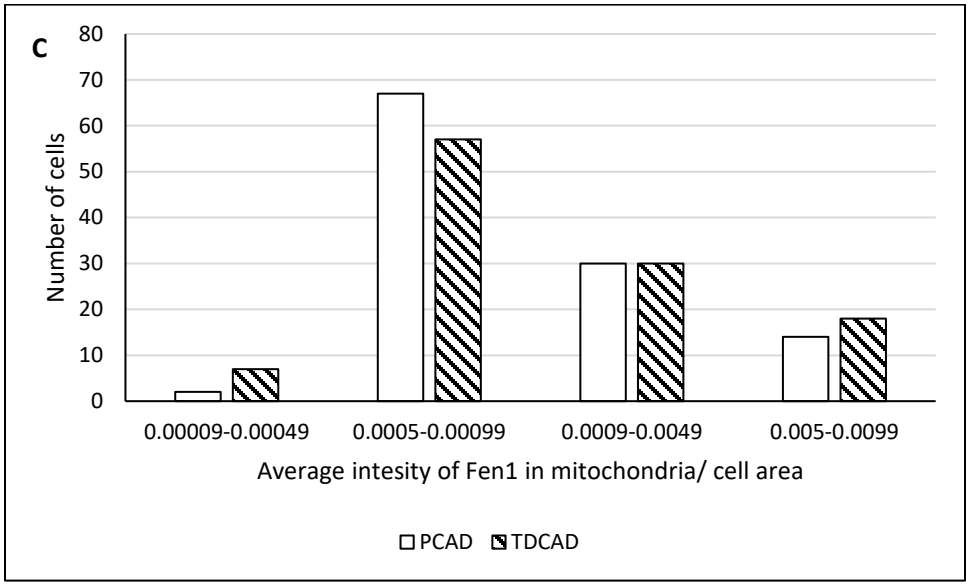

Figure 2.4. Fen1 expression measured by immunofluorescence. Cells were incubated with Mitotracker Red, then fixed with 4% PFA and labeled with a primary antibody against Fen1 and a secondary antibody tagged with FITC. Representative examples are shown of flattened Z-stack images for A. PCAD and B. TDCAD. C. Quantification of Fen1 signal from 113 cells of each type. The resulting values were binned based on the average intensity of mitochondrial Fen1 per cell.

1. One mitochondrial slice of Z-stack

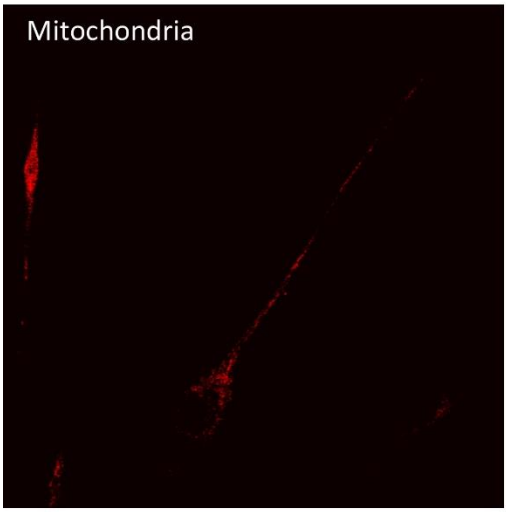

2. Theshold image

3. Select all positive pixels

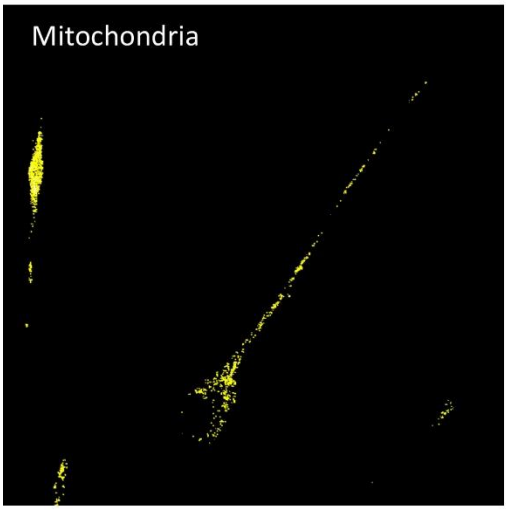

4. Move selection to Fen1 channel

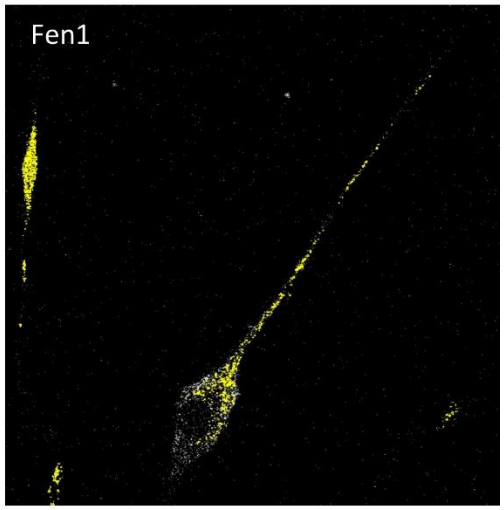

5. Copy and past selection to a new image

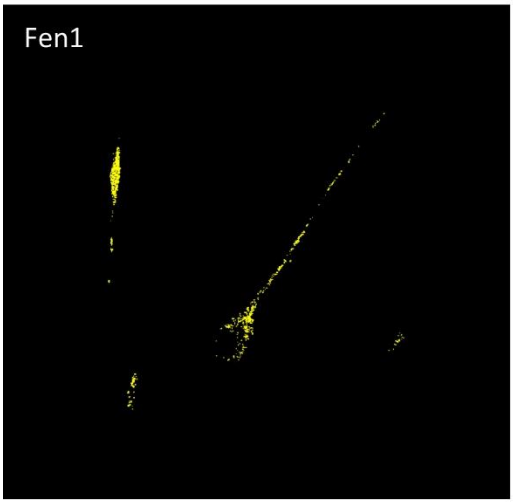

6. Select around one cells and quantify

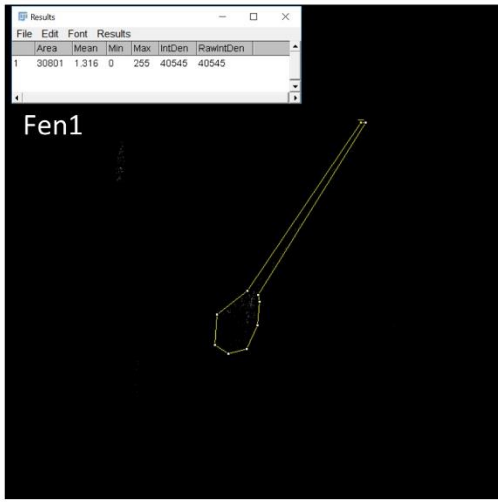

Figure 2.5. Schematic of immunofluorescence quantification. Images were quantified using the Image J program with the following steps. 1. A single mitochondrial Z-stack was selected in which the mitochondria were abundant. 2. The image was thresholded to remove background. The automatic threshold of the program was applied to every slice of the image. The automatic threshold is equal to the average of the mean background intensity and mean object intensity. 3. All positive pixels were selected by pressing Edit>Selection>Create Selection then Edit>Selection>Invert Selection. 4. The selection was moved to the Fen1 channel. 5. The selection was copied and pasted into a new image to remove any other cells in the image. 6. The area and density of the selection were measured.

2.3.2 Enzyme Activity

Along with measurements of protein localization, protein activity is important for assessing function. To generate a "flap" substrate, three synthetic oligonucleotides were annealed together to yield a molecule (Figure 2.6). The substrate was labeled with TAMRA (5-carboxytetramethylrhodamine) on the 5' end of the displaced strand to allow its detection after excision (Figure 2.6). Fen1 cleavage generates a 35-nucleotide flap containing the label[44].

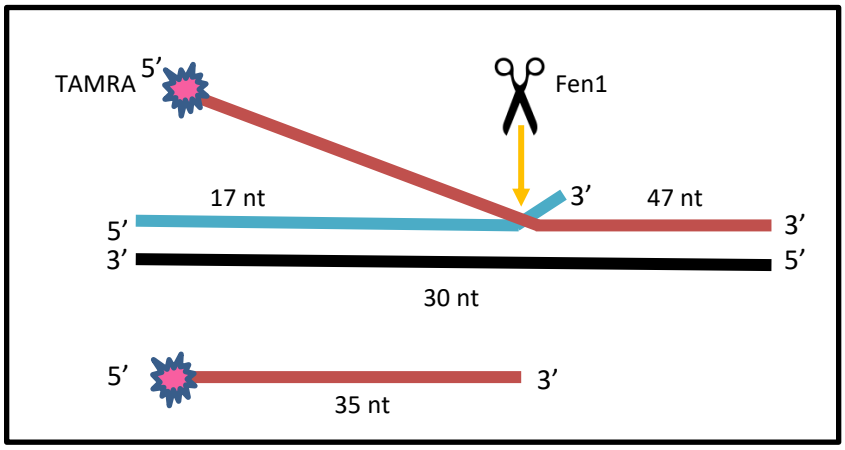

Figure 2.6. "Flap" substrate structure. This substrate was made by hybridizing three oligonucleotides, the lengths of which are labeled in nucleotides (nt). When cleaved by Fen1, a 35-nt product is generated. The single-stranded/double-stranded DNA junction is fixed, not mobile.

CAD cell extracts were made in a lysis buffer containing a non-ionic detergent in order to prevent protein denaturation, and reactions were incubated for 30 minutes (see Chapter 6: Materials and methods). The reaction conditions were modeled from the literature [43,69]. Increasing amounts of whole-cell extract from PCAD or TDCAD cells were incubated with the flap substrate; recombinant Fen1 was included as a positive control. The reactions with PCAD cell extracts reached a plateau of 50-60% cleavage that was not increased with proteins amounts ≥ 0.1 μg (Figure 2.7A). TDCAD cell extracts gave increasing amounts of product as the amount of extract was increased from 0.1 to 0.5 μg, but no further increase with 1 μg (Figure 2.7B). Since purified Fen1 gave nearly complete digestion, the plateau reached by the cell extracts does not appear to be due to defects in the substrate.

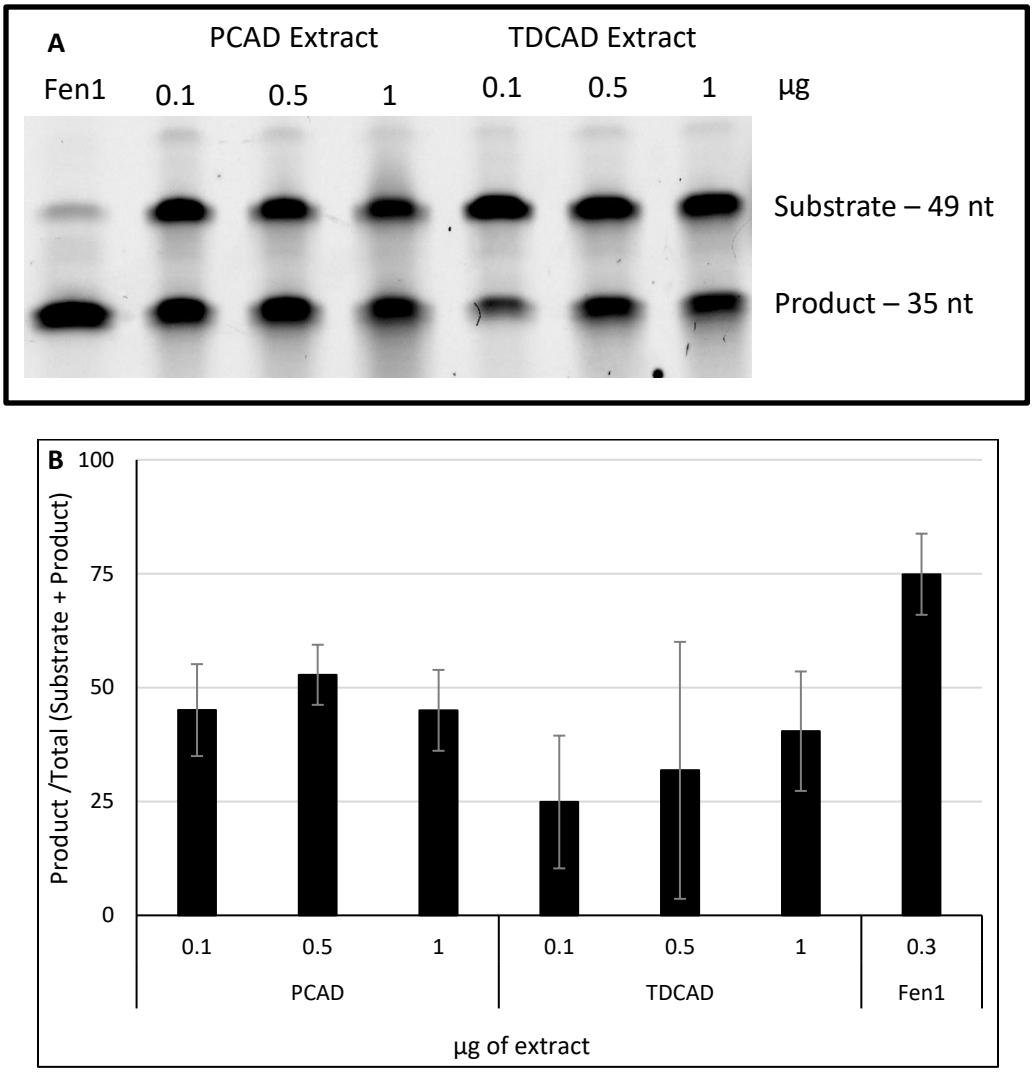

Figure 2.7. Flap excision activity in PCAD and TDCAD whole cell extracts. A. PCAD and TDCAD cells were incubated at increasing concentrations (0.1, 05, 1 µg) with the flap substrate (1 pmol) for 30 minutes at 37°C, then run on a 16% acrylamide-urea gel. Purified Fen1 (51 pmol) was incubated with 1 pmol of substrate for 30 minutes. A representative example is shown. B. Quantification of the 35 nt product in three independent experiments with Image J program. Error bars indicate standard deviation (n=3), except the 0.5 µg concentration that was performed twice.

I next assessed the flap excision activity in mitochondrial extracts. Protein extracts from isolated mitochondria were made for this purpose. The incubation conditions were the same as

for the whole-cell extracts, except instead of increasing the concentration of extract, the reaction was incubated for increasing amounts of time (Figure 2.8A). Increasing time points were used because, during initial experiments, mitochondrial extracts did not produce any product after 30 minutes with increasing concentrations of extract. However, this was resolved with optimization, as seen in the PCAD mitochondrial extracts at the 30 minute time-point. Both the PCAD and TDCAD mitochondria generated more product with time, but the PCAD mitochondrial extracts had more flap excision activity than the TDCAD mitochondrial extracts at every time point (Figure 2.8B).

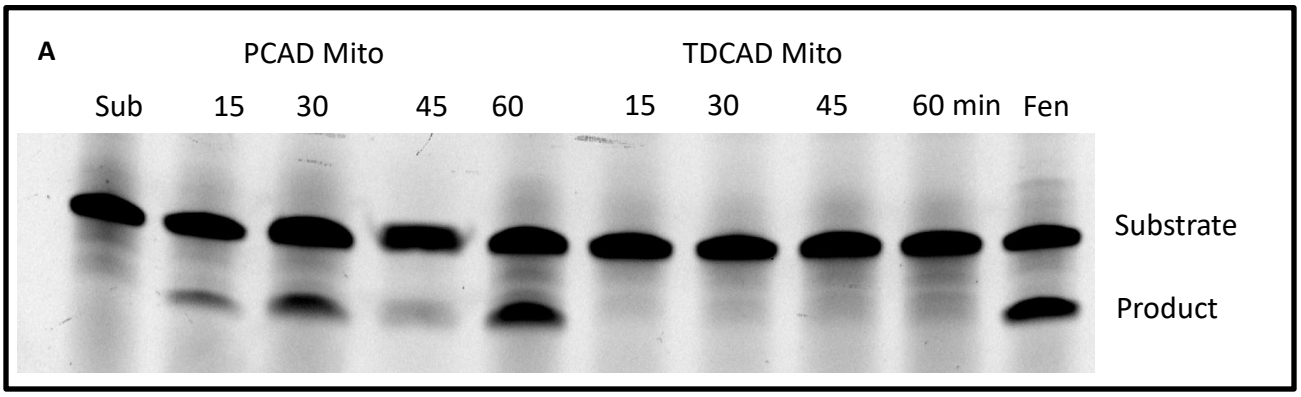

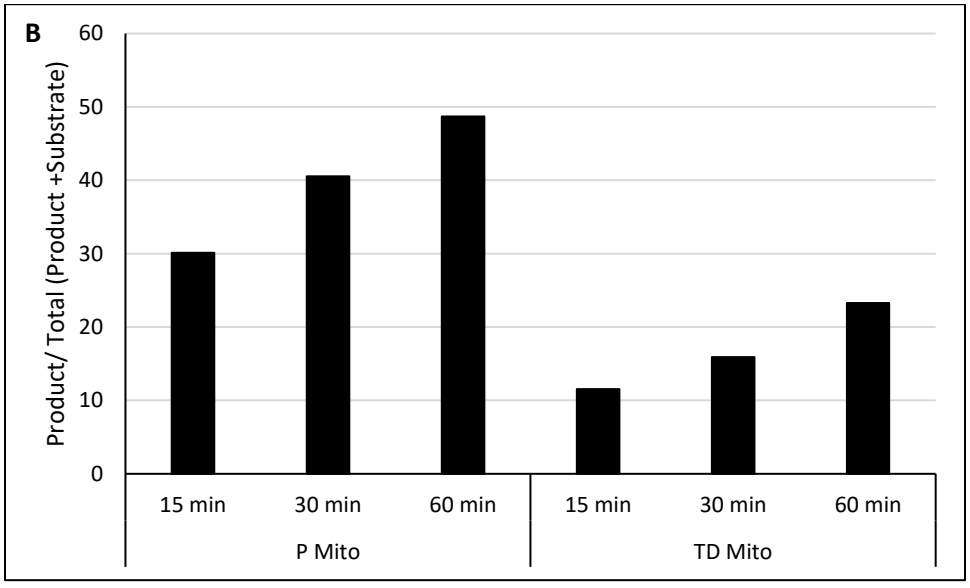

Figure 2.8. Flap excision activity of PCAD and TDCAD in mitochondrial extracts. A. A representative gel from a mitochondrial flap excision assay. PCAD or TDCAD mitochondrial extracts (0.5 μg) were incubated for increasing amounts of time (15, 30, 60 minutes) with the flap substrate (1 pmol) at 37°C, then run on a 16% polyacrylamide-urea gel. Purified Fen1 (51 nmol) was incubated for 30 minutes with 1 pmol substrate. The PCAD 45 minute time point was partially lost when loading the gel. B. Quantification of the experiments shown above. After background was subtracted, the product was divided by the total DNA (product + substrate). Error bars are not included because this experiment was completed only once.

2.3.3 Knockdown by siRNA

A key goal is to understand the role of the flap endonucleases in mitochondrial BER. To address this issue, mitochondrial endonucleases MGME1 and ExoG will be targeted for knockdown by siRNA. Since these proteins are mitochondria-specific, nuclear DNA repair should not be affected by their depletion. PCAD cells were incubated with a scrambled siRNA tagged with a fluorophore, and after 48 hours the cells were imaged in phase contrast and fluorescence ~500 nm (Figure 2.9). Transfection was successful in less than 50% of the PCAD cells. Since less than half of the cells were successfully transfected, assays which measure the entire population of cells will not give meaningful results. However, “cell-cased” measurements made with immunofluorescence would allow for transfected cells to be investigated without cell sorting. Cells may be marked for transfection and a protein of interest. For example, mitochondrial single strand binding protein (mtSSB) may be more prominent in mitochondria with uncleaved DNA flaps [45], as would be expected if the depleted endonuclease was necessary for long-patch BER. More general markers can also be investigated, such as total mtDNA content using Picogreen reagent [76], cytochrome c as a marker for apoptosis, or Parkin as a measure of mitophagy.

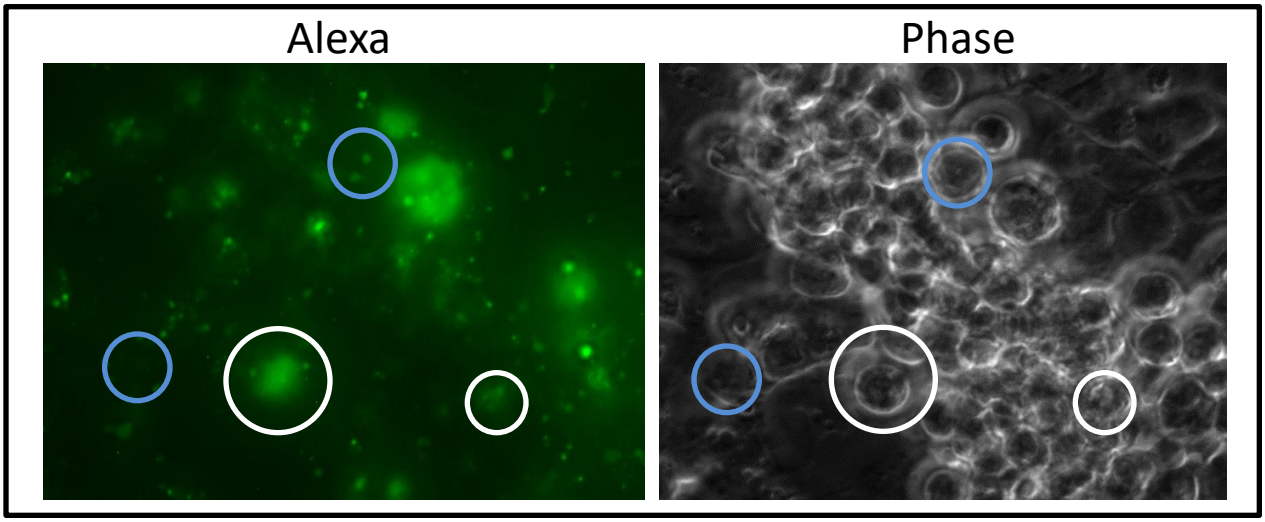

Figure 2.9. Transfection efficiency of PCAD cells. PCAD cells were incubated with Allstars Negative Control and Lipofectamine 2000 for 24 hours, then the medium was changed, and the cells were further incubated for 24 more hours at 37^{o}C. 182 PCAD cells were counted, with a representative example shown. Examples of cells scored as positive for transfection are circled in white, cells scored as negative are circles in blue.

Discussion

The results presented in this chapter are consistent with other reports of the down-regulation some DNA repair proteins and attenuated DNA repair activity upon cellular differentiation [57-59,61]. Both Fen1 and Ape1 mirror expression in differentiated SH-SY5Y cells with Ape1 modestly down-regulated and Fen1 reduced to ≤25% of previous expression in proliferating cells [57]. However, the mitochondrial levels of Fen1 show that the reduction is not as dramatic as the whole-cell level. These results are consistent with a role for Fen1 in mitochondria BER of differentiated cell mitochondria.

The slower flap excision activity in the mitochondria extracts of differentiated cells compared to the proliferating cells was not expected since the nucleases capable of flap cleavage are expressed in the differentiated cell mitochondria. However, mitochondria in differentiating cells tightly regulate their copy numbers [77,78], so perhaps with fewer mtDNA copies to repair there is less demand for flap excision activity.

There is a discrepancy in the western blot and immunofluorescence data for mitochondrial Fen1. The western blot shows that TDCAD mitochondrial Fen1 is expressed at 50% of previous expression in proliferating cell mitochondria, while the immunofluorescence shows both cell types' mitochondria at essentially equal levels. This inconsistency is likely due to differences in the assays. For example, Fen1 may bind to the outside of mitochondria [71], so some of the measurements taken with immunofluorescence may include Fen1 that is not within the mitochondria.

The down-regulation of Complex I in TDCAD mitochondria was unanticipated, but the regulation of Complex I is a dynamic process [79]. In rat tissues, Complex I is expressed differently among the tissues, with the levels in brain tissue falling below heart and muscle when subunit NDUFA9 was measured [80]. This subunit, the same I blotted against, is nuclear encoded. It is possible that changes in nuclear expression of proteins affect NDUFA9. However, the mitochondrial isolation process itself may result in degradation of complex I. The extracts were frozen for different lengths of time, as well as thawed various numbers of times. Each blot was run individually, and since there is no loading control across the entire blot, it is impossible to conclude that there is no error in the amount of protein that was loaded onto the gel. In

future experiments, mitochondrial extracts will be isolated with more consistencies to address these issues.

Overall, these data imply that non-cycling cells have the enzymes necessary to complete long-patch BER. The slower flap excision of the differentiated cell mitochondrial extracts may indicate that differentiated cell mitochondria depend more on short-patch than long-patch BER. However, there are lesions which require long-patch BER for repair, so continued function of this pathway is necessary unless the mitochondria depend upon another pathway, such as whole genome degradation.

Chapter 3

DNA Repair Capacity of Proliferating and Differentiated Cells

3.1 Abstract

Continued replication and repair of the mitochondrial genome is essential for mitochondria to function. Especially in the case of neurons, which generally do not regenerate, the mitochondria need to be replicated for the life of the organism, decades in the case of humans Failure to repair mitochondrial DNA (mtDNA) may lead to neuronal death, and most neurons will not be replaced. Therefore, the repair or clearance of damaged mtDNA is vital to prevent neurodegeneration.

In the research presented in this chapter, I establish that differentiated CAD cells have greater survival than proliferating CAD cells when challenged with the DNA damaging agents hydrogen peroxide or methyl methanesulfonate. In these experiments, differentiated CAD cells and differentiated muscle cells accumulated less mtDNA damage with these reagents than their proliferating cell progenitors. Finally, the overall rate of mtDNA repair was not significantly different between proliferating and differentiated cells. Taken together, these results indicate that neuronal cells continue to repair their mtDNA upon differentiation.

3.2 Introduction

The slower flap excision activity observed in differentiated CAD (TDCAD) cell compared to their proliferating precursors (PCAD) mitochondrial extracts implies that long-patch BER in is attenuated in the mitochondria of TDCAD cells (Chapter 2). However, continued replication and repair of the mtDNA is essential for mitochondria to function. Especially in the case of neurons, which do not regenerate, the mitochondria continue to replicate for the life of the organism [81]. Failure to repair mtDNA may lead to mitochondrial degradation and cell death, and the lost neurons are usually not replaced [82]. Therefore, repair or clearance of damaged mtDNA is vital to prevent neurodegeneration.

To address this issue, proliferating and differentiated cells were investigated for general mtDNA repair capacity. The cells were challenged with DNA damaging agents, and the presence of DNA lesions was assayed using a polymerase chain reaction (PCR) based assay. Since base excision DNA repair (BER) is the primary focus of this dissertation, agents were chosen that form DNA lesions that are repaired mainly by BER: hydrogen peroxide (H_2O_2) and methyl methanesulfonate (MMS). H_2O_2 is an oxidizing agent that generates single strand breaks, abasic residues, ring-opened derivatives of purines and pyrimidines, oxidized bases, etc [83]. MMS is an alkylating agent that reacts DNA to generate primarily with the N7 of guanine and the N3 of adenine, while generating smaller amounts of O-alkylated bases [84,85]. The lesions created by MMS are repaired primarily by the short-patch pathway of BER, while H_2O_2 generated lesions can be repaired by short-patch or long-patch BER. The long-patch BER pathway is necessary because some lesions can be repaired only by this pathway. For example, 2-deoxyribonolactone (2-dL), a C1’ oxidized AP site, forms a covalent crosslink with repair proteins during attempted

short-patch BER [64-66]. DNA-protein crosslinks are avoided in long-patch BER because DNA polymerase γ moves past the oxidized site when it adds the 2nd nucleotide.

The PCR-based assay allows analysis of the mtDNA without having to extract it from nuclear DNA [86]. Many types of lesions can slow down or block DNA polymerases [87]. Consequently, DNA with fewer lesions should be amplified more efficiently than DNA with more lesions (Figure 3.1).

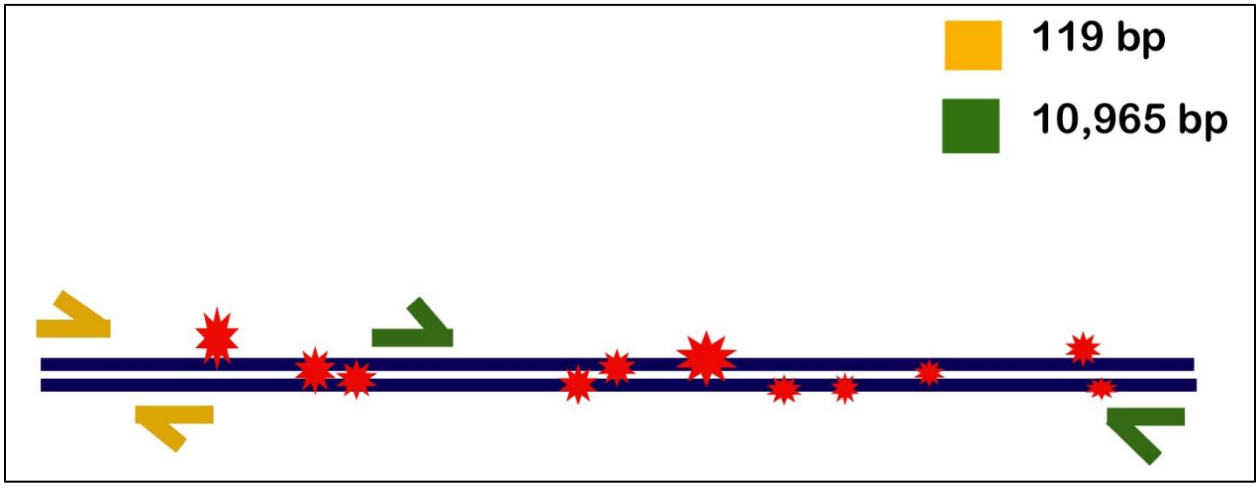

Figure 3.1. Schematic of PCR-based assay. The short PCR has primers (shown in yellow) generate a 119 base pairs (bp) product. This relatively small section of DNA is unlikely to contain many lesions. The long PCR primers (shown in green) generate a 10,965 bp product. Damage to the mtDNA is expected to be detected in this region.

The data presented in this chapter shows the mtDNA repair capacity in proliferating and differentiated CAD cells. I establish that the differentiated cells are more resistant to H_2O_2 and MMS killing them than are the proliferating cells. Additionally, differentiated CAD and mouse muscle cells accumulate less mtDNA damage than their proliferating counterparts. Finally, the overall rate of mtDNA repair between proliferating and differentiated cells was not

significantly different. Taken together, these results indicate that the general mtDNA repair capacity is not down-regulated in mitochondria upon CAD cell differentiation.

3.3 Results

3.3.1 Cell Survival

A previous study has shown that differentiated muscle cells had a greater survival than their proliferating precursors when challenge with MMS or the topoisomerase inhibitor camptothecin [61]. To investigate whether this difference also occurs in CAD cells, survival was assessed after treatment with H_2O_2 and MMS. Cell survival was measured in two way: trypan blue exclusion and 3-(4, 5-dimethylthiazolyl-2)-2, 5-diphenyltetrazolium bromide (MTT) assay were used to assess cell survival. Trypan blue is a dye excluded from living cells, but which penetrates dead or dying cells as the plasma membrane breaks down. After incubation with trypan blue, cells were scored as living (dye excluded) or dead (stained by dye). The MTT assay relies on metabolic activity to indicate viability. NAD(P)H-dependent oxidoreductase enzymes reduce the tetrazolium dye to an insoluble formazan. This reaction changes the dye from yellow to purple. The fluorescence of the cell medium was then measured in a fluorimeter.

PCAD and TDCAD cells were incubated with increasing concentrations of H_2O_2 for 30 minutes. When cell viability was assayed using the MTT reagent, it was clear than TDCAD cells survived H_2O_2 to a greater degree than PCAD cells (Figure 3.2A). With the trypan blue exclusion assay, a similar result was obtained but with greater variability for the PCAD cells (Figure 3.2B) than seen in the MTT assay (Figure 3.2A).

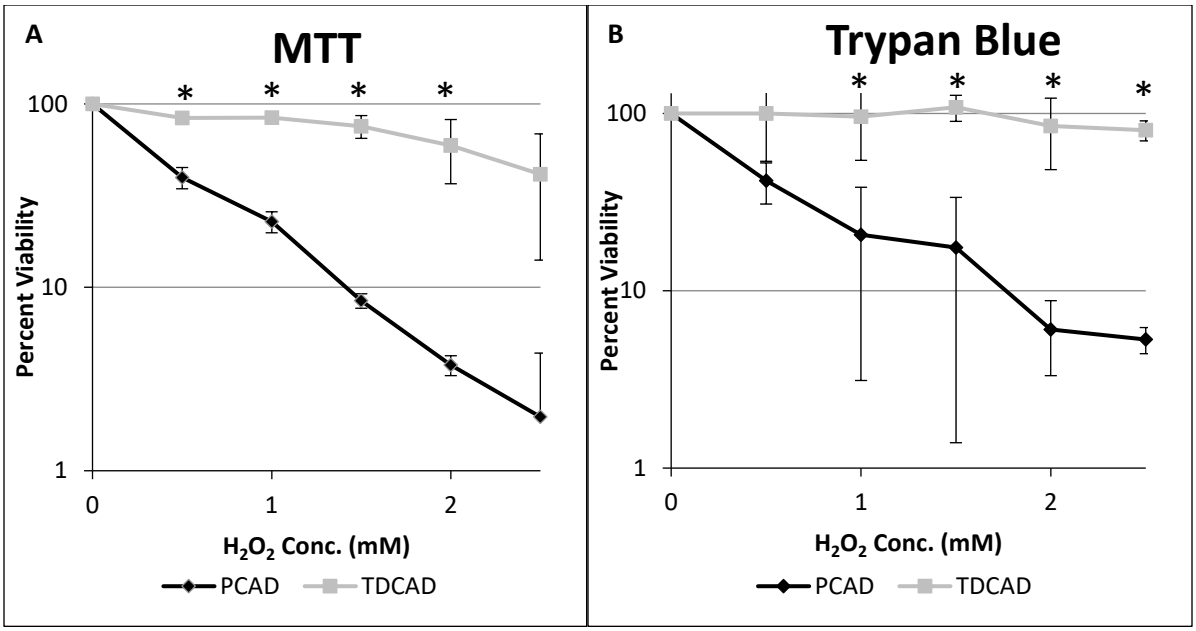

Figure 3.2. PCAD and TDCAD cell survival after treatment with H_2O_2. The cells were treated with H_2O_2 at the indicated concentration for 30 minutes, then allowed to recover in fresh medium for 24 hours before cell viability was measured. Cell survival was assayed with either A. MTT reagent or B. trypan blue dye. * denotes p>0.5 between PCAD and TDCAD as measured by student's t test (n=3).

The survival results for cells treated with MMS were less striking than were those seen with H_2O_2. The TDCAD cells did not show a greater survival than the PCAD cells for MTT (Figure 3.3A) and trypan blue due (Figure 3.3B). The TDCAD cells appear to be more resistant to oxidative damage than they are to alkylating damage at the levels generated in these experiments.

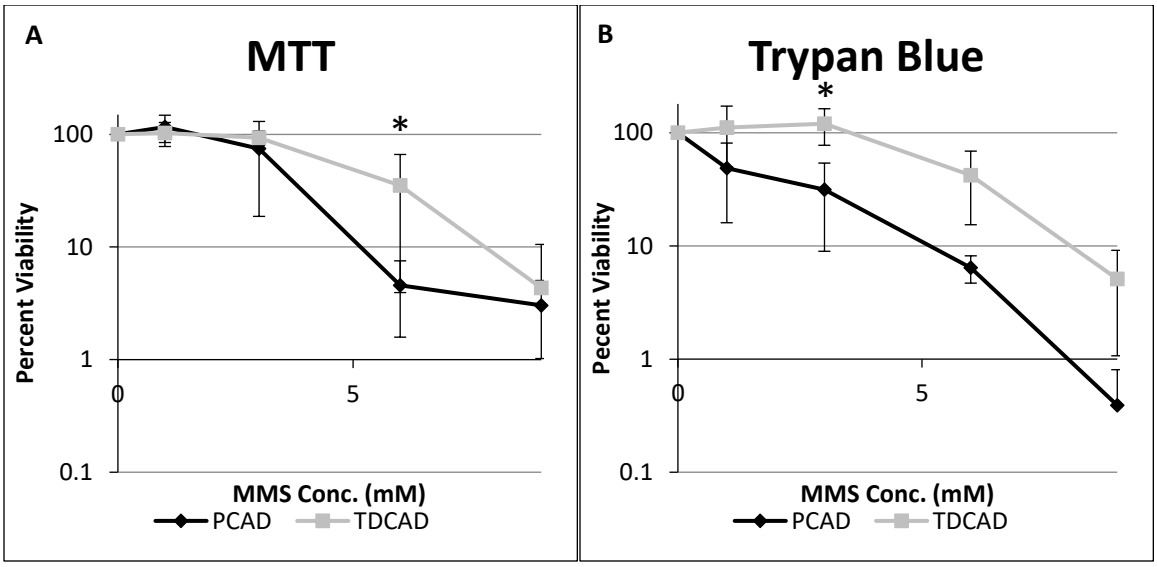

Figure 3.3. PCAD and TDCAD cell survival after incubation with MMS. Cells were treated with MMS for 30 minutes, then allowed 24 hours of recovery in fresh medium before cell viability was measured. Cell survival was assayed with either A. MTT reagent or B. trypan blue dye. * denotes p>0.5 between PCAD and TDCAD as measured by student's t test (n=3).

3.3.2 Mitochondrial DNA Damage

In order to measure mtDNA damage, incubation with the damaging agents was performed identically to the cell viability assays, with the exception that the total cellular DNA was harvested immediately at the end of the 30 minutes treatment. The PCR product generated by mtDNA in CAD cells after treatment with H_2O_2 was nearly equal across a 10 fold range of H_2O_2 concentrations (Figure 3.4A). The effect of MMS on DNA integrity paralleled the cell viability results, with increasing DNA damage at increasing doses (Figure 3.4B). Only after treatment with MMS did the differentiated cells produced more PCR product than the proliferating cells at the same dose of damaging agent.

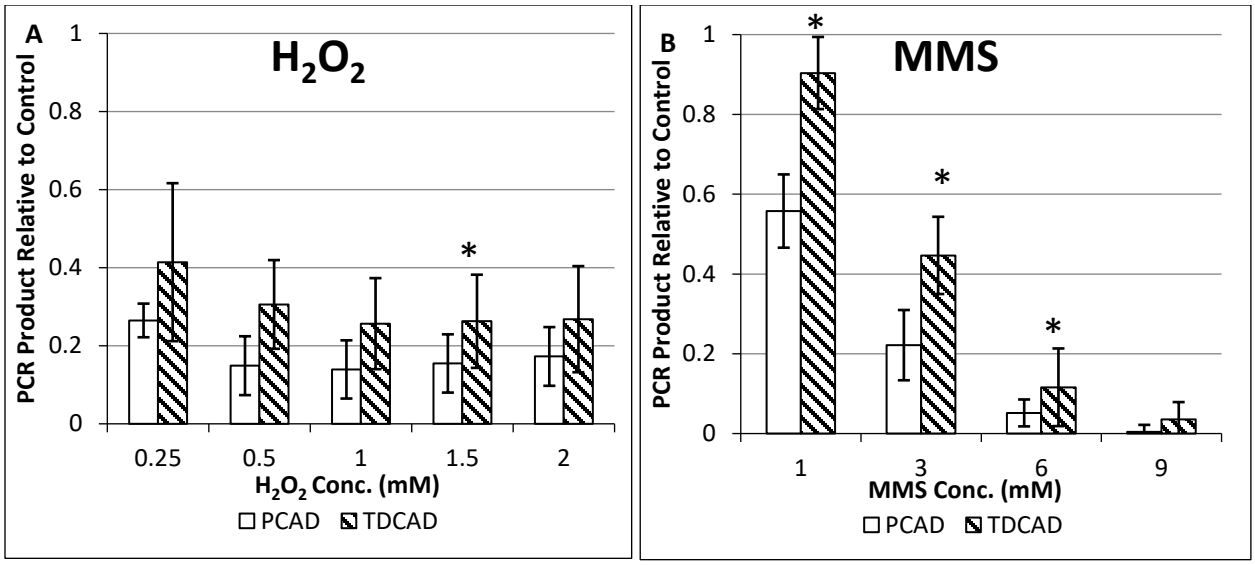

Figure 3.4. Mitochondrial DNA damage in TDCAD and PCAD mitochondria after treatment with H_2O_2 or MMS. The cells were treated for 30 minutes with A. H_2O_2 or B. MMS. Cells were lysed immediately after the treatment, and the DNA was extracted for PCR. Results from treated cells were normalized to results from untreated cells and the control was set to 1. The error bars indicate standard deviations. * denotes p>0.5 between PCAD and TDCAD cell mtDNA as measured by student's t test (n=3).

Nuclear DNA damage was also assessed in response to H_2O_2 (Figure 3.5). One advantage of the PCR assay is the ability to measure multiple genes from the DNA samples. However, the nuclear assay did not include a short PCR for normalization because the nuclear accounts for most of the total DNA quantification. Despite the evidence for mtDNA damage, there was no detectable damage in either the PCAD or TDCAD cells. Unfortunately, the error in this experiment was too large to draw any conclusions in comparison of the cell types. For this reason, and the focus of the dissertation on mitochondria and mtDNA, nuclear DNA damage was not assessed in the other samples from this data set.

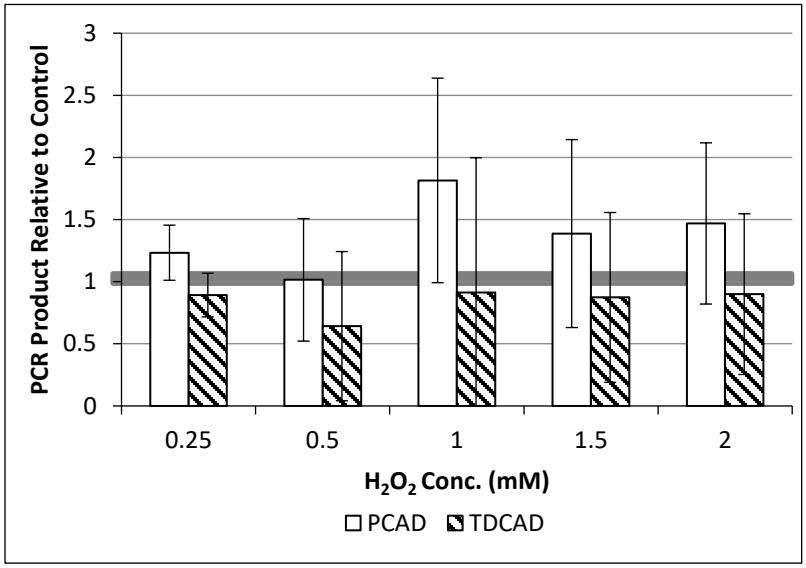

Figure 3.5. Nuclear DNA of CAD cells after incubation with H_2O_2. The same DNA samples used to measure mtDNA damage in Figure 3.4 were assessed with nuclear DNA specific primers. Cells were treated for 30 minutes with A. H_2O_2 or B. MMS. Cells were lysed immediately after the treatment, and the DNA was extracted for PCR. Results from treated cells were normalized to results from untreated cells and the control was set to 1. The error bars indicate standard deviation (n=3).

In addition to the CAD cells, muscle cells were cultured for these experiments by collaborators Prof. Eugena Dogliotti and Dr. Paula Fortini (Istituto Superiore di Sanita, Rome, Italy). Similar to neurons, muscles undergo mitochondria-dependent degeneration with age [88]. Mitochondrial volume as well as mtDNA copy number decrease in skeletal muscle with age [89].

Dr. Fortini extracted muscle cells from mice and grew them in culture, either as myoblasts (P-Muscle), or differentiated into myotubes (TD-Muscle). She treated the muscle

cells with H_2O_2 or MMS, then shipped the frozen cell pellets to us. I extracted the DNA from the pellets in the same manner as I did for the CAD cells.

When challenged with increasing concentrations of H_2O_2, the P-Muscle cells had more detectable mtDNA damage than did the TD-Muscle cells from concentrations ≥0.25 mM H_2O_2 (Figure 3.6A). After treatment with MMS, P-Muscle and TD-Muscle cells showed increasing levels of mtDNA damage with increasing concentrations of damaging agents, but not with a significant difference from one another. (Figure 6B). These results contrast with those seen in CAD cells, which showed a significant difference for MMS-induced mtDNA damage and no significant difference for H_2O_2 (Figure 3.4).

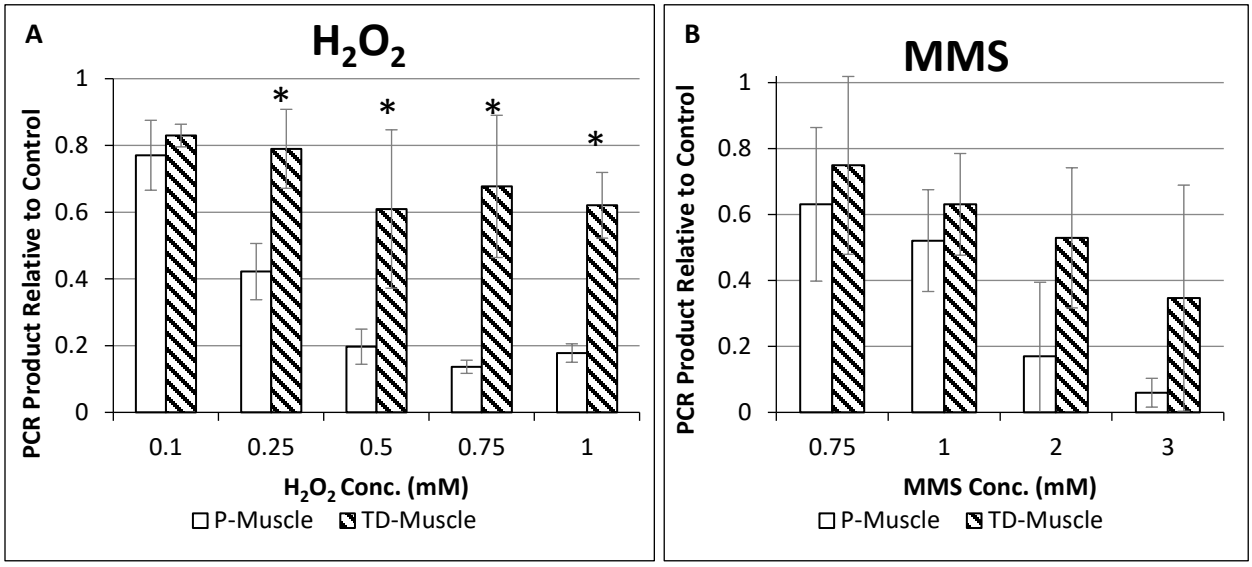

Figure 3.6. P-Muscle and TD-Muscles cells mtDNA damage after treatment with H_2O_2 and MMS. Cells were treated for 1 hour with A. H_2O_2 or B. MMS. Immediately after the treatment, cells were collected and frozen. Cell pellets were later lysed, and the DNA was extracted for PCR. Results from treated cells were normalized to results from untreated cells and the control was set to 1. The error bars indicate standard deviation (n=3). A * denoted p>0.5 between PCAD and TDCAD as measured by student's t test.

Mitochondrial DNA Repair

The previous experiments gave no information on the rate of mtDNA repair. To measure repair rates, CAD cells were treated with a single dose of H_2O_2 or MMS, and allowed to recover over time: 1.5 mM for H_2O_2 (Figure 3.7A) or 6 mM for MMS (Figure 3.7B). At these doses, mtDNA damage was ≥70% of the control, which allowed repair of the mtDNA to be observed. Recovery times up to 4 hours were employed initially to follow the kinetics of DNA repair. After treatment with either DNA-damaging agent, the majority of repair had happened by the 2h time point. Furthermore, in every condition except for the PCAD cells treated with H_2O_2, the repair lever never reached 100% instead plateauing around 50%. Unresolved mtDNA damage may be due to a failure to ligate the DNA, the last step of repair (Figure 1.2), although DNA ligase III is only modestly down-regulated after differentiation (~70%) [57,59]. Although, after treatment with MMS, both cell types failed to repair the mtDNA completely (Figure 3.7B).

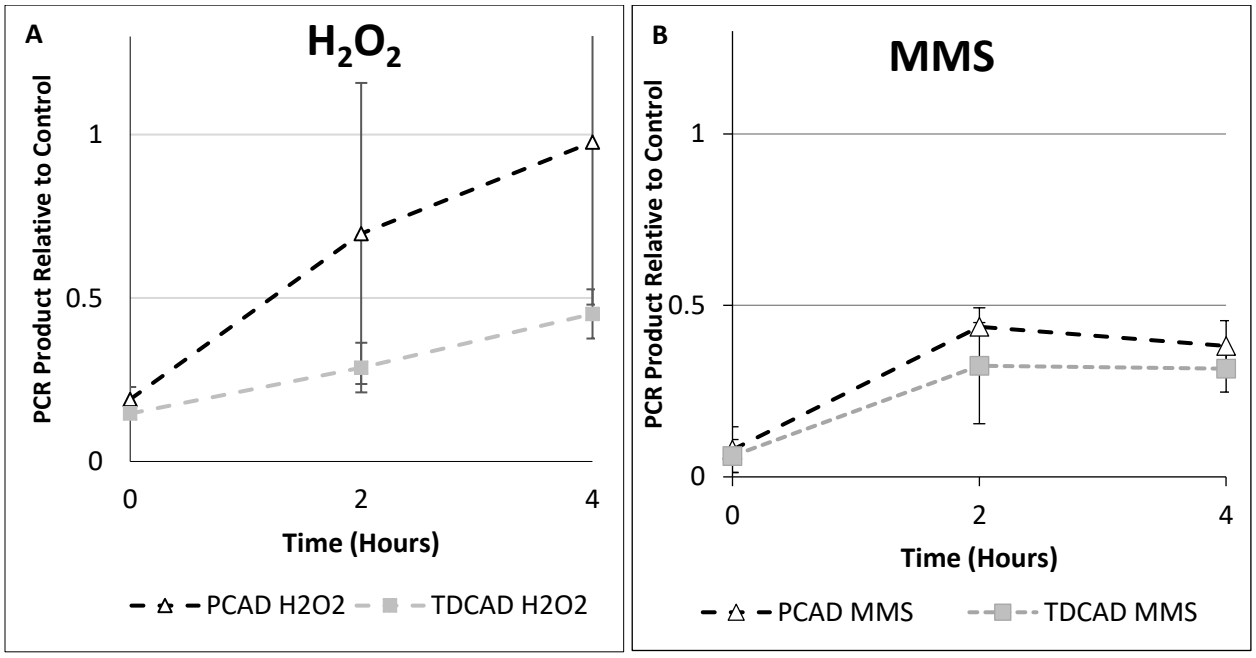

Figure 3.7. Repair of mtDNA by PCAD and TDCAD cells up to 4 hours. PCAD and TDCAD cells were challenged with 1.5 mM H_2O_2 or 6 mM MMS for 30 minutes, then allowed to recover in fresh medium for up to 4 hours. Time 0 is the start of the recovery phase. Results from treated cells were normalized to results from untreated cells and the control was set to 1. The error bars indicate standard deviation (n=3).

To get a more specific picture of the mtDNA repair kinetics, time points were taken in 15 minute intervals over an hour recovery period. This experiment has been done only with H_2O_2 at this time. The cells were challenged with 0.5 mM H_2O_2, rather than 1.5 mM H_2O_2, because the mtDNA damage was similar for PCAD and TDCAD at this concentration (Figure 3.5). Overall, there was no striking difference between the repair rates of the two cell types. However, repair does not appear to begin in earnest until the 30 minute time point. In future, time points will begin at 30 minutes and continue past 1 hour.

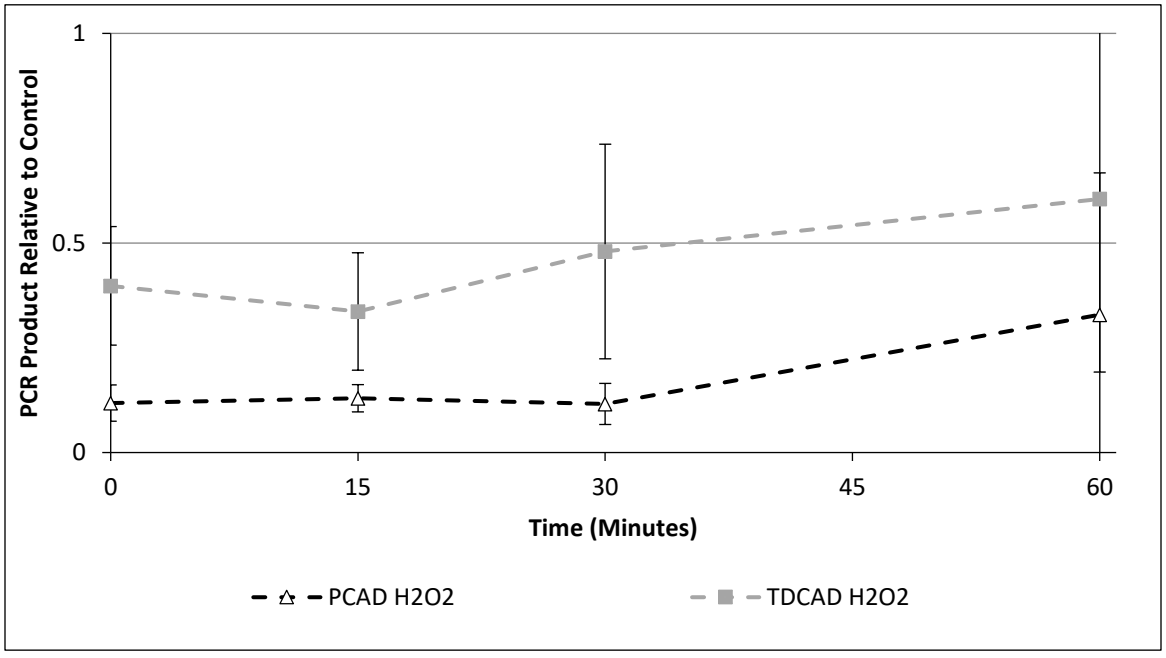

Figure 3.8. Repair of mtDNA by PCAD and TDCAD cells up to 4 hours up to 1 hour. PCAD and TDCAD cells were challenged with 0.5 mM H_2O_2 or 6 mM MMS for 30 minutes, then allowed to recover in fresh medium for up 1 hour. Time 0 is the end of the 30 minute treatment. Time points were taken by lysing cells and extracting DNA. Results from treated cells were

normalized to results from untreated cells and the control was set to 1. The error bars indicate standard deviation (n=3).

3.4 Discussion

The goal of the research presented in this chapter was to assess mtDNA repair capacity between PCAD and TDCAD cells. I present evidence that the mtDNA of differentiated CAD cells is protected somehow from accumulating some DNA lesions when compared to the mtDNA of proliferating cells after treatment with MMS. Similarly, differentiated mouse muscle cells accumulated fewer lesions than proliferating muscle cells after treatment with H_2O_2. This protective effect was seen in both CAD and mouse muscle cells, so it may be that this is a general phenomenon of differentiated cell mitochondria. It is possible that the DNA damaging agents are not causing as many lesions to the differentiated cell mtDNA.

In response to H_2O_2 and MMS, the muscle and neuronal cells responded differently (Figure 3.4 and 3.6). Both neuronal and muscles cells had less detectable mtDNA damage in the differentiated cells, but for neurons the trend was more obvious with treatment of MMS and with muscles it is significant with H_2O_2. The differences in mtDNA damage of the cells may be related to the DNA repair pathways on which they depend. As mentioned, MMS-induced lesions are repaired primarily by short-patch BER while H_2O_2 requires both short and long-patch BER. Chapter 2 implies that long-patch BER is slower in PCAD than TDCAD cells' mitochondria. If these cells due have attenuated long-patch BER, differentiated cells' mitochondria would be expected to be more sensitive to H_2O_2 than MMS, which appears to be the case (Figure 3.4).

Some assumptions are made when employing the PCR-based assay require which further discussion. Firstly, not all lesions will block the polymerase, and even those that do may

not consistently inhibit the polymerase. For example 8-hydroxydeoxyguanosine (8-oxo-G) is not efficiently detected by this assay, a lesion which accounts for about 10% of the DNA damage caused by H_2O_2 [90]. Furthermore, the assay does not measure all the lesions in the DNA. The polymerase can only begin transcribing the DNA at the primer. Once the polymerase encounters a blocking lesion, the remainder of the DNA will be un-transcribed. Therefore, any lesion beyond the initial blocking lesion cannot be measured. Overall, though, this remains an efficient means of measuring mtDNA damage without isolating mitochondria.

Chapter 4

Genotoxic effects of lunar soil simulants

This Chapter has been submitted as a manuscript to GeoHealth.

Title: Assessing Toxicity and Nuclear and Mitochondrial DNA Damage Caused by Exposure of Mammalian Cells to Lunar Regolith Simulant

4.1 Abstract

Previous missions to the lunar surface implicated potential dangers of lunar soil. In future explorations, astronauts may spend weeks or months on the Moon, increasing the risk of inhaling lunar dust. In an effort to understand the biological impact of lunar regolith, cell cultures derived from lung or neuronal cells were challenged with lunar soil simulants to assess cell survival and genotoxicity. Lunar soil simulants were capable of causing cell death and DNA damage in neuronal and lung cells, and freshly crushed lunar soil simulants were more effective at causing cell death and DNA damage than simulants as received from the supplier. The ability of the simulants to generate reactive oxygen species was not correlated with their cytotoxic or genotoxic affects. Furthermore, the cytotoxicity was not correlated with the accumulation of detectable DNA lesions. These results determine that lunar soil simulants are cytotoxic and genotoxic.

4.2 Introduction

4.2.1 Lunar Soil Properties

One aspect of the lunar environment that warrants more study in preparation for human exploration is the lunar regolith, or soil. Lunar soil is affected by a combination of processes that include meteorite impacts and resulting agglutination, as well as solar wind [91]. There are important differences between the lunar and terrestrial environments that affect the surface material. The Moon has no liquid component in the soil, so water-containing minerals, such as clay or mica, are not present [91]. The lack of lunar atmosphere also allows the Moon's surface to be perpetually bombarded by solar wind. This constant chemical reduction causes the lunar soil to become electrostatically charged. This charge can be so strong that the soil particles actually levitate above the lunar surface[92,93].

When astronauts visited the Moon during the Apollo missions, the lunar soil clung to spacesuits due to its electrostatic charge, and the lunar dust was tracked into the living environment by astronauts who had been exploring the lunar surface [62]. Astronaut Harrison Schmitt described his reaction to lunar dust as "lunar hay fever", including sneezing, watering eyes, and sore throat [63]. Lunar dust in the lunar exploration module represents a biological hazard to the astronauts, with particles 5-10 microns capable of accumulating in the central airways and smaller particles, 0.5-5 microns, infiltrating the alveoli [94]. The still smaller sizes of dust, 0.1 micron and below, can be transported through the olfactory bulb into the brain [95]. However, it is not known how deep into the brain lunar dust might infiltrate nor how removal might occur.

The overall geology of the Moon further affects the soil composition. The bright and dark regions on the lunar surface are the highlands and maria, respectively [96]. The maria are the result of lava flows on the Moon. In general, the maria coincide with the lowlands, but there are exceptions in which lowland areas are not covered in mare, for example the South Pole-Aitken basin [97]. The highlands are composed primarily of anorthosite, while the maria is basaltic. This means that there is variation in the mineral composition of lunar soil in different places that is accounted for in the lunar soil simulants chosen for this project.

4.2.2 Biological Effects of Lunar Soil

From terrestrial studies, we understand some of the risks of breathing toxic dust. The most relevant situations occur following occupational incidents and volcanic ash exposure. For example, people who were exposed to volcanic ash after the eruption of Mt. St. Helens in 1980 suffered acute effects including bronchitis, wheezing, and eye irritation [98]., 1983). Those with chronic lung diseases such as asthma and emphysema were disproportionately affected [98]. A recent study involving the lungs of rats exposed to ashes from Arizona lava fields exhibited chronic inflammation, septal thickening, and fibrosis [99]. Furthermore, workers in the mining industry are repeatedly exposed to dust from recently uncovered mineral deposits. A common outcome of this exposure is silicosis, a disease that develops from long-term exposure to silicate dust [100]. Silicosis is characterized by coughing and shortness of breath, caused by the silica dust particles embedded in the alveolar sacs [100].

There is also an accumulating body of evidence on the detrimental effects of particulate matter in the brain. However, due to the inaccessibility of the brain, concrete conclusions about these effects can be difficult to obtain. General inflammation is one result, as seen in the brains

of mice exposed to airborne particles which developed neuronal inflammation, including the increased expression of the inflammatory cytokines Il-1α, TNFα, and NFκB [101].

While not as well studied, damage to the DNA resulting from dust exposure is also possible. DNA damage can be both a short-term and a long-term problem. Mutations in nuclear DNA may lead to cell death or cancer, though the two are not mutually exclusive [102,103], since dying cells can signal to neighboring cells to promote cell division [104]. Limitations in the repair of mitochondrial DNA are associated with neurodegenerative disorders [27]. In an animal study, rats exposed to particles isolated from air pollution developed nuclear DNA mutations in their sperm [105]. For the human A549 lung cell line, treatment with various particulate materials caused DNA strand breaks and activated caspase-9, an enzyme released from mitochondria in a process of cell death [106].

4.2.3 Lunar Soil Simulants

Due to the scarcity of lunar soil available for research, lunar soil simulants are used as a substitute [93]. The simulants are designed to mimic various aspects of lunar soil. This project uses five lunar soil simulants and two control particulate materials (Table 4.1). The simulants in this set exemplify different types of lunar soil with distinctive compositions. For example, chemically reactive simulants are categorized here as those that generate reactive oxygen species (ROS). ROS are formed by metals exposed at surface defects in the soil particles that interact with oxygen when exposed to aqueous solution [107]. However, even some simulants selected for their physical characteristics may indirectly generate ROS in cells by upregulating the immune response after upon contact with the cells [108].

JSC-1A and the agglutinated form of JSC-1A are physical and chemical replicates of regolith from the lunar mare [109]. NU-LHT-2M and its agglutinated form are chemical replicates of regolith from the lunar highlands [110]. CSM-CLF is a chemically reactive soil intended to mirror the ability of lunar soil to generate ROS (Kaur et al., 2016). Quartz, a mineral, is included because its dust is known to cause silicosis [111]. Compared to the lunar soil simulants, quartz does not generate high concentrations of ROS in solution [112]. Anatase also produces low ROS concentration in solution and serves as a control for the physical response of the cells to particulate matter.

The experiments were performed using two cell lines. The Cath.-a-differentiated (CAD) cells were isolated from a mouse neuroblastoma [74]. CAD cells can be cultured for active proliferation or induced to differentiate in culture by serum starvation [74]. These cells allow for proliferating progenitors and terminally differentiated neurons to be compared directly. The A549 cell line was developed from a human lung carcinoma. A549 cells are used to represent lung exposure.

I present data showing that exposure to lunar soil simulants cytotoxic and DNA-damaging in both the neuronal and the lung cells lines. However, the ability of the simulants to ROS was not correlated with these cytotoxic or genotoxic effects. I also observed that freshly crushed lunar soil simulants were more effective at causing cell death and DNA damage than were the unprocessed simulants as received from the suppliers.

Table 4.1. **Characterization of lunar soil simulants**

Particulate Name	**Purpose or Emulated Location**	**Description**
JSC-1A	Low-Titanium Mare	Volcanic ash from Arizona that resembles lunar maria [109]
JSC-1A Agglutinated	Low-Titanium Mare	Treated to form glassy agglutinates [110]
NU-LHT-2M	Highland	Replicate of lunar highland basalts [110]
NU-LHT-2M Agglutinated	Highland	Treated to form glassy agglutinates [110]
CSM-CLF	Geotechnical	Developed from Colorado lava [110]
Quartz	Control Material	Little found on Moon; Known to be cytotoxic [113]
Anatase (TiO_2)	Control Material	Non-chemically reactive particulate [114]

4.3 Results

Lunar soil simulants were stored and prepared by Joel Hurowitz and Donald Hendrix at Stony Brook University (See Chapter 6 for details).

Experiments were performed on two cell lines. The cell line Cath.-a-differentiated (CAD) were cultured from a mouse neuroblastoma [74]. The cells can be grown proliferatively or differentiated in culture by serum starvation. These cells allow for proliferating progenitors and terminally differentiated neurons to be compared directly. The A549 cell line was developed from a human lung carcinoma. A549 cells are used to represent lung exposure.

4.3.1 Cell survival after treatment with lunar soil simulants

In order to understand the effect of lunar soil simulants on cell survival, viability was measured in CAD cells exposed to various materials. The cells were challenged with JSC-1A as-

received, size sorted to ≤63 μm, or JSC-1A ground to ≤10 μm and re-ground 1 hour before use. Size-sorting or grinding the simulants was employed for several reasons. Grinding the soil ensures that the average size is small enough that some particles can be engulfed by cells. Because the simulants as-received are naturally varied in size, there may be difficulty in generating consistent responses. Grinding and size-sorting produce a more uniform distribution of particle sizes. Crushing the simulants also increases their ability to generate ROS [110,112]. Moreover, in the lunar environment, the surface material is continuously subjected to micrometeor impacts [115], and crushing the soil partially simulates this physical effect.

A dose-dependent cytotoxic effect was observed for PCAD cells for each of the JSC-1A size classes, with the most significant lethality noted for particles ≤10 μm in size, which reduced cell survival to 10% at 20 mg/3.8 cm^2 (Figure 4.1A). In the differentiated cells, the ≤63 μm and ≤10 μm size classes caused similar cytotoxicity, but the as-received JSC-1A did not generate detectable cytotoxicity at doses lower than 20 mg/3.8 cm^2 (Figure 4.1B). In response to as-received JSC-1A, TDCAD cells showed greater survival than did PCAD cells at every simulant level.

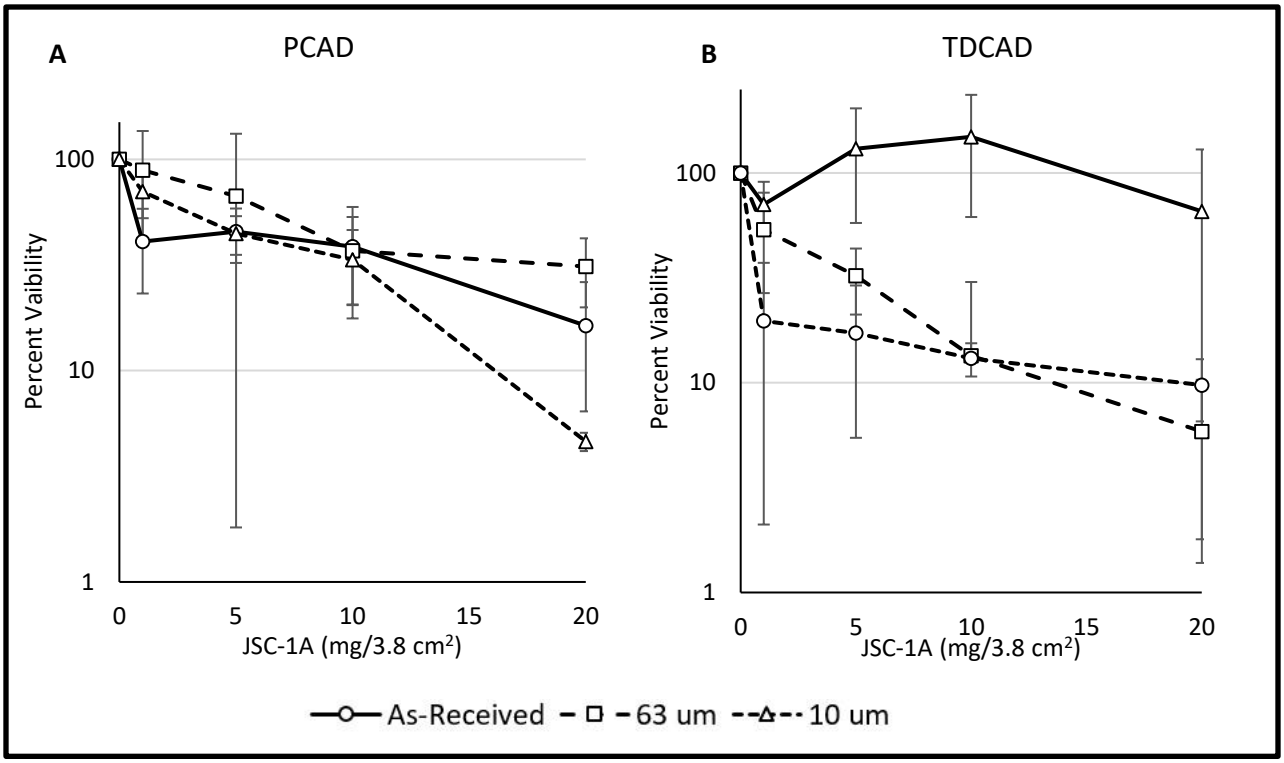

Figure 4.1. Freshly grinding JSC-1A may increase its cytotoxicity. Toxicity of JSC-1A, as-received or ground, on A. PCAD and B. TDCAD cells. Cells were treated for 1 hour with JSC-1A as-received, sieved to 63 µm or freshly ground to 10 µm. Cell viability was measured using trypan blue exclusion dye. Results are normalized to untreated cells which are set to 100%. The error bars indicate the standard deviation (N=3).

The observed cytotoxicity might be caused by either physical or chemical interaction of the cells with the simulants. To address this question, cells were treated with simulants that were shown to generate ROS with varying effectiveness. CSM-CLF generates ROS in the highest amounts, followed by JSC-1A, with quartz generating the least ROS [110,112]. Despite these differences, the three materials were similarly cytotoxic to both PCAD (Figure 4.2A) and TDCAD cells (Figure 4.2B). The A549 cells were more sensitive than were the CAD cells to both quartz and CSM-CLF (Figure 4.2C). Conversely, cell killing by JSC-1A was slightly *less* for A549 cells than it was for CAD cells (Figure 4.2C).

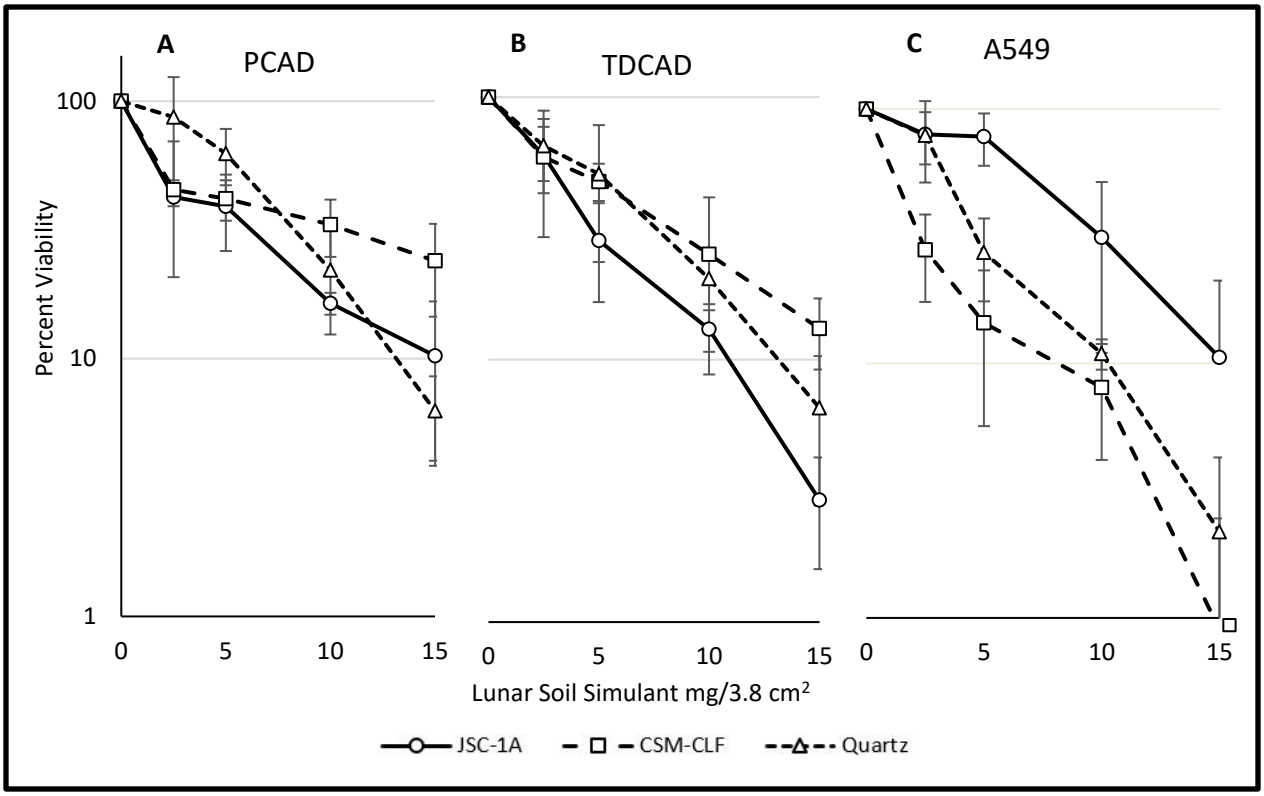

Figure 4.2. Cytotoxicity is not correlated with ROS-generating activity. A. PCAD, B. TDCAD, or C. A549 cells were treated with increasing concentrations of 10 µm, freshly ground JSC-1A, CSM-CLF, or quartz. Cell viability was assessed using the trypan blue exclusion dye. These results are normalized to untreated cells, which are set to 100%. The error bars are standard deviation (N=3).

When the simulants were used in that state received from the suppliers (i.e., not freshly ground), significant CAD cell death was observed only in response to CSM-CLF or anatase (Figure 4.3A). With freshly ground simulants, 20 mg/cm^2 of material resulted in high levels of cytotoxicity, but exposure to 10 mg/cm^2 allowed >10% survival with the majority of the materials. For PCAD and TDCAD cells, fresh grinding increased the cytotoxicity of all the simulants, in some cases slightly more dramatically for TDCAD than for PCAD cells (e.g., both JSC-1A and JSC-1A AGGL) (Figure 4.3B). A549 cells were more sensitive to every simulant than were the CAD cells (Figure 4.3C). Notably, the two agglutinated simulants caused more cell

death in the A549 cells did than their un-agglutinated counterparts, but such a difference was not seen for CAD cells (Figure 4.3C).

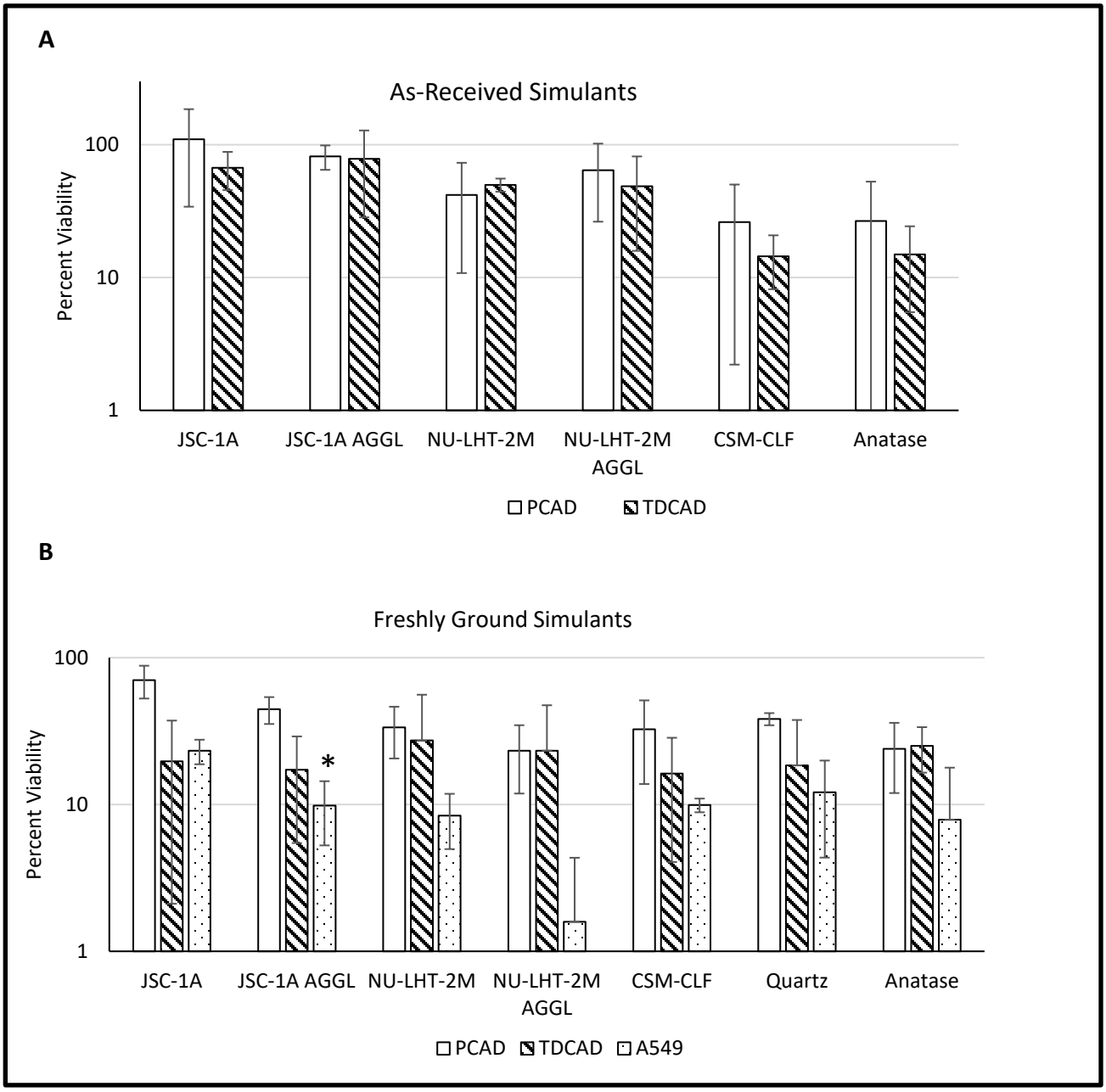

Figure 4.3. Differential sensitivity of neuronal and lung epithelial cells to various lunar soil simulants. The cytotoxicity of simulants was compared for A. 20 mg/3.8 cm^2 as-received material, or B. 10 mg/3.8 cm^2 10 µm material freshly ground one hour before use. Cell viability was measured using the trypan blue exclusion dye. The results are normalized to untreated cells, which are set to 100%. The error bars are standard deviation (n=3). * denotes $p<0.05$ between JSC-1A and JSC-1A AGGL.

4.3.2 DNA damage from lunar soil simulants

Damage to cellular DNA can lead to mutations, which may be propagated for the life of the organism [116]. The cytotoxic effects of DNA damage can also potentiate cancer by stimulating cell proliferation to replace dead tissue [104]. In order to assay the DNA damage resulting from exposure to lunar soil simulants, a PCR-based assay [86] was applied to nuclear and mitochondrial DNA isolated from cells after treatment with the simulants. This technique allowed for amplification of the mtDNA specifically, without separately extracting it [86]. Many DNA template lesions can slow down or block DNA polymerases [86,117], so this assay is not specific for the type of damage. However, DNA with fewer lesions is amplified more efficiently than is DNA with greater lesion density, thus giving an indirect measure of the damage.

The ratio of mitochondrial to nuclear DNA can vary as a result of the isolation procedure, the cell treatment, or cell-type differences. Thus, a separate set of PCR reactions was performed to amplify a small (~100-base-pair) region of either mtDNA or a single-copy nuclear gene, and the resulting values were used to normalize the respective long-PCR values that are sensitive to the presence of DNA lesions. The short segments used for this normalization are unlikely to contain a lesion at biologically relevant levels of DNA damage [86,117].

PCAD cells and TDCAD cells showed strikingly different levels of DNA damage after simulant exposure (Figure 4.4). The PCAD cells had little detectable damage in their nuclear DNA after exposure to any of the freshly ground simulants at 10 mg/cm^2, while the DNA damage detected in TDCAD cells was very high for all the simulants (Figure 4.4a). The DNA damage caused by quartz and anatase was measured at 5 mg/cm^2, because greater amounts of

those materials gave levels of DNA damage too high to permit a measurement. The TDCAD cells suffered modest but significant nuclear DNA damage after quartz or anatase treatment, while little or no DNA damage was detected in PCAD cells (Figure 4.4b). The DNA damage results contrast with the cell viability data, which showed similar survival outcomes for PCAD and TDCAD cells for most of the simulants (Figure 4.1). We were not able to measure DNA damage in A549 cells for technical reasons, and possible nuclear DNA damage from exposure to the as-received simulants was not assessed owing to material limitations.

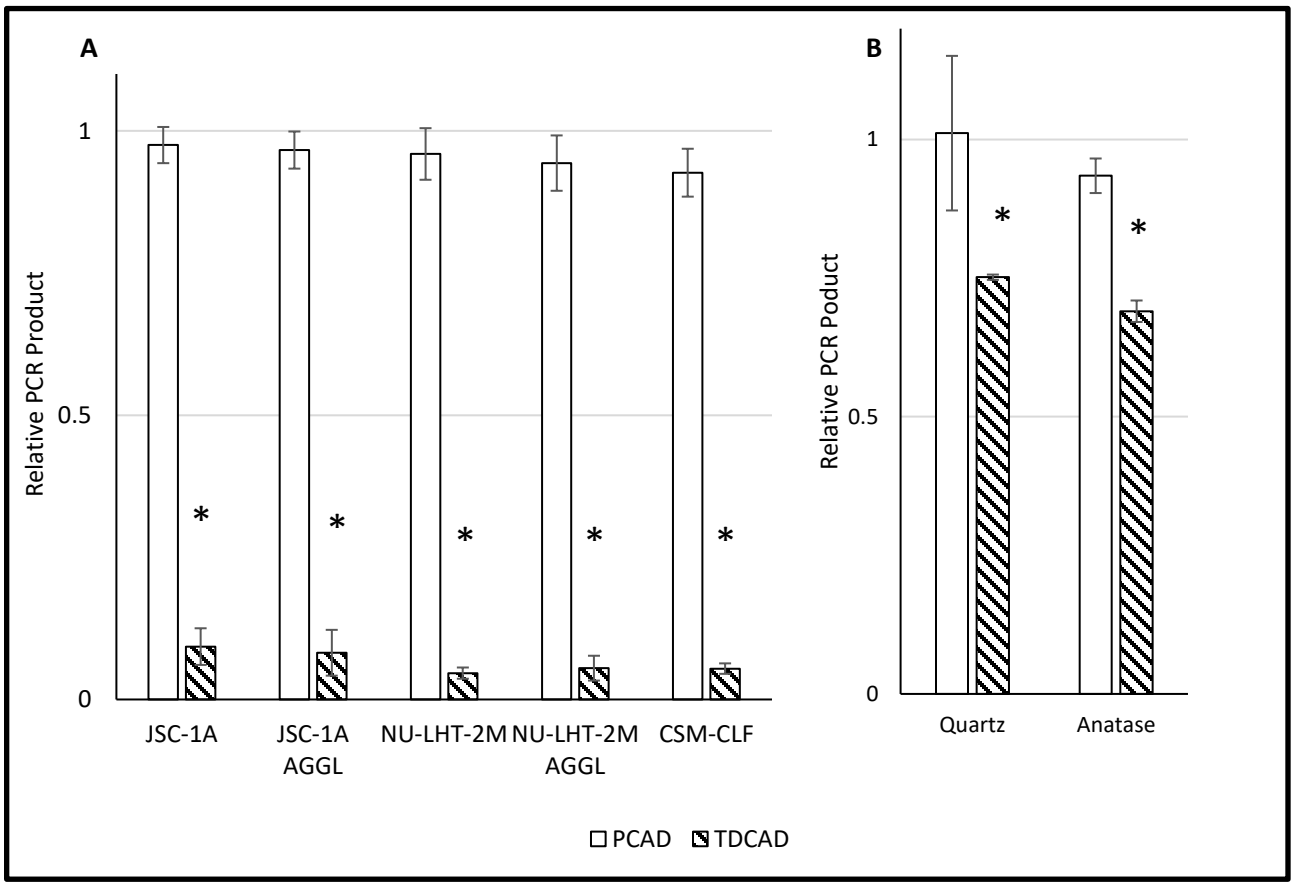

Figure 4.4. Greater nuclear DNA damage in TDCAD than in PCAD cells exposed to lunar soil simulants. Cells were treated with the indicated simulant for 1 hour, then total DNA was immediately extracted for PCR. A. 10 mg/3.8 cm^2 simulant or B. 5 mg/3.8 cm^2 simulant. Results

are normalized to untreated cells which are set to 1. The error bars indicate standard deviation (n=3). * denotes $p<0.05$ between PCAD and TDCAD treatments.

The results for mtDNA damage were mostly reversed from those observed for nuclear DNA. Exposure to most of the freshly ground simulants generated less detectable DNA damage (i.e., greater amounts of PCR product) in the TDCAD than in the PCAD cells (Figure 4.5A). The converse was seen for cells exposed to quartz or anatase (Figure 4.5B). Of the unground simulants, only CSM-CLF caused significant mtDNA damage in CAD cells, at about equal levels for PCAD and TDCAD (Figure 4.5C). The A549 cells suffered only moderate levels of mtDNA damage after exposure to any of the freshly ground simulants (Figure 4.5A).

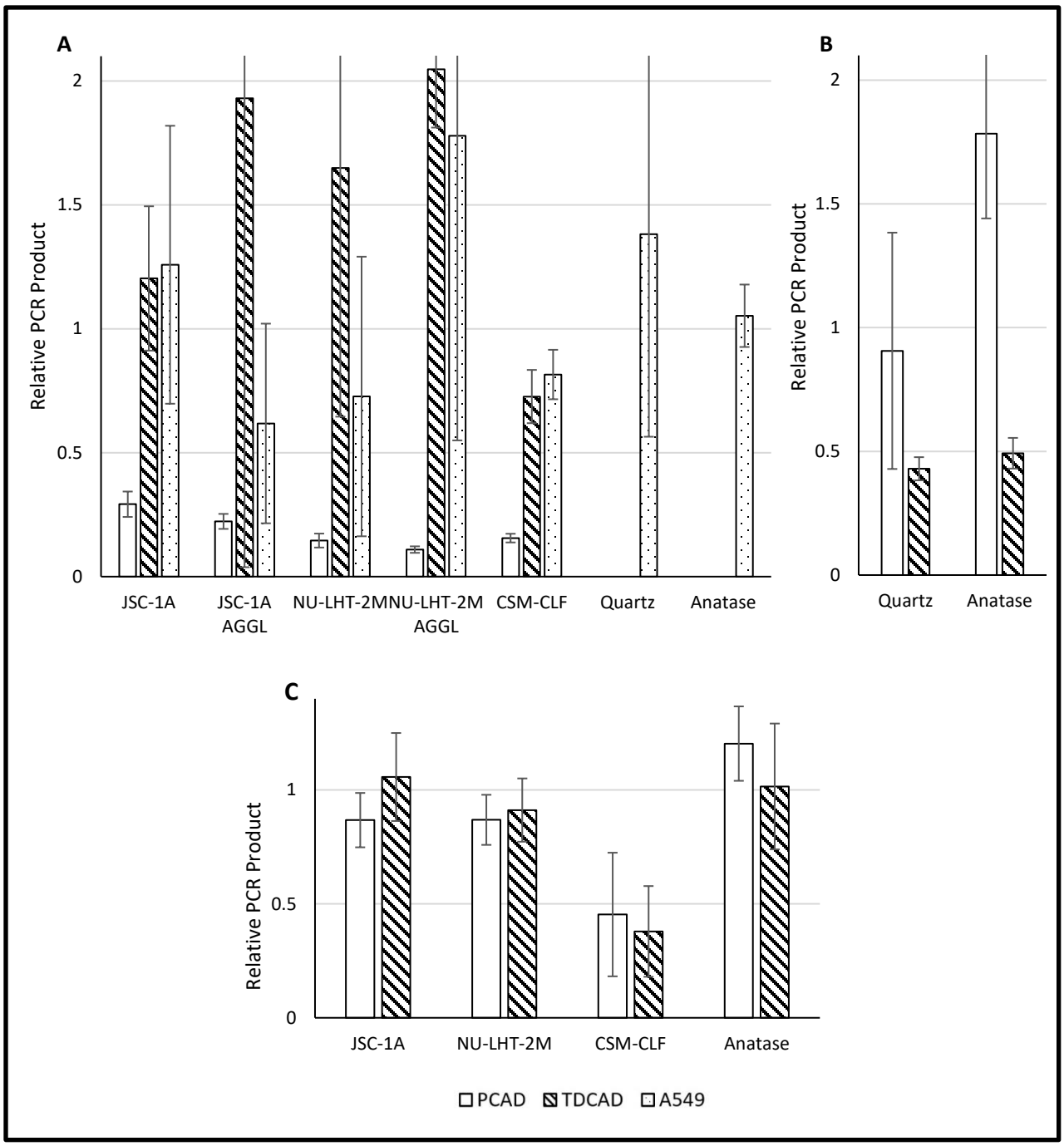

Figure 4.5. PCAD cells may undergo more mtDNA damage than do TDCAD or A549 cells. Cells were treated with the indicated simulant for 1 hour, followed by immediate DNA was extracted for PCR. A. Cells treated with 10 mg/cm^2 freshly ground lunar soil simulants. B. Cells treated with 5 mg/cm^2 freshly ground quartz and anatase. C. Cells treated with by 20 mg/cm^2 lunar soil simulants as-received. Results are normalized to untreated cells which are set to 1. The error bars indicate standard deviation (n=3).

4.4 Discussion

We found that exposure of neuronal and lung epithelial cells in culture to several types of lunar soil simulants caused cell death and DNA damage. The effects varied with the cell type, including whether the CAD cells were in the proliferating (precursor) or the fully differentiated (neuronal) state. In general, using material that had been freshly ground produced much greater effects than were seen with the simulants as received from the supplier. At first glance, our results would thus seem in line with the prior observations on ROS production [110,112]. However, there was no consistent variation of either the cytotoxicity or the DNA-damaging capacity of the materials with their ability to generate ROS in solution. Thus, the cellular (and likely, the tissue-level) effects of these particulate, regolith-simulating materials is more complex than simply the ability to generate measurable ROS.

The grinding procedure has at least two effects that could increase the biological impact of the lunar soil simulants. The increase in surface area per unit volume would certainly increase the availability of reactive components, such as reduced iron, to participate in ROS-generating reactions. Perhaps more importantly, the smaller sizes of the particles resulting from grinding would bring them into the range of microscopic interaction with the cells, which could even enable cellular uptake of the smallest particles [118]. It is worth noting in this context that ROS generated by internalized (phagocytosed) particles would likely be undetectable in the surrounding solution. Uptake of even chemically inert particles also

stimulates active ROS production by a wide range of cell types via an inflammatory response [118,119].

Conversely, the impact of externally generated ROS would be greatly dampened by cellular antioxidant enzymes such as catalase, glutathione peroxidase, superoxide dismutase, and by small molecules such as glutathione [120]. The potential impact of lunar regolith on human tissues and the resulting health effects of the particles will thus have to be assessed in light of their ability to be engulfed by cells or transmitted to deeper tissues, as occurs with particle uptake into the brain following nasal inhalation [121]. In addition, the results indicate that the ability of the particles to generate ROS *within* cells should be investigated, as this capacity might differ significantly from what is measured with the materials alone in solution [122].

The cell-type differences in the effects of the various simulants merit some comment. The similar cell-killing ability of the freshly-ground materials for PCAD and TDCAD cells was unexpected, as cycling cells are typically more sensitive to DNA-damaging agents than are non-replicating cells. This typical pattern results from the vulnerability of cellular DNA to damage during replication, and from the need for an undamaged DNA template for efficient DNA synthesis [123]. The similar responses to simulant exposure of PCAD and TDCAD cells is thus a further indication that damage to DNA is not necessarily a critical component of the cytotoxicity.

The A549 lung epithelial cells appeared to be less sensitive to killing by freshly-ground JSC1A than were either PCAD or TDCAD cells. Whether this difference indicates greater

protective mechanisms in lung epithelial cells than in neurons will require additional study. However, the observation suggests that the extended projections of TDCAD cells [74], like the axons and dendrites in neuronal tissues, do not necessarily render them more susceptible to lethal damage to cellular membranes, proteins, mitochondria or other vital organelles.

It is noteworthy that mtDNA damage was not well correlated with cell survival. The apparent lack of mtDNA damage in the simulant-treated TDCAD cells could arise in two ways. The rate of capacity of mtDNA repair could be greater in the differentiated than in the proliferating CAD cells. However, our other studies suggest that this is not the case for TDCAD cells treated with chemical DNA-damaging agents (Caston et al., in preparation). It is also possible that damaged mtDNA is eliminated rapidly in TDCAD cells, within the 1-hour treatment period we used, such that none is detected in the assay. Elimination of heavily damaged mtDNA has been observed in other cases [124,125] and is an effective option for mitochondria owing to the presence of multiple copies of mtDNA within a single compartment in the cell.

Clearly, avoidance of lunar dust inhalation will be important for future explorers, but with increased human activity on the Moon it is likely that adventitious exposure will occur, particularly for individuals spending long periods of time on that body. A detailed understanding of the health effects of lunar dust exposure is thus important, and further defining the cellular and biological impact of materials from various parts of the lunar surface is warranted. It will be especially critical eventually to study actual lunar regolith samples for their effects on cell function and the integrity of the cellular DNA.

Chapter 5

Conclusions and perspectives

5.1 Conclusions and discussion

The research presented in this dissertation provides an updated picture of mtDNA repair in differentiated cells. Overall, the DNA repair capacity of mitochondria in CAD cells was not down-regulated after differentiation. This conclusion is supported by the evidence that shows that the endonuclease MGME1 was not down-regulated in differentiated CAD cells, and that ExoG and Fen1 were only modestly diminished to ~50% of their expression in the mitochondria of proliferating CAD cells (Chapter 2; Figures 2.1, 2.2, and 2.4). The reduction of Fen1 and ExoG in the mitochondria after differentiation to ~50% may be biologically significant. The relative abundance of these proteins compared to their need in proliferating cell mitochondria is not known, nor how many copies are necessary after differentiation. However, since the level of MGME1 did not change upon differentiation, this enzyme is an obvious candidate for future study of long-patch BER in mitochondria.

Despite the availability of these endonucleases, DNA flap excision was diminished in both nuclear and mitochondrial extracts in differentiated cells compared to cycling precursors (Chapter 2, Figures 2.7 and 2.8). It may be that both short- and long-patch BER are down-regulated, as has been observed previously in whole-cell extracts from differentiated cells [57,59]. However, these flap endonucleases may not be the rate limiting step in DNA repair. If another enzyme in the pathway catalyzes its reaction at a slower rate, the slower flap excision activity of differentiated cells would not affect overall repair kinetics. For example, if a glycosylase activity at the first step of the reactions is reduced, then both short- and long-patch BER would continue more slowly upon differentiation. Alternatively, if there is diminished activity of DNA ligase activity, an enzyme that both pathways depend upon, both short- and

long-patch BER would appear slower. However, there is evidence that DNA ligase III, found in the mitochondria, continues to be expressed upon differentiation [57]. Investigation of DNA ligase III expression in CAD cells will be necessary to gain further insight.

Differentiated neuronal and muscle cells accumulated less mtDNA damage than proliferating cells when challenged with chemical reagents or lunar soil simulants (Chapters 3 and 4; Figures 3.4, 3.6, and 4.5). This result implies that mtDNA repair in differentiated cells is faster than that in proliferating cells, which would contrast with the results from Chapter 2, which show that flap excision in differentiated cells is attenuated. However, since the mitochondria have multiple genomes per mitochondrion, the failure to detect damage in the mtDNA of differentiated cells does not necessary imply that the DNA was repaired. Heavily damaged mitochondrial genomes can be degraded rather than repaired [125,126]. It may also be true that the differentiated cell mtDNA is somehow protected from accumulating damage. For instance, mitochondrial targeted antioxidants may neutralize the reactive oxygen species generated by hydrogen peroxide or exposure to lunar soil simulants [120].

The TDCAD cells represent a non-cycling neuronal cell. Failure of TDCAD cells to repair their DNA may be an indication failing DNA repair in aging neurons. As discussed previously, neurodegeneration is correlated with decreased mitochondrial DNA repair capacity [27,127], which may result in an increased sensitivity to DNA damaging agents [128,129]. BER seems to be particularly down-regulated during the aging process [130,131], and the results reported in Chapter 2 are consistent with this change in level. For example, mitochondrial DNA glycosylases studied in five regions of the mouse brain showed a pronounced decline in activity associated

with age [132]. Nuclear DNA glycosylase activities also declined, but decline was limited to the cerebellum [132]. The diminished enzyme activity in these reports reflects the decreased flap excision activity seen in the TDCAD cells compared to PCAD cells.

5.2 Future directions

Experiments need to be performed that elucidate if short-patch BER is attenuated in mitochondrial of differentiated cells. In order to assess the ability of differentiated cells to complete short-patch repair BER, cell extracts may be incubated with an oligonucleotide substrate that mimics a lesion that is normally repaired using the short-patch pathway, for example an abasic site [44,57]. Using both whole-cell and mitochondria extracts will elucidate whether the BER is diminished upstream of long-patch flap excision.

There is also a possibility that mitochondria or mtDNA are being degraded before the DNA damage and repair can be assayed. Mitophagy can be measured in the cells using immunofluorescence by marking mitochondria which co-localize with the autophagosome, usually marked by Parkin [51]. If mitochondria in CAD cells are found to be going through mitophagy, inhibition of this pathway should prevent degradation of damaged mtDNA, which could then be analyzed using the PCR-assay. There are multiple ways to inhibit mitophagy using small molecule inhibitors. Bafilomycin and chloroquine both inhibit autophagy, which would prevent mitophagy in addition to degradation of other organelles [133]. Alternatively, mitochondrial fission, a step in mitophagy, can be inhibited using mdivi-1, a chemical inhibitor of mitochondrial fission protein Drp-1 [134]. However, mitochondrial fission is necessary for general mitochondrial function, as well, including cell growth, cell division, and redistribution of mitochondria after differentiation [135,136].

In Chapter 2, I discussed knock-down of BER proteins as the next logical step to understand mitochondrial BER. Reducing expression of the mitochondrial BER endonucleases MGME1 and ExoG will test their requirement in for mtDNA repair. In consideration of the published literature, other relevant proteins would include OGG1 and Lig3, both implied to be diminished in aging and diseases neurons [137,138]. OGG1 has a mitochondria-specific isoform, OGG1-2a [139]. DNA ligase III is not mitochondria specific, but the protein does contain a known mitochondrial targeting signal that could be targeted to deplete only mitochondrial DNA ligase III [33,140]. There are other mitochondrial-specific proteins involved in BER that could be studied, for example isoforms of the DNA glycosylases MYHα and UNG1 [141,142].

Potential outcomes of protein knock-downs to measure should include DNA integrity as well as signs of neurodegenerative disease. The condition of the mtDNA can be measured by assessing the quantity of lesions, such as oxidized bases, oxidized AP sites, or double strand breaks. As mentioned, Alzheimer's disease may involve impaired BER [137,143-145]. Inability to complete BER may be causative to neurodegenerative diseases. The most obvious measurement of Alzheimer's disease would be amyloid beta plaques [146], but other measures of neuronal health, such as calcium signaling [147] or optical measurements of neuronal activity [148], with allow for a more general understanding of neuronal function [149].

In addition to cell culture work, mouse knockout models would allow for disease progression to be measured in absence of BER enzymes. A mouse knockout would more directly measurement of causality between deficient BER and neurodegeneration. A knock-out

mouse model has been characterized for OGG1 [150], and a conditional mouse knock-out was developed for Ape1 [151]. Both of these mouse models display increased oxidative damage compared to wild type mice. Moreover, transient focal cerebral ischemia induced in mice with Ape1 deficiency impaired cognitive recovery, as well as resulting in the long-term loss of white matter [151]. Neurodegeneration was not observed in mice without induced neuronal damage, but at only 12 weeks of age these mice may not have been old enough to develop neurodegeneration. Allowing the *APE1* knock-out mice to mature or combining *APE1* and *OGG1* knockout may induce neurodegeneration. In this case, the BER knockout phenotype could be compared to a neuronal disease mouse model, such as that for Alzheimer's disease. Comparing the onset of disease markers, such as onset of amyloid beta plaque formation [65,152], neurofilament light chain present in the cerebrospinal fluid [153], and apoptosis [154] will reveal any role of these proteins in neurodegeneration. Another benefit of using a mouse model is the ability to test behavior as well as molecular markers [155]. The insights gained by these experiments will be useful not only for understanding the relationship between BER and neurodegeneration, but also for developing useful pharmaceuticals for treating neurodegenerative diseases.

Chapter 6

Materials and methods

6.1 Cell Culture

Proliferating CAD cells were grown in Dulbecco's Modified Eagle Medium mixed in equal proportion with Ham's F12 medium (DMEM/F12) (HyClone #SH30271.01), then supplemented with 10% fetal bovine serum (Corning # 35-010-CV) and 1% of a penicillin/streptomycin mixture (Gibco #10378016). Differentiation was stimulated by growing CAD cells in serum-free DMEM/F12, supplemented with 20 μg/ml transferrin and 50 ng/ml sodium selenite. Differentiated CAD cells were grown on plates coated with poly-L-lysine at 20 mg/ml. Cells were fully differentiated after 5 days [74].

A549 Cells were grown in Ham's F12K (Kaighn's) nutrient medium supplemented with 10% fetal bovine serum and 1% of a penicillin/streptomycin mixture.

Muscle cell culture as performed by Dr. Paula Fortini, Istituto Superiore di Sanita, Rome Italy

From[61]: Murineskeletal MSCs were isolated from the hind limb muscles of young FVB;129 mice. MSCs were maintained as actively proliferating adult stem cells (myoblasts) and induced to differentiate in post-mitotic myotubes by modifying the cell growth conditions. In particular, myoblasts were subcultured in the growth medium (GM; F-10 nutrient mixture plus glutamax supplemented with 10% of fetal calf serum, 100 U/ml penicillin/streptomycin, 3% chicken embryo extract (obtained from 10- to 11-day-old embryos) and 2.5 mg/ml of recombinant human FGF-basic (Peprotech, Rocky Hill, NJ, USA)). To induce terminal differentiation, the GM was replaced with the differentiation medium (Dulbecco's modified Eagle medium plus glutamax, supplemented with 10% fetal calf serum and 100 U/ml penicillin/ streptomycin). Cells were incubated at 38 1C, 10% CO2. The efficiency of cell differentiation

was routinely controlled by staining with MHC antibodies, and evaluation of the differentiation and fusion indexes. The differentiation index is calculated as the percentage of nuclei belonging to MHC-positive cells on total nuclei. The fusion index is calculated as the percentage of nuclei belonging to MHC-positive cells possessing three or more nuclei on total MHC-positive cells

6.2 Western blotting

Cells were lysed using an SDS based buffer (Cell Signaling #9803), on ice for 30 minutes with vortexing. Cell debris was spun out at 10,000 xg for 10 minutes. Protein content was measured using Bradford reagent. Protein extracts were loaded in a 12% poly-acrylamide gel (Invitrogen #NP0343BOX) and run at 116 volts for two hours in MOPS buffer (NuPAGE #NP0001). Transfer was done for 3 hours on ice onto a PDVF membrane in transfer buffer (NuPAGE #NP0006-1), followed by ponceau staining to confirm transfer. The membrane was blocked for one hour in 3% bovine serum albumin (BSA) at room temperature. Primary antibodies and secondary were diluted into 3% BSA and incubated one hour with the membrane at room temperature. Between primary and secondary antibodies the membrane was washed for 30 minutes in phosphate buffered saline (PBS) +0.1% tween. After the secondary antibody the membrane was washed three times for ten minutes each in PBS with 0.1% tween, then washed once for ten minutes in PBS before imaging. Primary antibodies included anti-Ape1 1:100 (Novus NB100-101), anti-DNA2 1:500 (abcam ab96488), anti-ExoG (abcam ab77736), anti-Fen1 1:700 (novus NB100-320), anti-NDYFA9 (Complex I) 1:1000 (abcam ab14713), anti-TFAM 1:1000 (cell signaling 7495). Secondary antibodies were Goat anti-Rabbit 1:10,000 (licor) and Goat anti-Mouse 1:10,000 (licor). Imaging was performed on Licor Odyssey (Classic ODY-1716).

6.3 Immunofluorescence

Cells were grown in 12 well plates on top of coverslips to a density of 20,000 cells. The cells were incubated in Mitotracker Red diluted to 0.3 ug/ml in FBS-free media for 30 minutes. Cells were fixed in 4% PFA for 20 minutes at room temperature. The cells were then blocked for 2 hours in 0.3% BSA, 0.2% Triton X in PBS at room temperature followed by Fen1 (abcam 70815) diluted 1:700 in blocking buffer (0.3% BSA, 0.2% triton x, in PBS) overnight at 4^{o}C. Cells were washed twice in PBS for 10 minutes, then incubated in FITC anti-rabbit (1:50) for 1 hour at room temperature in the dark. Cells were washed twice for 10 minutes in PBS and mounted using Fluormount-G (SouthernBiotech #0100-01). Imaging was done on a confocal microscope.

Cell-by-cell quantification was performed on the immunofluorescence images by first applying a threshold to the image to remove background fluorescence. Then a region including the mitochondria of one cell was selected and the average Fen1 fluorescence intensity within the mitochondria was measured. The average intensity of Fen1 in the mitochondria was then divided by the cell area. This resulted in numbers ranging from 0.0001 to 0.009. The average intensities per cell were then binned into intervals of 0.00039. This analysis indicates that PCAD cells and TDCAD cells have nearly equal distributions of Fen1 in their mitochondria.

6.4 Whole Cell and Mitochondrial Extract Flap Assay

Extracts were made into enzyme lysis buffer (10 mM Tris-HCl, 200 mM KCl, 600 mM KCl, 2 mM EDTA, 40% (v/v) glycerol, 0.2% NP-40, 2 mM DTT, 0.5 mM PMSF, 1x protease inhibitor cocktail) and incubated for 1.5 hours, then spun down at 10k xg. The extracts were mixed with 1 ul of 1 µM flap substrate (1pmol) (Table 6.1) and 10x reaction buffer (50 mM Tris-HCl (pH 8.0)

30 mM NaCl, 2 mM DTT, 0.1 ug/ul BSA, 2 mM MgCl2, 5% glycerol, 10 m ATP). Whole cell extracts were incubated for 30 minutes at 37^{o}C with 0.1, 0.5, or 1 µg of extract in a0 µl reaction. Mitochondrial extracts were incubated for 15, 30, 45, or 60 minutes at 37^{o}C in a 10 µl reaction. For positive control, 0.5 ul of 4ng/ul Fen1 (51 nmol) was mixed with 1 pmol substrate. Reactions were terminated with an equal volume of formamide (10 µl) and run on a 16% TBE/Urea gel (15% acrylamide, 1x TBE (tris-borate-EDTA), 7M Urea, 26% formamide (v/v), 0.004% TEMED (v/v), 1% ammonium persulfate (w/v)) in TBE buffer.

Band intensity was measured by selecting equally sized sections around each band. Quantitation of the gel data was accomplished by dividing the band density of the product by the band density of the substrate and product combined. The substrate-product ratio generated by purified Fen1 was set to 100% and each sample was normalized to that ratio.

Table 6.1. Flap substrate oligonucleotides.

Name	Sequence (5'-3')
FBR1G	GGACTCTGCCTCAAGACGGTAGTCAACGTG
FLAPGT13	TAMARA-GATGTCAAGCAGTCCTAACTTTTTTTTTTTTTTTGAGGCAGAGTCC
FLAP3B1	CACGTTGACTACCGTC

6.5 Mitochondrial Extraction

Cells were grown in three-tier tissue culture flasks (nunc) until confluent. Four flasks of cells were used per experiment. Cells were trypsonized and spun down at 900xg in a sorvall RT legend centrifuge. Cells were resuspended in hypotonic buffer (20mM HEPES-KOH pH 7.4, 5mM MgCl2, 5mM KCl, 1 mM DTT) and spun again, then suspended in fresh hypotonic buffer for 10

minutes. Cells were homogenized with 20 strokes of a dounce homogenizer, or until 90% of cells were broken when viewed under a microscope. Then 6 ml of 2xMSH buffer (20Mm HEPES-KOH pH 7.4, 4mM EDTA, 2 mM EGTA, 5mM DTT, 0.42 mannitol, 0.14 M sucrose) was added per 9 ml of homogenate and spun down at 9000xg in the Sorvall Legend RT for five minutes twice, to remove nuclei. The supernatant was layered onto 0.8 M sucrose in a centrifuge tube and spin at 10,000 rpm for 10 minutes in a HB6 rotor (16,000xg). This pellet was re-suspended in 1ml MSH buffer supplemented with 50 ug/ul BSA. A sucrose step gradient was made using 0.8 M and 1.5 M sucrose in a 3:1 ratio. The solution containing the mitochondria was layered onto the sucrose and spin at 23K rpm for 30 minutes in an ultracentrifuge in an SW32 rotor (40,000xg). The band of mitochondria was diluted into 4 volumes of MSH and spun at 14k rpm for 10 minutes to repellet. Mitochondria were then lysed using RIPA buffer and protein concentration was measured using Bradford reagent.

6.6 siRNA Knockdown

PCAD cells were plated in 6 well plates and allowed to grow overnight. 1 µl of Allstar Negative Control siRNA Alexa Fluor 488 (Qiagen # SI03650318) was mixed with 250 µl DMEM and, in a separate tube, 10 µl of Lipofectamine 2000 (ThermoFisher Scientific #11668027) was mixed with 250 µl DMEM. Each solution was incubated separately for 5 minutes, then mixed and incubated 25 minutes. Media in plates was replaced with 1.5 ml DMEM. 500 µl of siRNA/ lipofectamine mixture was added to each well. Cells were incubated for 24 hours, then media was replaced with fully supplemented DMEM/F12. 48 hours after transfection cells were imaged.

6.7 Cell Viability

6.7.1 Trypan Blue Exclusion Dye

Cells were plated in 6 well plates and allowed to grow over night for proliferating cells, or 5 days for differentiated cells. After treatment with a DNA damaging agent in serum free media, the media was replaced with fully supplemented media and the cells were allowed to recover for 24 hours. Cells were released from the plate with 2 ml of trypsin for 10 minutes, then 80 µl of cells was mixed with 40 µl of trypan blue dye. Cells were counted with a hemocytometer under the microscope.

6.7.2 (3-(4,5-Dimethylthiazol-2-yl)-2,5-Diphenyltetrazolium Bromide) (MTT)

20,000 cells/well were plated into 96 well plates and allowed to grow over night for proliferating cells, or 5 days for differentiated cells. After treatment with a DNA damaging agent in serum free media, the media was replaced with fully supplemented media and the cells were allowed to recover for 24 hours. The media was then removed and replaced with phenol free media containing 1.2 mM MTT reagent. After a two hour incubation, the media was removed and cells were lysed with 0.04% HCl in isopropanol. The plates was read at 595 nm and 660 nm. The 660 nm reading accounted for cellular debris and was subtracted from the 595 nm reading.

6.8 qPCR Assay

For dose response experiments, cells were incubated for the indicated time with DNA damaging agent in serum-free medium. Immediately after the treatment, the chromosomal DNA was extracted using the Qiagen 20/G DNA extraction kit (Qiagen #10223). To avoid

removing the mitochondrial DNA, the cell lysate was not pelleted before applying the samples to the DNA isolation columns. DNA was resuspended in Tris-EDTA and incubated overnight at 4^{o}C. DNA quantification was performed using the Picogreen reagent (Thermo-Fisher P11496).

The PCR assay was based on a previously described protocol [156]. Briefly, the long PCR amplification measures the amount of damage to the DNA. If the polymerase encounters a lesion, it may be blocked, resulting in less product. Since the mitochondrial and nuclear DNA are both present in the sample, the DNA quantification used to prepare the PCR consists mostly of nuclear DNA. In order to account for any changes in the mitochondria-nuclear DNA ratio which might affect the interpretation of the long PCR result, a short PCR is used to measure the total amount of mtDNA present in the sample. During the short PCR, the polymerase is less likely to come across lesions than the long PCR due to the fewer nucleotides the polymerase will encounter. This assay has the advantages of requiring only nanograms of DNA, enabling gene specific measurement of DNA damage, and allowing for direct comparison of mitochondrial and nuclear DNA in the same samples.

Primers were altered as listed in Table 2. Amplification reaction was performed with the mouse mitochondrial primers, both long and short, in a total volume of 50 µl containing 15 ng DNA template, KAPA Long Range Buffer, 100 ng/µl bovine serum albium 800 µM dNTPs, 400 nM primer forward and reverse, 1.5 mM $MgCl_2$, and 1 unit KAPA Long Range Hotstart DNA polymerase. The nuclear PCR was identical with the exception of using 100 mM primer. For the short mitochondrial PCR, the thermocycler was programmed for 3 min at 95°C as initial denaturation, followed by 22 cycles of 15 sec at 95°C for denaturation, 45 sec at 59°C as annealing, 1 min at 68°C for extension, and final extension at 72°C for 10 min. For the long

mitochondrial PCR, the thermocycler was programmed for 3 min at 95°C as initial denaturation, followed by 22 cycles of 15 sec at 95°C for denaturation and 12 min at 66°C as annealing and extension, and final extension at 72°C for 10 min. The long nuclear PCR was programmed for 3 min at 95°C as initial denaturation, followed by 27 cycles of 15 seconds at 95°C for denaturation and 12 min at 64°C for annealing and extension, and final extension at 72°C for 10 min.

The long PCR product is 10,965 bp, and the short PCR product is 119 bp, so in order to normalize for this difference, the raw PCR data were divided by the product lengths. The control was then normalized to 1.

Table 6.2. Primers for qPCR

Primer Name	Primer Sequence (5'-3')
Mouse Mitochondrial Long Sense	CCATTCTAATCGCCATAGCCTTCC
Mouse Mitochondrial Long Antisense	GAGGACTGGAATGCTGGTTGGTGG
Mouse Mitochondrial Short Sense	CCCAGCTACTACCATCATTCAAGT
Mouse Mitochondrial Short Antisense	GATGGTTTGGGAGATTGGTTGATG
Mouse Nuclear (β Globin) Sense	TTGAGACTGTGATTGGCAATGCCT
Mouse Nuclear (β Globin) Antisense	CCTTTAATGCCCATCCCGGACT
Human Mitochondrial Long Sense	TCTAAGCCTCCTTATTCGAGCCCGA
Human Mitochondrial Long Antisense	TTTCATCATGCGGAGATGTTGGATGG
Human Mitochondrial Short Sense	CCCCACAAACCCCATTACTAAACCCA
Human Mitochondrial Short Antisense	TTTCATCATGCGGAGATGTTGGATGG

Lunar Soil Simulant Storage and Grinding

As performed by Donald Hendrix, Stony Brook University, Stony Brook, NY

Lunar soil simulants were ground to ≤10 μm in a planetary ball mill (Retch PM 100) fitted with an agate grinding container and agate grinding balls at 350 rpm for 10 minutes. After grinding, samples were placed in vacuum storage in a Labconco vacuum desiccator at ~10mbar

pressure over desiccant. Samples were removed when an aliquot was required for experimentation.

One hour before experiments, 0.2 g of each lunar simulant was reground by hand in an agate mortar and pestle for 10 min. Lunar simulant accumulated on the sides of the mortar were scraped off regularly to ensure effective grinding of the entire aliquot. Both the mortar and pestle were thoroughly rinsed with water and ethanol before switching samples to prevent contamination between samples.

Appendix I
DNA-protein crosslink formation in mitochondria

Appendix 1.1: Introduction

……Previously Published…….

Rachel Audrey Caston and Bruce Demple. Risky repair: DNA-protein crosslinks formed by mitochondrial base excision DNA repair enzymes acting on free radical lesions. Free Radical Biology and Medicine 107 (2017) 146–150 [13]

Appendix 1.1.1 Formation of DNA-Protein Crosslinks (DPC)

In the nucleus, the majority of lesions handled via BER can in principle be repaired using the short-patch pathway [157][158]. However, some lesions can be repaired only by the long-patch pathway. One reason is that BER polymerases, and certain DNA glycosylases, form covalent links to the DNA via transient Schiff base intermediates during their lyase reactions. However, enzyme attack on some lesions forms an amide linkage that traps the protein in a stable covalent link to the DNA (Figure 3A). A clear example is the trapping of DNA polymerase β (Polβ) [159] or *Escherichia coli* endonuclease III [160] by 2-deoxyribonolactone (dL). The dL lesion was the first characterized oxidative product in DNA, and it results from hydroxyl radical attack on the C1’ carbon of a nucleotide [161]. The 5’-dRP of Polβ attacks the oxidized carbon using a lysine nucleophile, generating a DPC anchored by an amide bond. Recently, the in vivo formation and removal of Polβ-DPC formed by oxidative agents was characterized in human and mouse cells[64,162]. Formation of Polβ DPC was a result of Polβ’s mechanistic role in BER. Cells treated with oxidizing agents generated Polβ DPC, with a low background level of Polβ DPC even in untreated cells. The effectiveness of an agent in producing the Polβ-DPC in cells

correlated directly with the agent's ability to generate dL lesions, and non-oxidative agents such as methyl methanesulfonate were not effective. A substitution of the Polβ lyase active-site lysine by alanine prevented the formation of oxidatively generated DPC. Even the background DPC in untreated cells was eliminated for the lyase-defective protein[64], which indicates that this spontaneous accumulation is due to lesion processing by the enzyme.

Some DNA glycosylases can also be trapped by dL or other oxidatively generated lesions. Oxanine in DNA traps bacterial Fpg, Nei/endonuclease VIII, and AlkA proteins, as well as eukaryotic Ogg1 [163]. 5-Hydroxy-5-methylhydantoin traps Fpg, Nei/Endo VIII, and mammalian NEIL1 [164]. These DPC differ from those formed by Polβ with dL in two ways: the mechanism of trapping in these two cases is via a direct reaction with the modified base, and they occur in an unbroken DNA strand. Relatively stable DPC can even be formed by some lyases acting on normal AP sites, as reported for poly(ADP-ribose) polymerase-1 [165].

There is evidence for the generation of mitochondrial DPC. Mitochondrial Pol γ is trapped in vitro by dL, either with the purified protein or in mitochondrial extracts from HeLa cells[44]. Preliminary evidence from our lab has also revealed the formation of DPC containing Pol γ in oxidant-treated whole mitochondria. The other mitochondrial DNA polymerase, PrimPol, has not been shown to have lyase activity. Although no studies have been reported on them, other mitochondrial lyases would likely also be trapped by dL in mitochondrial DNA.

Appendix 1.1.2 Repair of Oxidatively Generated DPC

It seems likely, even obvious, that DPC would need to be removed from DNA to prevent the disruption of transcription and replication. Nuclear Polβ-DPC accumulate in oxidant-treated

cells incubated with the proteasome inhibitor MG132, indicating that proteolysis is an early step in their excision from the DNA[64]. The accumulated DPC, which are cytotoxic, also contain ubiquitin, of which 65-75% depends on the Polβ lyase: the lyase-inactivating K72A substitution (preventing the formation of oxidative Polβ-DPC) eliminates the bulk of ubiquitin from oxidatively generated DPC in MG132-treated human cells[64]. Similarly, most of the ubiquitin trapped in DPC in oxidant-treated murine fibroblasts depends on Polβ[64]. These data imply that ubiquitylation of Polβ-DPC targets their processing by the proteasome.

Mitochondria contain their own set of proteases, located in the intermembrane space, the inner membrane, and the matrix [64]. So far, E3-ubiquitin ligases are reported only for the outer membrane of mitochondria, so their involvement in processing DPC in mtDNA seems unlikely. In the matrix, where the mtDNA is located, AAA proteases perform quality control degradation and the removal of mitochondrial targeting sequences. LONP1 and ClpP proteases degrade oxidized proteins in the mitochondrial matrix [166]. It is possible that one or more of these proteases also degrades the protein component of DPC.

In the absence of repair, cells may have damage tolerance pathways. For example, translesion DNA polymerases can synthesize past a DPC or its residual peptide in an unbroken DNA strand, thus using proteasome-coupled repair as a form of damage tolerance [167]. This process would not remove the peptide-DNA adduct, but it could prevent cytotoxicity. However, it is uncertain whether appropriate translesion DNA polymerases to support such a process occur in mitochondria. There is some evidence that PrimPol is capable of translesion synthesis across UV products, 8-oxo-7,8-dihydroguanine, or an abasic site [40,41,48]. In this context, though, it should be realized that the Polβ-DPC differ in an important way from the DPC

processed by translesion synthesis: the former are trapped at sites of a strand break, which is expected to prevent DNA synthesis across them.

……Not Previously Published ……..

Appendix 1.2 Methods

Isolated mitochondria were suspended in a buffer containing 1 mM ADP, 5 mM glutamic acid, 20 mM sodium-malate, 20 mM BSA, 1x MSH buffer (described in chapter 6), 60 mM KCl, 10 mM $MgCl_2$, and 1 mM K_2HPO_4. Copper ortho-phenanthroline (5 mM) was made by mixing 50 mg of phenanthroline in 300 µl of DMSO with 40 mg of copper in 50 ml dH_2O.

The slot-blot/RADAR assay was performed as previously described[64,168]. Briefly, mitochondria were lysed using DNAzol with 1% Sarkosyl for 30 minutes. DNA was precipitated with a half volume 100% ethanol, then washed twice with 70% ethanol before resuspending in 10mM Tris-HCl containing 1mM EDTA•Na_2 (1xTE). DNA (1 µg) from each sample was bound to a nitrocellulose membrane using a vacuum slot-blot manifold. The membrane was blocked in casein from bovine milk for 1 hour, then blotted for 1 hour with primary antiserum (against DNA polymerase γ) and secondary antibody goat anti-rabbit 1:10,000 (licor). Imaging was performed on a Licor Odyssey (Classic Edition, Serial #ODY-1716).

Appendix 1.3 Results

A slot-blot assay was used to measure DPC [64]. DNA was isolated from mitochondria using a combination of chaotropic salts and detergents that effectively separates DPC from free protein [168]. The DNA was adsorbed to a nitrocellulose membrane and immuno-blotted for DNA polymerase γ. The slot blot was not sensitive enough to detect polymerase γ in whole-cell

samples, so mitochondria were isolated from HeLa cells to measure DNA polymerase γ DPC formation.

The ability of polymerase γ to be trapped in oxidative DPC was shown by incubating the mitochondria with increasing concentrations of copper ortho-phenanthroline (CuOP) (Figure S1.1). The trapping of polymerase γ appeared to increase with the concentration of CuOP used to treat the mitochondria.

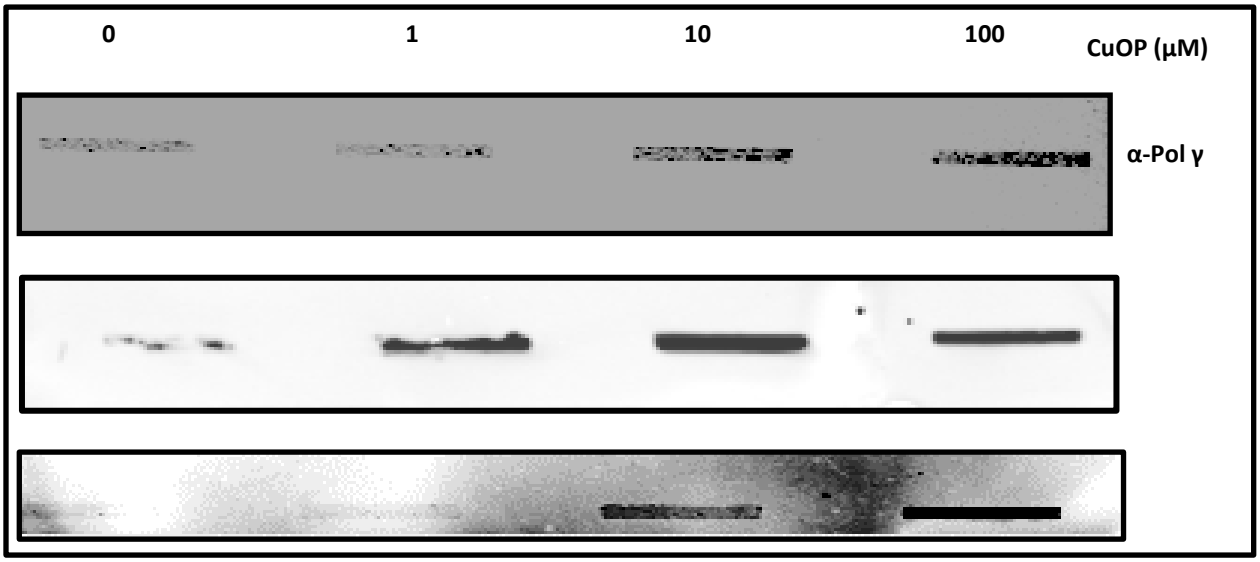

Figure Appendix1.1 Mitochondria accumulate DNA polymerase γ DPC. Isolated mitochondria from HeLa cells were treated with increasing concentrations of CuOP for 30 minutes. Due to the variability of the DPC detection at the lower concentrations, all three replicates are shown.

Mitochondria are lacking in some DNA repair pathways, but it is expected that DPC will need to be removed. The turnover rate of DPC in mitochondria was addressed by incubating mitochondria with CUOP for 30 minutes (and transfer to buffer without CuOP), then following the DPC levels during 4 hours of recovery (Figure S1.2). A 4 hour control was included to

account for changes in mitochondrial function with time and mitochondria activity was measured using MTT reagent at the beginning and end of the time course.

Removal of the DPC was not consistent between experiments. For example, the second and fourth rows have no DPC at 1 hour of recovery, but at later time points DPC is detected again (Figure S1.2). The fourth row also has more DPC at 0.5 hour recovery than at 0 hour recovery. The variability of the assay does not allow for any solid conclusion to be drawn about DPC clearance in mitochondria.

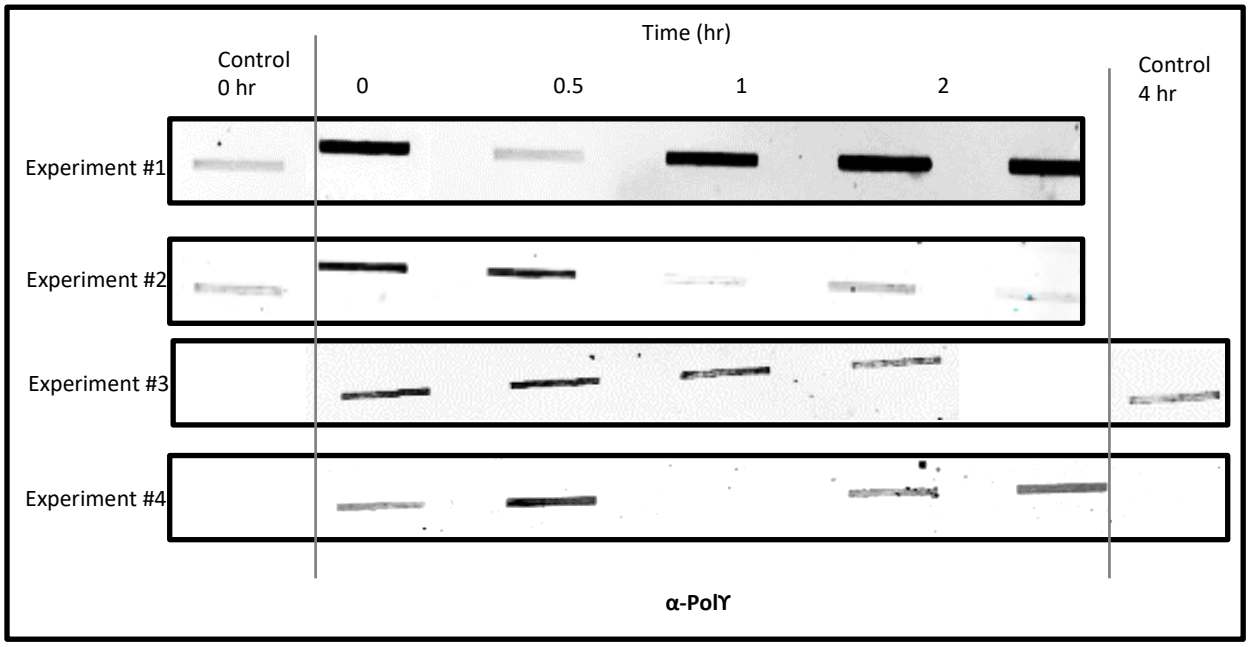

Figure Appendix1.2 DNA polymerase γ DPC may be cleared from mitochondria. Mitochondria isolated from HeLa were treated with 10 µM CUOP for 30 minutes, then collected by centrifugation at 15kxg and resuspended in fresh buffer. Mitochondria were then allowed to recover up to 4 hours. An untreated sample was also incubated for 4 hours. Four experiments are shown.

Appendix 1.4 Concluding Remarks and Future Directions

……..Previously Published…..……..

Rachel Audrey Caston and Bruce Demple. Risky repair: DNA-protein crosslinks formed by mitochondrial base excision DNA repair enzymes acting on free radical lesions. Free Radical Biology and Medicine 107 (2017) 146–150 [13]

The generation of oxidatively generated DPC during mitochondrial BER is coming into focus. Polγ-DPC are formed in mitochondrial extracts incubated with the oxidatively generated lesion dL[44,159], and preliminary data indicate the formation of Polγ-DPC in isolated mitochondria treated with dL-forming oxidants. Whether Polγ-DPC can be detected in intact cells remains to be seen. In the nucleus, the lyase active site of Polβ is essential for the observed protein trapping. The active site of the lyase in Polγ has yet to be characterized, however, making a similar mechanistic test of Polγ trapping difficult. Moreover, processes for removing mitochondrial DPC have not yet been described. The nuclear DPC degradation mechanism is dependent upon E3-ubiquitin ligase activity and the proteasome, which do not seem to have mitochondrial counterparts. Thus, new mechanisms for coping with DPC may emerge as the processing of these lesions in mitochondria is defined.

References

[1] Friedman, J. R.; Nunnari, J. Mitochondrial form and function. *Nature* **505**: 335–343; 2014.

[2] Cotrina, M. L.; Lin, J. H. C.; Alves-Rodrigues, A.; Liu, S.; Li, J.; Azmi-Ghadimi, H.; Kang, J.; Naus, C. C. G.; Nedergaard, M. Connexins regulate calcium signaling by controlling ATP release. *Proceedings of the National Academy of Sciences* **95**: 15735-40; 1998.

[3] Blanchoin, L.; Boujemaa-Paterski, R.; Sykes, C.; Plastino, J. Actin Dynamics, Architecture, and Mechanics in Cell Motility. *Physiological Reviews* **94**: 235-263; 2014.

[4] Bugyi, B.; Carlier, M.-F. Control of Actin Filament Treadmilling in Cell Motility. *Annual Review of Biophysics* **39**: 449-470; 2010.

[5] Mishra, P.; Chan, D. C. Mitochondrial dynamics and inheritance during cell division, development and disease. *Nature Reviews Molecular Cell Biology* **15**: 634–646; 2014.

[6] Seong, I. S.; Oh, J. Y.; Yoo, S. J.; Seol, J. H.; Chung, C. H. ATP-dependent degradation of SulA, a cell division inhibitor, by the HslVU protease in Escherichia coli. *FEBS Letters* **456**: 211-214; 1999.

[7] Pfeiffer, T.; Schuster, S.; Bonhoeffer, S. Cooperation and competition in the evolution of ATP-producing pathways. *Science (New York, NY)* **292**: 504–507; 2001.

[8] Hüttemann, M.; Lee, I.; Pecinova, A.; Pecina, P.; Przyklenk, K.; Doan, J. W. Regulation of oxidative phosphorylation, the mitochondrial membrane potential, and their role in human disease. *J Bioenerg Biomembr* **40**: 445–456; 2008.

[9] Ray, P. D.; Huang, B.-W.; Tsuji, Y. Reactive oxygen species (ROS) homeostasis and redox regulation in cellular signaling. *Cell Signal* **24**: 981–990; 2012.

[10] Wang, Y.; Bogenhagen, D. F. Human mitochondrial DNA nucleoids are linked to protein folding machinery and metabolic enzymes at the mitochondrial inner membrane. *The Journal of biological chemistry* **281**: 25791–25802; 2006.

[11] Bohr, V. A. Repair of oxidative DNA damage in nuclear and mitochondrial DNA, and some changes with aging in mammalian cells. *Free Radical Biology and Medicine* **32**: 804; 2002.

[12] Muftuoglu, M.; Mori, M. P. Formation and repair of oxidative damage in the mitochondrial DNA. *Mitochondrion* **17**: 164–181; 2014.

[13] Caston, R. A.; Demple, B. Risky repair: DNA-protein crosslinks formed by mitochondrial base excision DNA repair enzymes acting on free radical lesions. *Free Radical Biology and Medicine* **107**: 146–150; 2016.

[14] Schon, E. A.; DiMauro, S.; Hirano, M. Human mitochondrial DNA: roles of inherited and somatic mutations. *Nature Reviews Genetics* **13**: 878–890; 2012.

[15] Suzuki, T.; Nagao, A.; Suzuki, T. Human mitochondrial tRNAs: biogenesis, function, structural aspects, and diseases. *Annu Rev Genet* **45**: 299–329; 2011.

[16] Johnston, I. G.; Williams, B. P. Evolutionary Inference across Eukaryotes Identifies Specific Pressures Favoring Mitochondrial Gene Retention. *Cell Systems* **2**: 101–111; 2016.

[17] Kukat, C.; Wurm, C. A.; Spåhr, H.; Falkenberg, M.; Larsson, N.-G.; Jakobs, S. Super-resolution microscopy reveals that mammalian mitochondrial nucleoids have a uniform size and frequently contain a single copy of mtDNA. *Proc Natl Acad Sci USA* **108**: 13534–13539; 2011.

[18] Falkenberg, M.; Larsson, N.-G.; Gustafsson, C. M. DNA replication and transcription in mammalian mitochondria. *Annual Review of Biochemistry* **76**: 679–699; 2007.

[19] Gustafsson, C. M.; Falkenberg, M.; Larsson, N.-G. Maintenance and Expression of Mammalian Mitochondrial DNA. *Annual Review of Biochemistry* **85**: 133–160; 2016.

[20] Bonawitz, N. D.; Clayton, D. A.; Shadel, G. S. Initiation and beyond: multiple functions of the human mitochondrial transcription machinery. *Molecular Cell* **24**: 813–825; 2006.

[21] DiMauro, S.; Davidzon, G. Mitochondrial DNA and disease. *Annals of Medicine* **37**: 222–232; 2005.

[22] Wallace, D. C. Mitochondrial Diseases in Man and Mouse. *Science* **283**: 1482–1488; 1999.

[23] Harman, D. Aging: A Theory Based on Free Radical and Radiation Chemistry. *Journal of Gerontology* **11**: 298–300; 1956.

[24] Sun, N.; Youle, R. J.; Finkel, T. The Mitochondrial Basis of Aging. *Molecular Cell* **61**: 654–666; 2016.

[25] Taylor, R. W.; Turnbull, D. M. Mitochondrial DNA mutations in human disease. *Nature Reviews Genetics, Published online: 16 November 2012; | doi:101038/nrg3275* **6**: 389–402; 2005.

[26] Lin, M. T. High aggregate burden of somatic mtDNA point mutations in aging and Alzheimer's disease brain. *Human Molecular Genetics* **11**: 133; 2002.

[27] Cha, M.-Y.; Kim, D. K.; Mook-Jung, I. The role of mitochondrial DNA mutation on neurodegenerative diseases. *Exp Mol Med* **47**: e150–158; 2015.

[28] Sanders, L. H.; McCoy, J.; Hu, X.; Mastroberardino, P. G.; Dickinson, B. C.; Chang, C. J.; Chu, C. T.; van Houten, B.; Greenamyre, J. T. Mitochondrial DNA damage: molecular marker of vulnerable nigral neurons in Parkinson's disease. *Neurobiology of Disease* **70**: 214–223; 2014.

[29] Dölle, C.; Flønes, I.; Nido, G. S.; Miletic, H.; Osuagwu, N.; Kristoffersen, S.; Lilleng, P. K.; Larsen, J. P.; Tysnes, O.-B.; Haugarvoll, K.; Bindoff, L. A.; Tzoulis, C. Defective mitochondrial DNA homeostasis in the substantia nigra in Parkinson disease. *Nature communications* **7**: 13548–1369; 2016.

[30] Lin, M. T.; Cantuti-Castelvetri, I.; Zheng, K.; Jackson, K. E.; Tan, Y. B.; Arzberger, T.; Lees, A. J.; Betensky, R. A.; Beal, M. F.; Simon, D. K. Somatic mitochondrial DNA mutations in early Parkinson and incidental Lewy body disease. *Annals of Neurology* **71**: 850–854; 2012.

[31] Blanch, M.; Mosquera, J. L.; Ansoleaga, B.; Ferrer, I.; Barrachina, M. Altered Mitochondrial DNA Methylation Pattern in Alzheimer Disease-Related Pathology and in Parkinson Disease. *Elsevier* **186**: 385–397; 2016.

[32] Arning, L.; Haghikia, A.; Taherzadeh-Fard, E.; Saft, C.; Andrich, J.; Pula, B.; Höxtermann, S.; Wieczorek, S.; Akkad, D. A.; Perrech, M.; Gold, R.; Epplen, J. T.; Chan, A. Mitochondrial haplogroup H correlates with ATP levels and age at onset in Huntington disease. *J Mol Med* **88**: 431–436; 2010.

[33] Coskun, P. E.; Wallace, D. C. Alzheimer's brains harbor somatic mtDNA control-region mutations that suppress mitochondrial transcription and replication. *Proceedings of the National Academy of Sciences* **101**: 10726–10731; 2004.

[34] Lakatos, A.; Derbeneva, O.; Younes, D.; Keator, D.; Bakken, T.; Lvova, M.; Brandon, M.; Guffanti, G.; Reglodi, D.; Saykin, A.; Weiner, M.; Macciardi, F.; Schork, N.; Wallace, D. C.; Potkin, S. G. Association between mitochondrial DNA variations and Alzheimer's disease in the ADNI cohort. *Neurobiology of Aging* **31**: 1355–1363; 2010.

[35] Horton, T. M.; Graham, B. H.; Corral-Debrinski, M.; Shoffner, J. M.; Kaufman, A. E.; Beal, M. F. Marked increase in mitochondrial DNA deletion levels in the cerebral cortex of Huntington's disease patients. *Neurology* **45**: 1879–1883; 1995.

[36] Acevedo-Torres, K.; Berríos, L.; Rosario, N.; Dufault, V.; Skatchkov, S.; Eaton, M. J.; Torres-Ramos, C. A.; Ayala-Torres, S. Mitochondrial DNA damage is a hallmark of chemically induced and the R6/2 transgenic model of Huntington's disease. *DNA Repair* **8**: 126–136; 2008.

[37]Kazak, L.; Reyes, A.; Holt, I. J. Minimizing the damage: repair pathways keep mitochondrial DNA intact. *Nature Reviews Molecular Cell Biology* **13**: 659–671; 2012.

[38] Krokan, H. E.; Bjørås, M. Base excision repair. *Cold Spring Harb Perspect Biol* **5**: a012583–012605; 2013.

[39] Prakash, A.; Doublié, S. Base Excision Repair in the Mitochondria. *J Cell Biochem* **116**: 1490–1499; 2015.

[40] Martínez-Jiménez, M. I.; García-Gómez, S.; Bebenek, K.; Sastre-Moreno, G.; Calvo, P. A.; Díaz-Talavera, A.; Kunkel, T. A.; Blanco, L. Alternative solutions and new scenarios for translesion DNA synthesis by human PrimPol. *DNA Repair* **29**: 127–138; 2015.

[41] García-Gómez, S.; Reyes, A.; Martínez-Jiménez, M. I.; Chocrón, E. S.; Mourón, S.; Terrados, G.; Powell, C.; Salido, E.; Méndez, J.; Holt, I. J.; Blanco, L. PrimPol, an archaic primase/polymerase operating in human cells. *Molecular Cell* **52**: 541–553; 2013.

[42] Sykora, P.; Kanno, S.; Akbari, M.; Kulikowicz, T.; Baptiste, B. A.; Leandro, G. S.; Lu, H.; Tian, J.; May, A.; Becker, K. A.; Croteau, D. L.; Wilson, D. M.; Sobol, R. W.; Yasui, A.; Bohr, V. A. DNA polymerase beta participates in mitochondrial DNA repair. *Molecular and Cellular Biology* : MCB.00237–17; 2017.

[43] Zheng, L.; Zhou, M.; Guo, Z.; Lu, H.; Qian, L.; Dai, H.; Qiu, J.; Yakubovskaya, E.; Bogenhagen, D. F.; Demple, B.; Shen, B. Human DNA2 is a mitochondrial nuclease/helicase for efficient processing of DNA replication and repair intermediates. *Molecular Cell* **32**: 325–336; 2008.

[44] Liu, P.; Qian, L.; Sung, J.-S.; de Souza-Pinto, N. C.; Zheng, L.; Bogenhagen, D. F.; Bohr, V. A.; Wilson, D. M.; Shen, B.; Demple, B. Removal of oxidative DNA damage via FEN1-dependent long-patch base excision repair in human cell mitochondria. *Molecular and Cellular Biology* **28**: 4975–4987; 2008.

[45] Uhler, J. P.; Thörn, C.; Nicholls, T. J.; Matic, S.; Milenkovic, D.; Gustafsson, C. M.; Falkenberg, M. MGME1 processes flaps into ligatable nicks in concert with DNA polymerase γ during mtDNA replication. *Nucleic Acids Research* **44**: 5861–5871; 2016.

[46] Cymerman, I. A.; Chung, I.; Beckmann, B. M.; Bujnicki, J. M.; Meiss, G. EXOG, a novel paralog of Endonuclease G in higher eukaryotes. *Nucleic Acids Research* **36**: 1369–1379; 2008.

[47] Guilliam, T. A.; Jozwiakowski, S.; Ehlinger, A.; Barnes, R. P.; Rudd, S.; Bailey, L.; Skehel, J. M.; Eckert, K. A.; Chazin, W. J.; Doherty, A. Human PrimPol is a highly error-prone polymerase regulated by single-stranded DNA binding proteins. *Nucleic Acids Research* **43**: 1056–1068; 2014.

[48] Bianchi, J.; Rudd, S.; Jozwiakowski, S.; Bailey, L.; Soura, V.; Taylor, E.; Stevanovic, I.; Green, A.; Stracker, T.; Lindsay, H.; Doherty, A. PrimPol Bypasses UV Photoproducts during Eukaryotic Chromosomal DNA Replication. *Molecular Cell* **52**: 566–573; 2013.

[49] Mourón, S.; Rodriguez-Acebes, S.; Martínez-Jiménez, M. I.; García-Gómez, S.; Chocrón, S.; Blanco, L.; Méndez, J. Repriming of DNA synthesis at stalled replication forks by human PrimPol. *Nat Struct Mol Biol* **20**: 1383–1389; 2013.

[50] Stojkovič, G.; Makarova, A. V.; Wanrooij, P. H.; Forslund, J.; Burgers, P. M.; Wanrooij, S. Oxidative DNA damage stalls the human mitochondrial replisome. *Sci Rep* **6**: 28942–28955; 2016.

[51] Ding, W.-X.; Yin, X.-M. Mitophagy: mechanisms, pathophysiological roles, and analysis. *Biological Chemistry* **393**: 547–564; 2012.

[52] Course, M. M.; Wang, X. Transporting mitochondria in neurons. *F1000Res* **5**: 1–10; 2016.

[53] Ashrafi, G.; Schlehe, J. S.; LaVoie, M. J.; Schwarz, T. L. Mitophagy of damaged mitochondria occurs locally in distal neuronal axons and requires PINK1 and Parkin. *The Journal of Cell Biology* **206**: 655–670; 2014.

[54] Saxton, W. M.; Hollenbeck, P. J. The axonal transport of mitochondria. *jcsbiologistsorg* **125**: 2095–2104; 2012.

[55] Davis, C.-H. O.; Kim, K.-Y.; Bushong, E. A.; Mills, E. A.; Boassa, D.; Shih, T.; Kinebuchi, M.; Phan, S.; Zhou, Y.; Bihlmeyer, N. A.; Nguyen, J. V.; Jin, Y.; Ellisman, M. H.; Marsh-Armstrong, N. Transcellular degradation of axonal mitochondria. *Proceedings of the National Academy of Sciences* **111**: 9633–9638; 2014.

[56] Lu, B. Neuronal mitophagy: long-distance delivery or eating locally? *Curr Biol* **24**: R1006–1008; 2014.

[57] Sykora, P.; Yang, J.-L.; Ferrarelli, L. K.; Tian, J.; Tadokoro, T.; Kulkarni, A.; Weissman, L.; Keijzers, G.; Wilson, D. M.; Mattson, M. P.; Bohr, V. A. Modulation of DNA base excision repair during neuronal differentiation. *Neurobiology of Aging* **34**: 1717–1727; 2013.

[58 Szczesny, B.; Olah, G.; Walker, D. K.; Volpi, E.; Rasmussen, B. B.; Szabo, C.; Mitra, S. Deficiency in repair of the mitochondrial genome sensitizes proliferating myoblasts to oxidative damage. *PLoS ONE* **8**: e75201; 2013.

[59] Narciso, L.; Fortini, P.; Pajalunga, D.; Franchitto, A.; Liu, P.; Degan, P.; Frechet, M.; Demple, B.; Crescenzi, M.; Dogliotti, E. Terminally differentiated muscle cells are defective in base excision DNA repair and hypersensitive to oxygen injury. *Proceedings of the National Academy of Sciences* **104**: 17010–17015; 2007.

[60] Poovathingal, S. K.; Gruber, J.; Lakshmanan, L.; Halliwell, B.; Gunawan, R. Is mitochondrial DNA turnover slower than commonly assumed? *Biogerontology* **13**: 557–564; 2012.

[61] Fortini, P.; Ferretti, C.; Pascucci, B.; Narciso, L.; Pajalunga, D.; Puggioni, E. M. R.; Castino, R.; Isidoro, C.; Crescenzi, M.; Dogliotti, E. DNA damage response by single-strand breaks in terminally differentiated muscle cells and the control of muscle integrity. *Cell Death and Differentiation* **19**: 1741–1749; 2012.

[62] Gaier, J. R. The effects of lunar dust on EVA systems during the Apollo missions. *NASA* SPACE TRANSPORTATION AND SAFETY. **NASA/TM-2005-213610/REV1**: 1–73; 2007.

[63] Wagner, S. The Apollo experience lessons learned for constellation lunar dust management NASA. *NASA* LUNAR AND PLANETARY SCIENCE AND EXPLORATION. : 1–54; 2008.

[64] Quinones, J. L.; Thapar, U.; Yu, K.; Fang, Q.; Sobol, R. W.; Demple, B. Enzyme mechanism-based, oxidative DNA-protein cross-links formed with DNA polymerase β in vivo. *Proc Natl Acad Sci USA* **112**: 8602–8607; 2015.

[65] Pannee, J.; Portelius, E.; Minthon, L.; Gobom, J.; Andreasson, U.; Zetterberg, H.; Hansson, O.; Blennow, K. Reference measurement procedure for CSF amyloid beta (Aβ)1-42 and the CSF Aβ1-42 /Aβ1-40 ratio - a cross-validation study against amyloid PET. *J Neurochem* **139**: 651–658; 2016.

[66] Sung, J.-S.; DeMott, M. S.; Demple, B. Long-patch base excision DNA repair of 2-deoxyribonolactone prevents the formation of DNA-protein cross-links with DNA polymerase beta. *The Journal of biological chemistry* **280**: 39095–39103; 2005.

[67] Qiu, J.; Li, X.; Frank, G.; Shen, B. Cell cycle-dependent and DNA damage-inducible nuclear localization of FEN-1 nuclease is consistent with its dual functions in DNA replication and repair. *The Journal of biological chemistry* **276**: 4901–4908; 2000.

[68] Duxin, J. P.; Dao, B.; Martinsson, P.; Rajala, N.; Guittat, L.; Campbell, J. L.; Spelbrink, J. N.; Stewart, S. A. Human Dna2 is a nuclear and mitochondrial DNA maintenance protein. *Molecular and Cellular Biology* **29**: 4274–4282; 2009.

[69] Stewart, J. A.; Campbell, J. L.; Bambara, R. A. Flap endonuclease disengages Dna2 helicase/nuclease from Okazaki fragment flaps. *The Journal of biological chemistry* **281**: 38565–38572; 2006.

[70] Tarantino, M. E.; Bilotti, K.; Huang, J.; Delaney, S. Rate-determining Step of Flap Endonuclease 1 (FEN1) Reflects a Kinetic Bias against Long Flaps and Trinucleotide Repeat Sequences. *Journal of Biological Chemistry* **290**: 21154–21162; 2015.

[71] Kazak, L.; Reyes, A.; He, J.; Wood, S. R.; Brea-Calvo, G.; Holen, T. T.; Holt, I. J. A cryptic targeting signal creates a mitochondrial FEN1 isoform with tailed R-Loop binding properties. *PLoS ONE* **8**: e62340; 2013.

[72] Cymerman, I. A.; Chung, I.; Beckmann, B. M.; Bujnicki, J. M.; Meiss, G.; Chung, I.; Beckmann, B. M.; Bujnicki, J. M.; Meiss, G. EXOG, a novel paralog of Endonuclease G in higher eukaryotes. *Nucleic Acids Research* Oxford University Press; **36**: 1369–1379; 2008.

[73] Tann, A. W.; Boldogh, I.; Meiss, G.; Qian, W.; van Van Houten, B.; van Houten, B.; Mitra, S.; Szczesny, B. Apoptosis Induced by Persistent Single-strand Breaks in Mitochondrial Genome: CRITICAL ROLE OF EXOG (5'-EXO/ENDONUCLEASE) IN THEIR REPAIR. *Journal of Biological Chemistry* **286**: 31975–31983; 2011.

[74] Qi, Y.; Wang, J. K.; McMillian, M.; Chikaraishi, D. M. Characterization of a CNS cell line, CAD, in which morphological differentiation is initiated by serum deprivation. *J Neurosci* **17**: 1217–1225; 1997.

[75] Watkins, J.; Basu, S. A quantitative proteomic analysis of mitochondrial participation in p19 cell neuronal differentiation. *J Proteome Res* **7**: 328–338; 2007.

[76] Farr, C. L.; Kaguni, L. S. Purification strategies for Drosophila mtDNA replication proteins in native and recombinant form. Mitochondrial single-stranded DNA-binding protein. *Methods Mol Biol* **197**: 285–294; 2002.

[77] Dickinson, A.; Yeung, K. Y.; Donoghue, J.; Baker, M. J.; Kelly, R. D.; McKenzie, M.; Johns, T. G.; John, J. C. S. The regulation of mitochondrial DNA copy number in glioblastoma cells. *Cell Death and Differentiation* **20**: 1644–1653; 2013.

[78] Facucho-Oliveira, J. M.; Alderson, J.; Spikings, E. C.; Egginton, S.; John, J. C. S. Mitochondrial DNA replication during differentiation of murine embryonic stem cells. *jcsbiologistsorg* **120**: 4025–4034; 2007.

[79] Roestenberg, P.; Valsecchi, F. Mammalian mitochondrial complex I: biogenesis, regulation, and reactive oxygen species generation. *Antioxid Redox Signal* **12**: 1431–1470; 2009.

[80] Benard, G.; Faustin, B.; Passerieux, E.; Galinier, A.; Rocher, C.; Bellance, N.; Delage, J.-P.; Casteilla, L.; Letellier, T.; Rossignol, R. Physiological diversity of mitochondrial oxidative phosphorylation. *AJP: Cell Physiology* **291**: C1172–1182; 2006.

[81] Bhardwaj, R. D.; Curtis, M. A.; Spalding, K. L.; Buchholz, B. A.; Fink, D.; Björk-Eriksson, T.; Nordborg, C.; Gage, F. H.; Druid, H.; Eriksson, P. S.; Frisén, J. Neocortical neurogenesis in humans is restricted to development. *Proceedings of the National Academy of Sciences* **103**: 12564–12568; 2006.

[82] Silver, J.; Schwab, M. E.; Popovich, P. G. Central nervous system regenerative failure: role of oligodendrocytes, astrocytes, and microglia. *Cold Spring Harb Perspect Biol* **7**: a020602; 2014.

[83] Bjelland, S. Mutagenicity, toxicity and repair of DNA base damage induced by oxidation. *Mutation Research/Fundamental and Molecular Mechanisms of Mutagenesis* **531**: 37–80; 2003.

[84] Tarun, M.; Rusling, J. F. Quantitative measurement of DNA adducts using neutral hydrolysis and LC-MS. Validation of genotoxicity sensors. *Analytical Chemistry* **77**: 2056–2062; 2005.

[85] Singer, B.; Kusmierek, J. T. Chemical Mutagenesis. *Annual Review of Biochemistry* **51**: 655–693; 1982.

[86] Furda, A.; Santos, J. H.; Meyer, J. N.; van Houten, B. Quantitative PCR-based measurement of nuclear and mitochondrial DNA damage and repair in mammalian cells. *Methods Mol Biol* **1105**: 419–437; 2014.

[87] Livneh, Z.; Ziv, O.; Shachar, S. Multiple two-polymerase mechanisms in mammalian translesion DNA synthesis. *Cell Cycle* **9**: 729–735; 2010.

[88] Brioche, T.; Pagano, A. F.; Py, G.; Chopard, A. Muscle wasting and aging: Experimental models, fatty infiltrations, and prevention. *Mol Aspects Med* **50**: 56–87; 2016.

[89] Short, K. R.; Bigelow, M. L.; Kahl, J.; Singh, R.; Coenen-Schimke, J.; Raghavakaimal, S.; Nair, K. S. Decline in skeletal muscle mitochondrial function with aging in humans. *Proceedings of the National Academy of Sciences* **102**: 5618–5623; 2005.

[90] Termini, J. Hydroperoxide-induced DNA damage and mutations. *Radiation Research: A Twentieth-century Perspective* **450**: 107–124; 2000.

[91] Heiken, G.; Vaniman, D.; French, B. Lunar sourcebook. A user's guide to the moon. *Endeavour* **16**: 1–171; 1992.

[92] Stubbs, T. J.; Vondrak, R. R.; Farrell, W. M. A dynamic fountain model for lunar dust. *Advances in Space Research* **37**: 59–66; 2006.

[93] Colwell, J. E.; Batiste, S.; Horányi, M.; Robertson, S.; Sture, S. Lunar surface: Dust dynamics and regolith mechanics. *Wiley Online Library* **45**; 2007.

[94] Jabbal, S.; Poli, G.; Lipworth, B. Does size really matter?: Relationship of particle size to lung deposition and exhaled fraction. *J Allergy Clin Immunol* **139**: 2013–2014.e1; 2017.

[95] Oberdörster, G.; Sharp, Z.; Atudorei, V.; Elder, A.; Gelein, R.; Kreyling, W.; Cox, C. Translocation of inhaled ultrafine particles to the brain. *Inhalation Toxicology* **16**: 437–445; 2004.

[96] Grove, T. L.; Krawczynski, M. J. Lunar Mare Volcanism: Where Did the Magmas Come From? *Elements* **5**: 29–34; 2009.

[97] Garrick-Bethell, I.; Zuber, M. T. Elliptical structure of the lunar South Pole-Aitken basin. *Icarus* **204**: 399–408; 2009.

[98] Baxter, P. J.; Ing, R.; Falk, H.; Plikaytis, B. Mount St. Helens eruptions: the acute respiratory effects of volcanic ash in a North American community. *Archives of environmental health* **38**: 138–143; 1983.

[99] Lam, C.-W.; James, J. T.; McCluskey, R.; Cowper, S.; Balis, J.; Muro-Cacho, C. Pulmonary toxicity of simulated lunar and Martian dusts in mice: I. Histopathology 7 and 90 days after intratracheal instillation. *Inhalation Toxicology* **14**: 901–916; 2002.

[100] Rimal, B.; Greenberg, A. K.; Rom, W. N. Basic pathogenetic mechanisms in silicosis: current understanding. *Curr Opin Pulm Med* **11**: 169–173; 2005.

[101] Campbell, A.; Oldham, M.; Becaria, A.; Bondy, S. C.; Meacher, D.; Sioutas, C.; Misra, C.; Mendez, L. B.; Kleinman, M. Particulate matter in polluted air may increase biomarkers of inflammation in mouse brain. *NeuroToxicology* **26**: 133–140; 2004.

[102] Roos, W. P.; Kaina, B. DNA damage-induced cell death: from specific DNA lesions to the DNA damage response and apoptosis. *Cancer Letters* **332**: 237–248; 2012.

[103] Roos, W. P.; Thomas, A. D.; Kaina, B. DNA damage and the balance between survival and death in cancer biology. *Nature Reviews Cancer* **16**: 20–33; 2015.

[104] Labi, V.; Erlacher, M. How cell death shapes cancer. *Cell Death Dis* **6**: e1675; 2015.

[105] Yauk, C.; Polyzos, A.; Rowan-Carroll, A.; Somers, C. M.; Godschalk, R. W.; Van Schooten, F. J.; Berndt, M. L.; Pogribny, I. P.; Koturbash, I.; Williams, A.; Douglas, G. R.; Kovalchuk, O. Germ-line mutations, DNA damage, and global hypermethylation in mice exposed to particulate air pollution in an urban/industrial location. *Proceedings of the National Academy of Sciences* **105**: 605–610; 2008.

[106] Upadhyay, D.; Panduri, V.; Ghio, A.; Kamp, D. W. Particulate matter induces alveolar epithelial cell DNA damage and apoptosis: role of free radicals and the mitochondria. *American Journal of Respiratory Cell and Molecular Biology* **29**: 180–187; 2003.

[107] Turci, F.; Corazzari, I.; Alberto, G.; Martra, G.; Fubini, B. Free-radical chemistry as a means to evaluate lunar dust health hazard in view of future missions to the moon. *Astrobiology* **15**: 371–380; 2015.

[108] Sena, L.; Chandel, N. Physiological roles of mitochondrial reactive oxygen species. *Molecular Cell* **48**: 158–167; 2012.

[109] Ray, C. S.; Reis, S. T.; Sen, S.; O'Dell, J. S. JSC-1A lunar soil simulant: Characterization, glass formation, and selected glass properties. *Journal of Non-Crystalline Solids* **356**: 2369–2374; 2010.

[110] Kaur, J.; Rickman, D.; Schoonen, M. A. Reactive Oxygen Species (ROS) generation by lunar simulants. *Acta Astronautica* **122**: 196–208; 2016.

[111] Bhagia, L. J. Non-occupational exposure to silica dust. *Indian J Occup Environ Med* **16**: 95–100; 2013.

[112] Hurowitz, J. A.; Tosca, N. J.; McLennan, S. M. Production of hydrogen peroxide in Martian and lunar soils. *Earth and Planetary Science Letters* **255**: 41–52; 2007.

[113] van Berlo, D.; Wessels, A.; Boots, A. W.; Wilhelmi, V.; Scherbart, A. M.; Gerloff, K.; Van Schooten, F. J.; Albrecht, C. Neutrophil-derived ROS contribute to oxidative DNA damage induction by quartz particles. *Free Radical Biology and Medicine* **49**: 1685–1693; 2010.

[114] Wang, Y.; Sun, H.; Tan, S.; Feng, H.; Cheng, Z.; Zhao, J.; Zhao, A.; Wang, B.; Luo, Y.; Yang, J.; Hou, J. G. Role of point defects on the reactivity of reconstructed anatase titanium dioxide (001) surface. *Nature communications* **4**: 2214; 2013.

[115] Wallace, W. T.; TAYLOR, L. A.; LIU, Y.; Cooper, B. L.; McKay, D. S.; CHEN, B.; JEEVARAJAN, A. S. Lunar dust and lunar simulant activation and monitoring. *Meteoritics & Planetary Science* **44**: 961–970; 2009.

[116] Giglia, G. DNA damage response. *Cold Spring Harb Perspect Biol* **3**: a000745; 2011.

[117] Lehle, S.; Hildebrand, D. G.; Merz, B.; Malak, P. N.; Becker, M. S.; Schmezer, P.; Essmann, F.; Schulze-Osthoff, K.; Rothfuss, O. LORD-Q: a long-run real-time PCR-based DNA-damage

quantification method for nuclear and mitochondrial genome analysis. *Nucleic Acids Research* **42**: e41; 2013.

[118] Champion, J. A.; Walker, A.; Mitragotri, S. Role of particle size in phagocytosis of polymeric microspheres. *Springer* **25**: 1815–1821; 2008.

[119] Gustafson, H. H.; Holt-Casper, D.; Grainger, D. W.; Ghandehari, H. Nanoparticle Uptake: The Phagocyte Problem. *Nano Today* **10**: 487–510; 2015.

[120] Oyewole, A. O.; Birch-Machin, M. A. Mitochondria-targeted antioxidants. *FASEB J* **29**: 4766–4771; 2015.

[121] Hopkins, L. E.; Patchin, E. S.; Chiu, P.-L.; Brandenberger, C.; Smiley-Jewell, S.; Pinkerton, K. E. Nose-to-brain transport of aerosolised quantum dots following acute exposure. *Taylor & Francis* **8**: 885–893; 2013.

[122] Fu, P. P.; Xia, Q.; Hwang, H.-M.; Ray, P. C.; Yu, H. Mechanisms of nanotoxicity: generation of reactive oxygen species. *J Food Drug Anal* **22**: 64–75; 2014.

[123] Iyama, T.; Wilson, D. M. DNA repair mechanisms in dividing and non-dividing cells. *DNA Repair* **12**: 620–636; 2013.

[124] Kandul, N. P.; Zhang, T.; Hay, B. A.; Guo, M. Selective removal of deletion-bearing mitochondrial DNA in heteroplasmic Drosophila. *Nature communications* **7**: 13100; 2016.

[125] Moretton, A.; Morel, F.; Macao, B.; Lachaume, P.; Ishak, L.; Lefebvre, M.; Garreau-Balandier, I.; Vernet, P.; Falkenberg, M.; Farge, G. Selective mitochondrial DNA degradation following double-strand breaks. *PLoS ONE* **12**: e0176795; 2017.

[126] Shokolenko, I. N.; Wilson, G. L.; Alexeyev, M. F. The "fast" and the “slow” modes of mitochondrial DNA degradation. *Mitochondrial DNA* **27**: 490–498; 2014.

[127] Keogh, M. J.; Chinnery, P. F. Mitochondrial DNA mutations in neurodegeneration. *Biochim Biophys Acta* **1847**: 1401–1411; 2015.

[128] Sanders, L. H.; McCoy, J.; Hu, X.; Mastroberardino, P. G.; Dickinson, B. C.; Chang, C. J.; Chu, C. T.; van Houten, B.; Greenamyre, J. T. Mitochondrial DNA damage: molecular marker of vulnerable nigral neurons in Parkinson's disease. *Neurobiology of Disease* **70**: 214–223; 2014.

[129] Narciso, L.; Parlanti, E.; Racaniello, M.; Simonelli, V.; Cardinale, A.; Merlo, D.; Dogliotti, E. The Response to Oxidative DNA Damage in Neurons: Mechanisms and Disease. *Neural Plast* **2016**: 3619274–3619288; 2016.

[130] Xu, G.; Herzig, M.; Rotrekl, V.; Walter, C. A. Base excision repair, aging and health span. *Mechanisms of Ageing and Development* **129**: 366–382; 2008.

[131] Gredilla, R. DNA damage and base excision repair in mitochondria and their role in aging. *hindawicom*; 2011.

[132] Imam, S. Z.; Karahalil, B.; Hogue, B. A.; Bohr, V. A. Mitochondrial and nuclear DNA-repair capacity of various brain regions in mouse is altered in an age-dependent manner. *Neurobiology of Aging* **27**: 1129–1136; 2005.

[133] Dolman, N. J.; Chambers, K. M.; Mandavilli, B.; Batchelor, R. H.; Janes, M. S. Tools and techniques to measure mitophagy using fluorescence microscopy. *Autophagy* **9**: 1653–1662; 2013.

[134] Bordt, E. A.; Clerc, P.; Roelofs, B. A.; Saladino, A. J.; Tretter, L.; Adam-Vizi, V.; Cherok, E.; Khalil, A.; Yadava, N.; Ge, S. X.; Francis, T. C.; Kennedy, N. W.; Picton, L. K.; Kumar, T.; Uppuluri, S.; Miller, A. M.; Itoh, K.; Karbowski, M.; Sesaki, H.; Hill, R. B.; Polster, B. M. The Putative Drp1 Inhibitor mdivi-1 Is a Reversible Mitochondrial Complex I Inhibitor that Modulates Reactive Oxygen Species. *Developmental Cell* **40**: 583–594.e6; 2017.

[135] Youle, R. J.; van der Bliek, A. M. Mitochondrial fission, fusion, and stress. *Science (New York, NY)* **337**: 1062–1065; 2012.

[136]van der Bliek, A. M.; Shen, Q.; Kawajiri, S. Mechanisms of mitochondrial fission and fusion. *Cold Spring Harb Perspect Biol* **5**: a011072; 2013.

[137] Weissman, L.; Jo, D.-G.; Sørensen, M. M.; Markesbery, W. R.; Bohr, V. A. Defective DNA base excision repair in brain from individuals with Alzheimer's disease and amnestic mild cognitive impairment. *Nucleic Acids Research* **35**: 5545–5555; 2007.

[138] Wang, X.; Su, B.; Siedlak, S. L.; Fujioka, H.; Wang, Y.; Casadesus, G.; Zhu, X. Amyloid-beta overproduction causes abnormal mitochondrial dynamics via differential modulation of mitochondrial fission/fusion proteins. *Proceedings of the National Academy of Sciences* **105**: 19318–19323; 2008.

[139] Nishioka, K.; Ohtsubo, T.; Oda, H.; Fujiwara, T.; Kang, D.; Sugimachi, K.; Nakabeppu, Y. Expression and differential intracellular localization of two major forms of human 8-oxoguanine DNA glycosylase encoded by alternatively spliced OGG1 mRNAs. *Mol Biol Cell* **10**: 1637–1652; 1999.

[140] Lakshmipathy, U.; Campbell, C. The human DNA ligase III gene encodes nuclear and mitochondrial proteins. *Molecular and Cellular Biology* **19**: 3869–3876; 1999.

[141] Otterlei, M.; Haug, T.; Nagelhus, T. A.; Slupphaug, G.; Lindmo, T.; Krokan, H. E. Nuclear and mitochondrial splice forms of human uracil-DNA glycosylase contain a complex nuclear localisation signal and a strong classical mitochondrial localisation signal, respectively. *Nucleic Acids Research* **26**: 4611–4617; 1998.

[142] Takao, M.; Zhang, Q. M.; Yonei, S.; Yasui, A. Differential subcellular localization of human MutY homolog (hMYH) and the functional activity of adenine:8-oxoguanine DNA glycosylase. *Nucleic Acids Research* **27**: 3638–3644; 1999.

[143] Coppedè, F.; Migliore, L. DNA damage in neurodegenerative diseases. *Mutation Research/Fundamental and Molecular Mechanisms of Mutagenesis* **776**: 84–97; 2014.

[144] Canugovi, C.; Shamanna, R. A.; Croteau, D. L.; Bohr, V. A. Base excision DNA repair levels in mitochondrial lysates of Alzheimer's disease. *Neurobiology of Aging* **35**: 1293–1300; 2014.

[145] Wang, J.; Markesbery, W. R.; Lovell, M. A. Increased oxidative damage in nuclear and mitochondrial DNA in mild cognitive impairment. *J Neurochem* **96**: 825–832; 2006.

[146] Guo, J.-P.; Yu, S.; McGeer, P. L. Simple in vitro assays to identify amyloid-beta aggregation blockers for Alzheimer's disease therapy. *J Alzheimers Dis* **19**: 1359–1370; 2010.

[147] Chen, T.-W.; Wardill, T. J.; Sun, Y.; Pulver, S. R.; Renninger, S. L.; Baohan, A.; Schreiter, E. R.; Kerr, R. A.; Orger, M. B.; Jayaraman, V.; Looger, L. L.; Svoboda, K.; Kim, D. S. Ultrasensitive fluorescent proteins for imaging neuronal activity. *Nature* **499**: 295–300; 2013.

[148] Kim, S. A.; Jun, S. B. In-vivo Optical Measurement of Neural Activity in the Brain. *Exp Neurobiol* **22**: 158–166; 2013.

[149] Blennow, K.; Zetterberg, H. Understanding biomarkers of neurodegeneration: Ultrasensitive detection techniques pave the way for mechanistic understanding. *Nat Med* **21**: 217–219; 2015.

[150]Rosewell, I.; Hollenbach, S.; Daly, G.; Epe, B.; Lindahl, T.; Barnes, D. E. Accumulation of premutagenic DNA lesions in mice defective in removal of oxidative base damage. *Proceedings of the National Academy of Sciences* **96**: 13300–13305; 1999.

[151] Stetler, R. A.; Gao, Y.; Leak, R. K.; Weng, Z.; Shi, Y.; Zhang, L.; Pu, H.; Zhang, F.; Hu, X.; Hassan, S.; Ferguson, C.; Homanics, G. E.; Cao, G.; Bennett, M. V. L.; Chen, J. APE1/Ref-1 facilitates recovery of gray and white matter and neurological function after mild stroke injury. *Proceedings of the National Academy of Sciences* **113**: E3558–3567; 2016.

[152] Béduer, A.; Joris, P.; Mosser, S.; Fraering, P. C.; Renaud, P. Detection of Alzheimer's disease amyloid-beta plaque deposition by deep brain impedance profiling. *J Neural Eng* **12**: 024001; 2015.

[153] Bacioglu, M.; Maia, L. F.; Preische, O.; Schelle, J.; Apel, A.; Kaeser, S. A.; Schweighauser, M.; Eninger, T.; Lambert, M.; Pilotto, A.; Shimshek, D. R.; Neumann, U.; Kahle, P. J.; Staufenbiel, M.; Neumann, M.; Maetzler, W.; Kuhle, J.; Jucker, M. Neurofilament Light Chain in Blood and CSF as Marker of Disease Progression in Mouse Models and in Neurodegenerative Diseases. *Neuron* **91**: 494–496; 2016.

[154] Hollville, E.; Martin, S. J. Measuring Apoptosis by Microscopy and Flow Cytometry. *Curr Protoc Immunol* **112**: 14.38.1–14.38.24; 2016.

[155] Puzzo, D.; Lee, L.; Palmeri, A.; Calabrese, G.; Arancio, O. Behavioral assays with mouse models of Alzheimer's disease: practical considerations and guidelines. *Biochem Pharmacol* **88**: 450–467; 2014.

[156] Santos, J. H.; Mandavilli, B. S.; van Houten, B. Measuring oxidative mtDNA damage and repair using quantitative PCR. *Methods Mol Biol* **197**: 159–176; 2002.

[157] Dianov, G.; Lindahl, T. Reconstitution of the DNA base excision-repair pathway. *Curr Biol* **4**: 1069–1076; 1994.

[158] Fortini, P.; Dogliotti, E. Base damage and single-strand break repair: mechanisms and functional significance of short- and long-patch repair subpathways. *DNA Repair* **6**: 398–409; 2006.

[159] DeMott, M. S.; Beyret, E.; Wong, D.; Bales, B. C.; Hwang, J.-T.; Greenberg, M. M.; Demple, B. Covalent trapping of human DNA polymerase beta by the oxidative DNA lesion 2-deoxyribonolactone. *Journal of Biological Chemistry* **277**: 7637–7640; 2002.

[160] Hashimoto, M.; Greenberg, M. M.; Kow, Y. W.; Hwang, J.-T.; Cunningham, R. P. The 2-Deoxyribonolactone Lesion Produced in DNA by Neocarzinostatin and Other Damaging Agents Forms Cross-links with the Base-Excision Repair Enzyme Endonuclease III. *J Am Chem Soc* **123**: 3161–3162; 2001.

[161] Sonntag, von, C. The Chemical Basis of Radiation Biology. Taylor & Francis; 1989.

[162] Quiñones, J. L.; Demple, B. When DNA repair goes wrong: BER-generated DNA-protein crosslinks to oxidative lesions. *DNA Repair* **44**: 103–109; 2016.

[163] Nakano, T.; Terato, H.; Asagoshi, K.; Masaoka, A.; Mukuta, M.; Ohyama, Y.; Suzuki, T.; Makino, K.; Ide, H. DNA-protein cross-link formation mediated by oxanine. A novel genotoxic mechanism of nitric oxide-induced DNA damage. *The Journal of biological chemistry* **278**: 25264–25272; 2003.

[164] Le Bihan, Y.-V.; Izquierdo, M. A.; Coste, F.; Aller, P.; Culard, F.; Gehrke, T. H.; Essalhi, K.; Carell, T.; Castaing, B. 5-Hydroxy-5-methylhydantoin DNA lesion, a molecular trap for DNA glycosylases. *Nucleic Acids Research* **39**: 6277–6290; 2011.

[165] Prasad, R.; Horton, J. K.; Chastain, P. D.; Gassman, N. R.; Freudenthal, B. D.; Hou, E. W.; Wilson, S. H. Suicidal cross-linking of PARP-1 to AP site intermediates in cells undergoing base excision repair. *Nucleic Acids Research* **42**: 6337–6351; 2014.

[166] Hamon, M.-P.; Bulteau, A.-L.; Friguet, B. Mitochondrial proteases and protein quality control in ageing and longevity. *Ageing research reviews* **23**: 56–66; 2015.

[167] Duxin, J. P.; Dewar, J. M.; Yardimci, H.; Walter, J. C. Repair of a DNA-protein crosslink by replication-coupled proteolysis. *Cell* **159**: 346–357; 2014.

[168] Kiianitsa, K.; Maizels, N. A rapid and sensitive assay for DNA-protein covalent complexes in living cells. *Nucleic Acids Research* **41**: e104; 2013.